Numerical Study on the Formation and Early Development of Tropical Cyclones

A thesis submitted in fulfilment

of the requirements for the degree of

Doctor of Philosophy (PhD)

By

Guoping Zhang

Department of Environmental Sciences
Faculty of Science and Engineering
Macquarie University
Sydney, Australia

November 2016

THIS PAGE INTENTIONALLY LEFT BLANK

CONTENTS

LIST OF ACRONYMS

AISG..... the American Insurance Services Group

AMSU .....the Advanced Microwave Sounding Unit

ARW .....Advanced Research WRF

ATMS..... Advanced Technology Microwave Sounder

CAPE .....the convective available potential energy

CISK..... the convective instability of the Second Kind

CLASS..... Comprehensive Large Array-data Stewardship System

CVAs..... convectively induced vorticity anomalies

EP flux..... Eliassen_Palm flux

FOV..... The Field of View

GOES-9.....Geostationary Operational Environmental Satellite-9

ITCZ .....Intertropical Convergence Zone

MCC..... mesoscale convective complexes

MCS.....mesoscale convective system

MCV..... mesoscale convective vortex

NOAA..... the National Oceanic and Atmospheric Administration

MT..... monsoon trough

MTSAT .....the Multi-functional Transport Satellites

NWP..... numerical weather prediction

OW..... Okubo-Weiss parameter

OWZ.....the normalised Okubo-Weiss parameter

QuikSCAT..... Quick Scatterometer

SSM/I..... Special Sensor Microwave/Imager

SST..... sea surface temperature

TB.....brightness temperature

TC..... tropical cyclone

TD..... tropical depression

TPW..... total precipitable water

UCAR..... University Corporation for Atmospheric Research

VHT..... Vortical Hot Tower

VWS.....vertical wind shear

WISHE..... wind-induced surface heat exchange

WNP..... western North Pacific

WRF .....Weather Research and Forecasting Model

WRFDA .....WRF Variational Data Assimilation System

WSM6.....WRF single-moment 6-class microphysics scheme with graupel

YSU-PBL..... Yonsei University Planetary boundary layer

ABSTRACT

This study investigates the formation mechanisms and early development of tropical cyclones (TCs) through both observational data analysis and numerical model simulations. Typhoon Ketsana (2003) in the western North Pacific is the major case study and has been simulated using the Weather Research and Forecasting Model. First, the roles that mesoscale convective systems (MCSs) play in determining the rate of TC formation is investigated by comparing the simulation of Typhoon Ketsana, which involved multiple MCSs during its formation, with that of Typhoon Dan (1999) with only one MCS involved. Diagnoses of the convection activity, convective energy consumption and recovery show that the longer the convective heating supply from the convective clouds is, the longer is the preconditioning period before TC forms and starts to intensify.

In addition, this study further analyses the contribution from the convective-scale vortical hot towers, or, in more general convectively induced vorticity anomalies (CVAs), to the formation of Typhoon Ketsana. Scale separation showed that the activity of the convective-scale vortices correlate well with the development of the MCSs. These convectively induced vorticity anomalies have large values of positive relative vorticity induced by intense low-level convergence but at the same time large downdrafts associated with negative relative vorticity. The system dynamics through which the CVAs can get organised to form the system-scale surface vortex is analysed with several measures, such as merger index and OWZP.

Observed TC warm-core structure is also examined in this study. The warm core

structures of 17 TCs in monsoon trough of the western North Pacific are analysed using the AMSU-A microwave brightness temperature data. Although there is limitation of the data such as signal scattering by ice, with proper interpretation of the limitations on applications, the temperature retrieval from passive microwave data is able to indicate the warm-core development processes in TCs well. On the other hand, the WRF simulations indicate that every MCS was associated with strong mid- to upper-level heating as typically found in stratiform clouds. However, the simulated warm core development of Typhoon Ketsana shows some interesting development with variation in the warm core height and potential double warm core development. The relationship of such development to MCS activity is discussed.

DECLARATION

I certify that the work in this thesis entitled "Numerical study on the Formation and Early Development of Tropical Cyclones" has not previously been submitted for a degree nor has it been submitted as part of requirements for a degree to any other university or institution other than Macquarie University.

I also certify that the thesis is an original piece of research and it has been written by me. Any help and assistance that I have received in my research work and the preparation of the thesis itself have been appropriately acknowledged.

In addition, I certify that all information sources and literature used are indicated in the thesis.

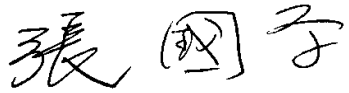

Guoping Zhang (42215714)

21-11-2016

ACKNOWLEDGEMENTS

I take this opportunity to express my gratitude to Dr. Kevin Cheung for the guidance, support, encouragement, help and trust he provided. His supervision and guidance is the foundation of my PhD project. His high scientific standards and his hard work is my example, without him it would be impossible for me to finish the PhD project.

Pursuing a PhD degree is not an easy task, especially after 17 years professional operation and in a foreign country, throughout the six years' study, accompanied with a lot of sleepless nights, hardships and frustration, and also with the help, encouragement and trust from so many wonderful people. Finally, I am on the way to reach the destination of the wonderful journey.

I am also grateful to my adjunct supervisors Dr Kazuo who has contributed heavily throughout my research. The help extended by the Higher Degree Research Council at Macquarie University for providing my scholarship (MQRES), and also the various funds that supported me to attend many national and international conferences and workshops.

In addition, I want to thank many other great people: Dr Xinyan Lu and Dr Yubin Li who helped me a lot with the WRF model; Xin Zhang from UCAR who helped me on the WRFDA models. I also would show my gratitude to Mr. George Antognelli from Open Wiring Systems who offered me a casual position to support my family when no more support from the University.

A number of resources on the Internet have proved invaluable in the research undertaken. The most useful among them are the websites UCAR, Monthly Weather Review and websites about Unix and Intel FORTRAN.

Finally, it is a hopeless understatement to say that I am sincerely grateful for their constant love and infinite support from my family members. All of them contribute a lot to my PhD project. My wife agreed to sell our property in China to cover the living cost of the two years and six months period without any financial support from the university. They are the basic reason of happiness, and they give me the energy to fly towards future.

November 2016

Guoping Zhang

THIS PAGE INTENTIONALLY LEFT BLANK

1 INTRODUCTION

1.1 Chapter Overview

This chapter reviews the research literature on tropical cyclone (TC) formation and early development, which is the main theme of this dissertation. After a general introduction to the background of TCs, previous studies on the roles of mesoscale convective systems (MCSs), convective-scale systems and their scale interaction in the TC formation process are discussed. The science behind the generation process of the warm core, which is a unique feature in TCs, is also a focus of this review. This chapter also sets up the objectives of the dissertation and reveals several specific research questions.

1.2 Literature Review

1.2.1 General Background of Tropical Cyclones

A TC is one of the most destructive weather phenomena, which develops over most of the tropical ocean basins. Its main characteristics include a low-pressure centre circled by spiral bands of clouds, high wind speeds of at least 34 knots (17 m s^{-1}) and the most unique feature of warm core structure but without any frontal system involved. The impacts from TCs occur worldwide including the tropical Australian regions, most Oceania countries and regions such as Southeast Asia, East Asia and North Indian Ocean, and the Caribbean, the Gulf and east coast of the U.S. as well as African countries located by the Southwest Indian Ocean (e.g., Madagascar). It is well known that the hazards

associated with landfalling TCs are multiple in nature and often interconnected. Direct damages to infrastructures are mostly due to the destructive winds within the core circulation of TCs and floods caused by heavy rainfall. In addition to strong winds and rain, TCs are capable of generating high waves, seas wells, damaging storm surge and tornadoes, all of these can result in loss of human lives and huge economic damage. Over the past two centuries, TCs have been responsible for the deaths of about 1.9 million people worldwide (Adler, 2005). Recently, Typhoon Haiyan (2013), the most intense TC in 2013 and the second most intense TC in history, caused catastrophic flooding in the Philippines and it was reported that it had caused more than 5,235 casualties in the Philippines directly. In the U.S., the total number of fatalities related to Hurricane Katrina (2005) was 1833; the American Insurance Services Group (AISG) estimated that Katrina was responsible for $41.1 billion of insured losses in the U.S. Recent Australian examples include the hazardous impacts from TC Yasi (2011) on the tropical resorts and mangrove-fringed coastline of northeast Queensland, which caused an estimated US$3.6 billion in damage (AU $3.5 billion, according to Forecasting service Tropical Storm Risk), making it the costliest TC to hit Australia in record.

1.2.2 Large-scale Environmental Features for TC Formation

For the sake of saving lives, mitigating property loss of TCs and improving economic efficiency, researchers have been focusing on TCs for centuries intending to understand these weather systems especially the formation processes and structures. There are numerous processes from small convective scale to large synoptic scale that are

involved in the TC formation process. Climatologists divided the thermal and kinematic evolution into a sequence of events, and the formation was defined by Frank (1987) as the transition from a disturbance to a tropical depression (TD). Lack of observational studies on TC formation in the literature was likely due to the limited number of observations, which resulted in hypotheses focusing more on the intensification processes of TCs when the storms approaching the coasts were better observed. Charney and Eliassen (1964) discussed the convective instability of the Second Kind (CISK) and formulated a theory for the response of tropical convective complexes to variations in the initial development of TCs formed from earlier conditional instability. Emanuel (1986) then re-examined Charney and Eliassen's hypothesis and developed an air-sea interaction theory for TCs about wind-induced surface heat exchange (WISHE), which was considered to play dominating role during formation rather than the convective instability.

In earlier studies on TC intensification, the basic kinematic structure was considered already built up and in some cases the warm core structure of TC has also established. However, how the unorganised disturbances develop into a well-organised tropical depression was believed to be a stochastic process. Gray (1968) identified six large-scale environmental conditions necessary for TC formation, namely, (i) large value of low-level cyclonic relative vorticity; (ii) a nonzero Coriolis parameter (at least 3°–5° off the equator); (iii) weak vertical wind shear between the lower and upper troposphere, (iv) high values of sea surface temperature (SST), usually exceeding 26.5 °C, which is now considered as a SST threshold for TC formation; (v) vertical instability as measured

by the equivalent potential temperature gradient between the surface and the 500-hPa level or by the convective available potential energy (CAPE); and (vi) large value of mid-tropospheric relative humidity. The first three conditions are dynamic, while the other three are thermodynamic.

Traditionally, areas of tropical cyclone formation are divided into seven basins. These include the North Atlantic Ocean, the eastern and western parts of the North Pacific Ocean, the south-western Pacific, the South Indian Ocean, and the North Indian Ocean (Arabian Sea and Bay of Bengal). On average there are about 80 to 90 named TCs per year (Gray 1985), which may has influences to the global energy budget (Emanuel, 2001). This range of annual TC number was remarkably steady within the last 40 years. Within each basin, however, the numbers often vary more dramatically than the global average (University Corporation for Atmospheric Research UCAR 2013, https://www2.ucar.edu/news/backgrounders/hurricanes-typhoons-cyclones). Gray (1968) showed that 80-90% of TCs formed within 20° of the equator and the majority of them formed in or near the monsoon trough (MT), which is part of the Intertropical Convergence Zone (ITCZ) with westerly winds on its equatorward side and easterly winds on the poleward side over the north Western Pacific; the ITCZ over the north East Pacific and the north Atlantic often has easterly in the south as well. Fig. 1.1 shows the frequency of TC occurrence in the main basins.

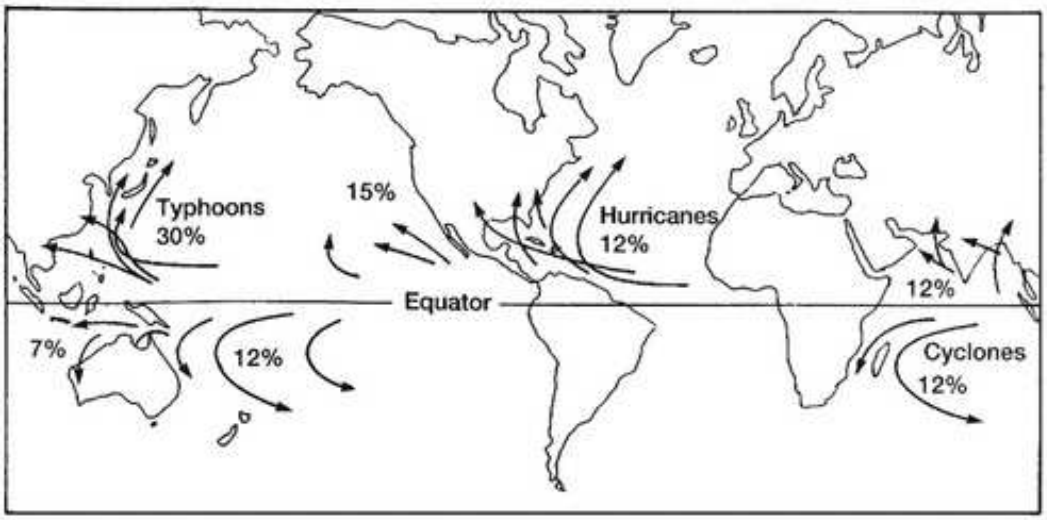

Fig. 1.1 Designation of various TC development regions and percentage of them occurring in each region relative to the global total. Numbers in parentheses are those of the average number of tropical storms occurring in each region per year (adapted from Abbott 2006).

Mcbride (1995), Lander (1996) and Chen (2004) illustrated that about 70% of TCs form in the MT in the western North Pacific (WNP). These studies suggested that a MT offers a favourable environment to fulfil the criteria for formation, such as high relative humidity in the lower to middle troposphere (Bister and Emanuel 1997), upper level anti-cyclonic relative vorticity, low level cyclonic vorticity (Zehr 1992), convective instability, strong low-level convergence and broad scale persistent cloud clusters (Lu et al. 2012). It became well known that tropical waves can trigger TC formation process by changing the spatial and temporal variation in the frequency of TC formation (Chang et al. 1996; Chen et al. 2004; Cheung 2004). However, the roles of mesoscale and convective-scale processes involved in the formation process of TCs, especially how disturbances develop into a TD, are not well understood (Tory and Frank 2010).

1.2.3 Contribution from MCSs to the formation of TCs

With the advances of satellite technologies, mesoscale convective complexes (MCCs), categorised as a subset of MCSs, were identified in the late 1970s and early 1980s (e.g., Maddox 1980). Many studies (e.g., Bosart and Sanders 1981; Cotton et al. 1989; Velsco and Fritsch 1987; Augustine and Howard 1988; Brandes 1990; Bartels and Maddox 1991) found that some convective systems did not satisfy the MCC's strict criteria but had similar structure. Zipser (1982) defined a MCS as a weather feature that exhibited moist convective overturning contiguous with or embedded within a mesoscale circulation, which was at least partially driven by the convective processes. However, such a broad definition includes a wide variety of mesoscale weather phenomena ranging from short-lived thunderstorms to well-organised squall lines to long-lived TCs. Ritchie and Holland (1999) revealed that MCSs frequently organised from the long-lived convection could develop midlevel mesoscale vortices and the probability of cyclogenesis might increase. After studying a 3-year period of TC formations in the WNP, they found that in 70% of all cases of TC genesis, MCSs developed at more than one time during the 72 h up to and including formation. In addition, in 44% of the cases, multiple mesoscale convective systems developed at a single time. Lee et al. (2008) used rigorous criteria on wind directions and speed to define synoptic patterns of TC formations, and found similar results on MCS developments as in Ritchie and Holland (1999). Namely, the easterly wave pattern often develops a TC from a single MCS,

while multiple MCSs developing at the same or different times are favourable in the monsoon shear and monsoon confluence patterns.

These findings illustrate that mesoscale convective processes are of importance in the formation of the majority of TCs. The interaction between MCSs and the large-scale environment, in which they form, is an important aspect of the cyclogenesis problem. These studies also show that MCS occurrence is common phenomenon during the formation. Furthermore, Bartels and Maddox (1991) showed that a midlevel mesoscale convective vortex (MCV) is frequently found within a MCS during the development of severe convective activity. The MCV may last longer than its parent MCS and exist even after the MCS dissipates. Zehr (1992) identified two pre-genesis stages in his conceptual model of TC formation (Fig. 1.2). In the first stage, convection increases within a persistent tropical perturbation, and a small vortex forms and remains, following with the process of stage two. The convection increases again and gradually gain all characteristics of a minimal TC with maximum wind of at least 17 m s^{-1} near the vortex centre, a warm core and its associated deep convection.

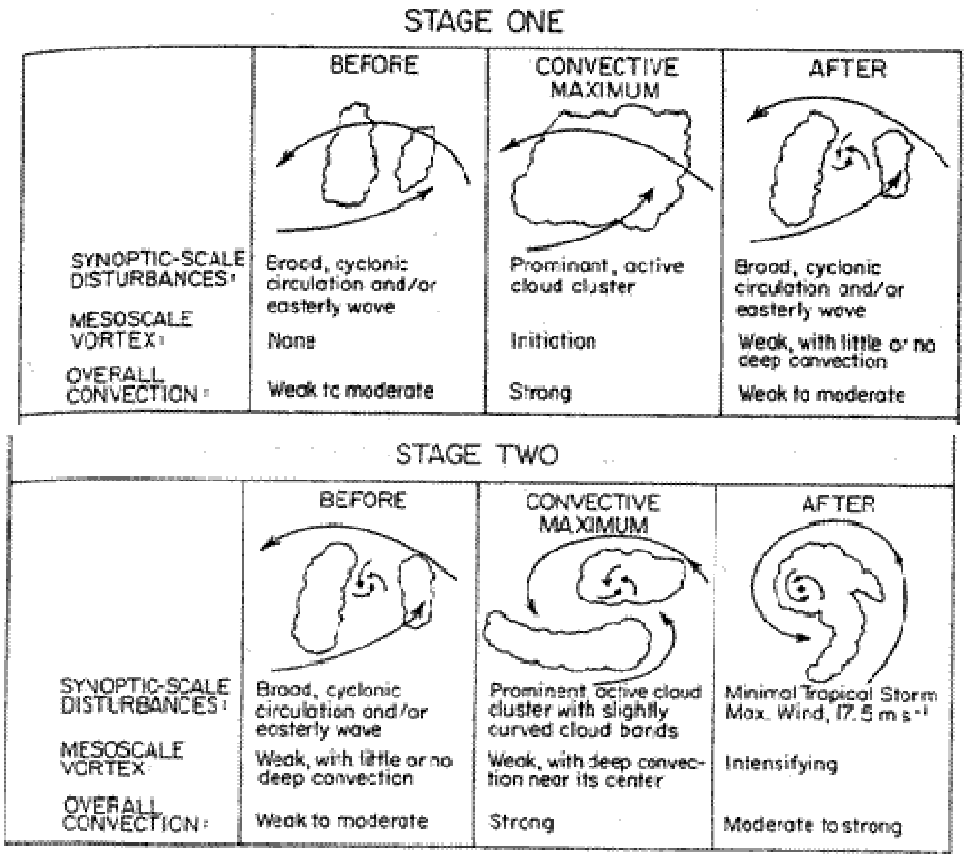

Fig. 1.2 Schematic of the pre-genesis stage of TC (adapted from Zehr 1992).

Although many studies including both observational and modelling studies confirmed that MCV plays very important roles on the formation process (Bosart and Sanders 1981; Harr and Elsberry 1996; Ritchie and Holland 1997; Simpson et al. 1997; Cheung and Elsberry 2006; Kieu and Zhang 2008), it has lasted for decades for scientists to debate how the MCSs influence cyclogensis, and finally they formed two main hypotheses. McBride (1995) introduced conceptions of large-scale formation and core-formation, and further pointed out that core formation can be categorised to two hypotheses. The first hypothesis is called the top-down theory and the second one is called the bottom-up theory which will be addressed in detail in Section 1.2.4. Ritchie

and Holland (1997) and Simpson et al. (1997) focused on the interaction of several midlevel MCVs that eventually merged together to form the TC core, which was likely due to the single vortex size and larger depth. The depth increased downward with the growth of vorticity. Emanuel (1993) also studied a single MCS with MCV through numerical simulation, and found that the enhancement of tangential wind and the midlevel vortex extended downward due to the downdrafts brought by heavy rainfall at the stratiform rain region of MCS (Fig. 1.3). Chen and Frank (1993) described the three stages of the MCV formation based on their numerical simulations: the initial MCS stage, mesovortex genesis stage and mesovortex intensification stage. It was illustrated that in these stages, the reduction of the Rossby radius of deformation leads to genesis of MCV in the stratiform rain region of the MCS, and midlevel short wave, low-level jet with high equivalent potential temperature and weak midlevel vertical wind shear are all critical dynamical factors for MCV development. It was also suggested that this conceptual model likely applies to mesovortices in the tropical cloud clusters as well. These three stages are described in more detail as follows.

a) Initial MCS stage

During this stage, deep convection develops in an unstable air mass, and due to the low-level convergence, an upper-tropospheric stratiform rain zone starts to develop behind the new cloud cluster, the upper ascent and lower descent stretch the midlevel air and induce convergence there, which results in enhanced vorticity.

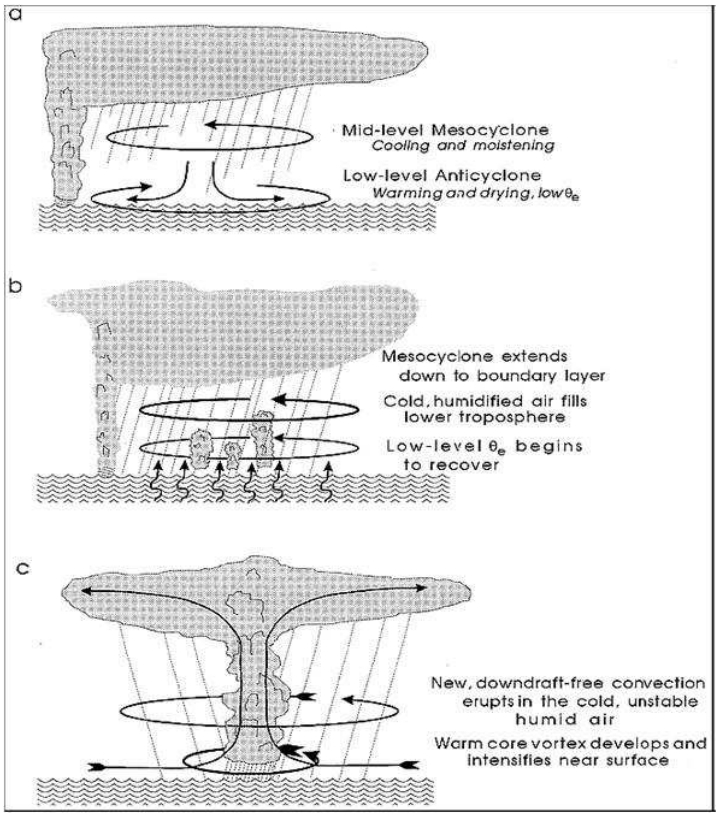

Fig. 1.3 Schematic of the MCS top-down development (adapted from Bister and Emanuel 1997).

b) Mesovortex genesis stage

During this stage, the mesoscale ascent within the stratiform rain zone extends to the upper troposphere, and a mid-level cyclonic vorticity centre forms due to the localised heating.

c) Mesovortex intensification stage

At the third stage, the mesovortex and warm core structure extend down to upper boundary layer above the cold pool, and intensify through the increasing low-level convergence and reduced Rossby radius (Hack and Schubert 1986).

1.2.4 Contribution from Convective-scale Systems to the Formation of TCs

Due to the advances in remote sensing techniques, small-scale weather systems of the order of 10 km associated with TCs have been identified. Riehl and Malkus (1958) suggested that undiluted updrafts in cumulonimbus maintained the mean thermodynamic stratification of the equatorial zone by transporting high moist static energy, and they directly observed and confirmed this phenomenon via a series of aircraft flights in the tropical Pacific zone. This landmark finding is largely accepted by the research community and named Hot Towers, which is a tropical cumulonimbus cloud that penetrates the tropopause and reaches out of the lowest layer of the atmosphere into the stratosphere. Marks and Houze (1984) identified small-scale vortices in the eyewall of a TC using airborne Doppler radar data. It was found that these Hot Towers were associated with the maximum values of convergence, vorticity, and wind speed in the TC, which illustrated that they played significant roles in the storm dynamics. Marks et al. (2008) presented a detailed observational study of a vortex in the eyewall of Hurricane Hugo (1989). This analysis revealed that the intense cyclonic vorticity maximum adjacent to the strongest convection in the eyewall was roughly 1 km in diameter.

Both Hendricks et al. (2004) and Montgomery et al. (2006) argued that the Vortical Hot Towers (VHTs) together mimic a quasi-steady diabatic heating forcing, which is responsible for the development of the secondary circulation. The intense vortices associated with individual cumulonimbus clouds identified by Sippel et al. (2006) through radar data from Tropical Storm Allison (2001) exhibited similar vortex

interactions, the small-scale vortices such as VHTs and their aggregate effects were also argued to play a prominent role in the rapid intensification of TCs. Tory et al. (2006a, b) found that the formation and merger of VHT-like anomalies resulted in the formation of a dominant vortex that became the TC core in simulations of TC formation in the Australian region. All of the aforementioned numerical studies suggest a new paradigm on TC formation. It was argued by these studies that the existence of sufficient CAPE and low-level cyclonic vorticity in the pre-TC environment facilitates the formation of VHTs by deep convective processes, which serve as the primary building blocks of the TC vortex. Some observational evidences also suggested that such a VHT pathway is closely related to tropical cyclogenesis and TC development.

Zehr (1992) observed a phenomenon that the low-level vortex intensification sometimes follows the bursts of deep convection within MCSs. Montgomery (2006) further pointed out that the low-level vorticity enhancement occurs first and then intensifies through the mechanisms of CISK and WISHE. He and other researchers then suggested that VHTs plays very important roles in the formation process of TC (Tory et al. 2006). Montgomery and Kallenbach (1997), Molinari et al. (2004), Reasor et al. (2005) and Sippel et al. (2006) provided observational evidence for the existence and interactions of intense vortices associated with individual cumulonimbus clouds of varying scales and intensity in developing cyclones, and summarised that axisymetrization and the stretching of VHT vorticity canters intensifies the initial surface vortex. Montgomery et al. (2006) further demonstrated that VHTs could effectively overcome the generally adverse effects of downdrafts and sustain for a relatively long

time period by consuming CAPE in their local environment, humidifying the middle and upper troposphere, and undergoing diabatic vortex mergers (i.e., new convection in between two existing centres) with neighbouring towers. In addition, Fang and Zhang (2011) found that there were large numbers of small-scale vorticity anomalies accompanying the VHT, which might be dissipated VHTs or future VHTs. These anomalies, together with the active VHTs, were collectively named as convectively induced vorticity anomalies (CVAs), and it was further showed that enhancing surface vortex during TC formation resulted in such bottom-up process.

1.2.5 Scale Interactions in TC Formation

Both the top-down and bottom-up hypotheses show the importance of MCS during the formation of TCs. However, the detailed mechanisms governing the relative contributions from MCSs and VHTs to the low-level vortex enhancement for forming the core of a TC during the TC formation process are still not fully understood. Although remote-sensing observation data showed the low-level vortex enhancement and rapid development of VHT (e.g., Lee et al. 2008), via the coarse-resolution satellite images, the mechanisms cannot be identified and determined whether the process is top-down, bottom-up or combination of the two hypotheses.

Many weather systems are involved in the TC formation process, including the large-scale environment, MCSs and MCVs, and convective-scale systems. However, the relative contributions from these weather systems and how they interact during the formation period may vary largely from case to case. For instance, Simpson et al. (1997)

identified several MCVs in the early stage of the cyclogenesis on TC Oliver (1993), four of them interacted and three of which merged to develop to the TC. Ritchie et al. (1997) observed many MCVs interacting with each other during the formation process of Typhoon Irving (1992). On the other hand, Houze et al. (2009) pointed out that the downdraft from MCSs involved in the formation of Hurricane Ophelia (2005) did not appear to be very strong and there was little evidence of strong downward motion to reach the boundary layer. Houze et al. (2009) concluded that the convective-scale perturbations at the lower levels and the mesoscale perturbations at the mid-levels, all derived from the deep convective cells, contributed together to the total storm circulation (Fig. 1.4).

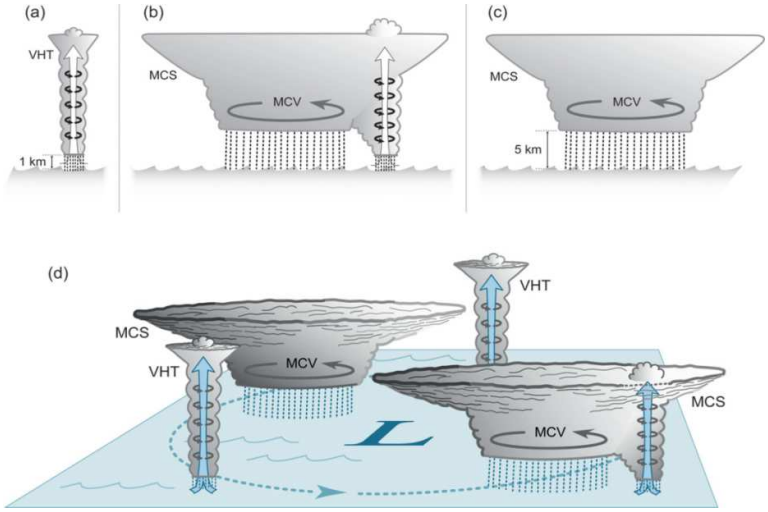

Fig. 1.4 MCS life cycle within a developing tropical cyclone. (a) The MCS begins as a set of one or more isolated deep VHTs. (b) The convective-scale cells are transient components of a larger and longer-lived MCS, and they form a precipitating stratiform cloud. (c) In the late stages of the MCS life cycle, new cell development ceases. (d) An idealised distribution of VHTs and MCSs in various stages of development (adapted from Houze et al. 2009).

Karyampudi and Pierce (2002) also found the merging of low-level and mid-level vortices when studying TC Ernesto (1994) and Hurricane Luis (1995). Hendricks et al. (2004) suggested that convective plumes with intense vertical vorticity in their cores, i.e. VHTs, were the favourable convective structures in tropical cyclogenesis, which could eventually result in the spin up of TCs through multiple mergers and axisymmetrization of these low-level potential vorticity (PV) anomalies. The evolution of negative vorticity anomalies in the development of TCs is another interesting issue associated with small-scale vortices. Many studies such as McWilliams (1984), Dritschel and Waugh (1992), and Ritchel and Holland (1993), pointed out that vortices of any scale would interact when in close enough proximity, giving rise to the well-recognised patterns of vortex orbiting, merging, shearing and axisymmetrization of like-signed anomaly. Through idealised numerical experiments based on a 3D quasi-geostrophic model, Montgomery and Enagonio (1998) showed that vortex intensification was preceded by the ingestion of like sign PV anomalies into the parent vortex and expulsion of opposite-sign PV anomalies during the axisymmetrization process. Nguyen et al. (2008) also argued that cyclonic vorticity anomalies in the negative vorticity gradient of the parent vortex would tend to move toward the centre, while anticyclonic anomalies would tend to move away from the centre. Wang(2014) suggested that cumulus congestus clouds also could amplify the low-level vorticity effiectively and intense the system. Although the above-mentioned studies suggested that the expulsion of the vortices with negative relative vorticity is a crucial factor for vortex enhancement, the detailed mechanisms and organization aspects of this process has not been clarified in detail in the

literature.

1.2.6 Warm Core Generation

The warm core structure of TC has long been of scientific interest for centuries because such structure is the most unique feature in a TC. The existence of warm core was first enunciated by Ferrel (1856). In addition, Shaw (1922) found that TCs were shallow disturbance via visualizing a TC that had a core composed of air that rose adiabatically from surface up to 15 km. Furthermore, Haurwitz (1935) concluded that the sea-level pressure could only be accounted for if the TC central air columns were warmer than its surroundings up to at least 10-11 km. Simpson (1947) presented the first aero evidence of TC warm core structure. Via flight observational data, La Seur and Hawkins (1963) drew the cross section of temperature in Hurricane Cleo (1958) with a 11 °C maximum temperature anomaly at the upper level. Hawkins and Rubsam (1968) interpolated downward the temperature anomaly and obtained the warm core structure via flight observations of Hurricane Hilda (1964) with a maximum temperature anomaly of 16 °C at around 250 hPa (Fig. 1.5). Although these studies were based on very limited observations, this plot of TC warm core structure is still widely believed to be typical. For example, Palmén and Newton (1969) emphasised the importance of warm core as a necessary condition with a quote “the formation of a warm core is the first decisive sign of TC formation”.

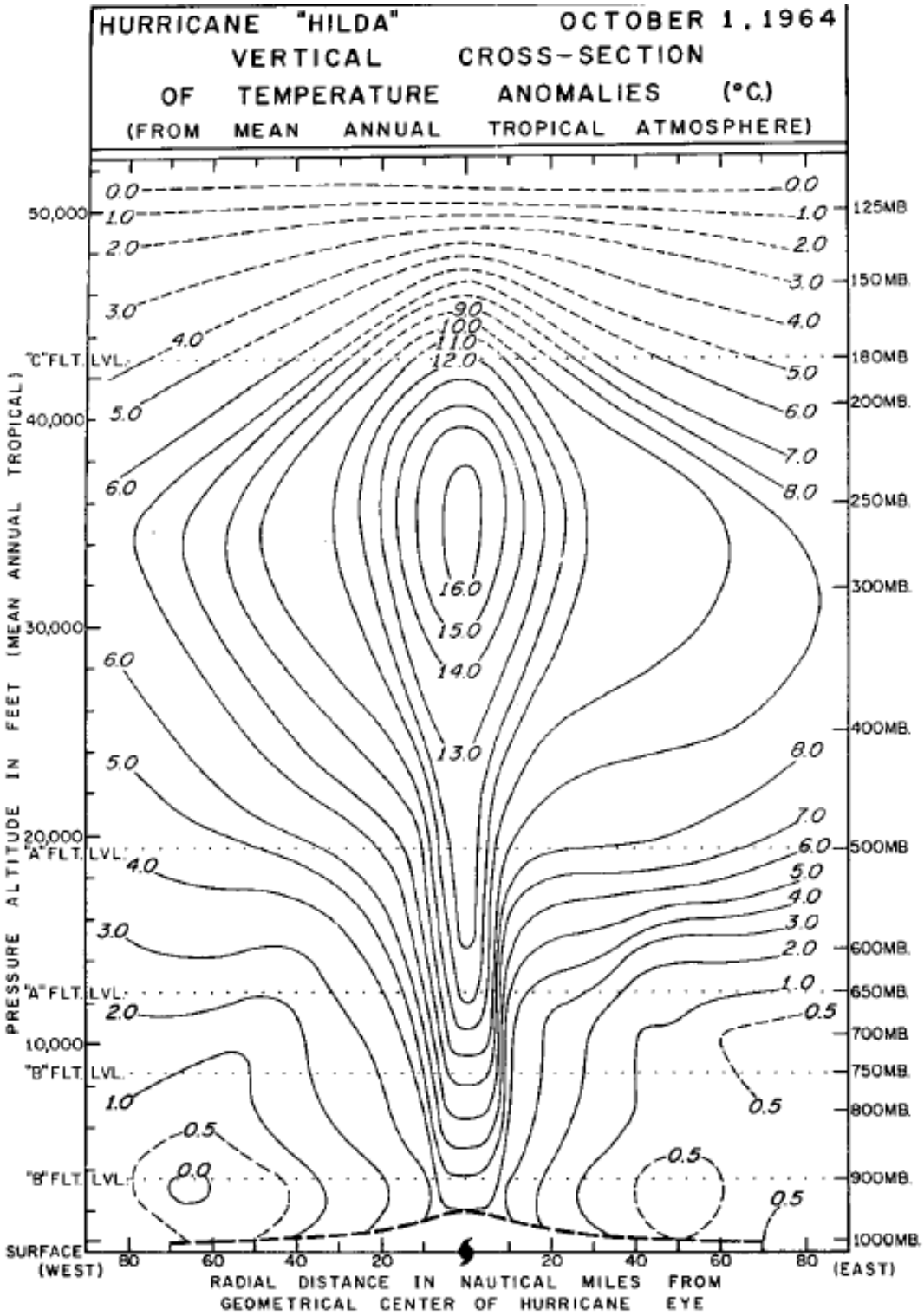

Fig. 1.5 Vertical cross section of temperature anomaly for Hurricane Hilda (1964) (Adapted from Hawkins and Rubsam (1968))

Many studies showed the three-dimensional characteristics that distinguish warm core from baroclinic systems (Bosart and Bartlo 1991). Montevedi and Edwards (2010) also found that even the inland redevelopment of Hurricane Erin (2001) resulted in a new warm-core system. Bessho et al. (2010) illustrated and confirmed that the maxima average temperature anomaly in 200 hPa was larger than that in lower levels. However, many other studies showed different warm core structures. Hawkins and Imbembo (1976) showed that the observed warm core was at around 600 hPa in Hurricane Inez (1966). Using the temperatures retrieved from Advanced Technology Microwave Sounder (ATMS), Zhu et al. (2013) also argued that unlike a typical TC, the height of maximum warm core in Hurricane Sandy (2012), the most devastating storm in 2012, was very low. Its maximum warm core was located around 400 hPa.

Stern and Nolan (2012) found that the maximum temperature perturbation occurs in the mid-troposphere (5-6 km), in contrast to the typical upper-tropospheric (>10 km) warm core. When Stern and Nolan (2012) reassessed the typical ones, results showed that the warm core was generally found at 4–8 km and a secondary maximum often developed near 13–14 km but was almost always weaker than the primary warm core, which resulted in their conclusion that the “typical” warm-core structure was actually not well known. They further demonstrated that microwave remote sensing instruments were of insufficient resolution to detect this mid-level warm core, with conclusions of some studies that have utilised these instruments may not be reliable. It was also argued that the height of the warm core was not necessarily related to either the height where the vertical shear of the tangential winds was maximised or the height where the radial

temperature gradient was maximised, and changes in the height of the warm core needed not imply changes in either the intensity of the storm or in the manner in which the winds in the eyewall decay with height. Braun (2002) also simulated a maximum temperature anomaly of Hurricane Bob (1991) that was located about 5 km in height, but it was believed that this came from the domain-averaged reference state. On the other hand, Liu et al. (1997) simulated the warm core of Hurricane Andrew (1992) at about 500 hPa.

Halverson et al. (2006) confirmed the existence of warm core through ER-2 dropsondes data but the largest temperature anomaly was located near 500 hPa due to the strong inversion present between 760 and 800 hPa. Halverson et al. (2006) further pointed out that the concentration of the warming leading to the pressure drop was not as significant in the layers above 300 hPa and the warm anomaly at low level was generated by subsidence in the core zone (Fig 1.6).

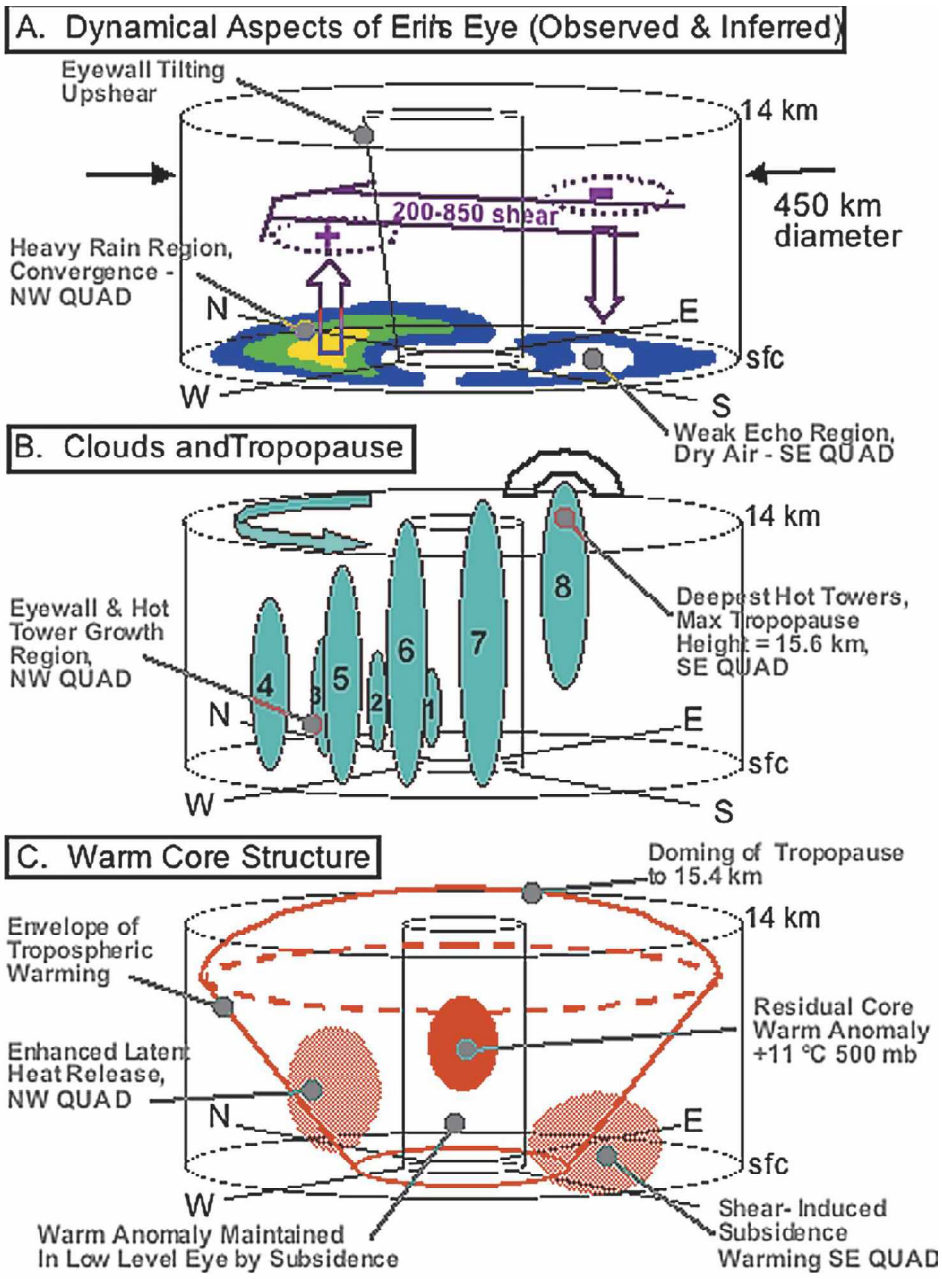

Fig. 1.6 Schematic synthesizing dropsonde, aircraft, and satellite observations on the structure of Hurricane Erin's inner core. (a) The relationship of shear to the rainfall distribution and hypothesised vertical motions. (b) The evolution of eyewall hot towers and tropopause height anomaly. (c) The general warm core structure and asymmetrics in the warming that are hypothesised to arise from the vortex–shear interaction (adapted from Halverson et al. 2006).

Via GPS sondes, Dolling and Barnes (2012) found that the warm core of Hurricane Humberto (2001) was located at 2-3 km in height with different intensities. They pointed out the warm core was located in the subsidence region below the base of the trailing edge of the MCS anvil, and dry adiabatic descent leads to warming at the lower levels (Fig 1.7). This represents a possible mechanism through which a MCS evolves into a TC's warm core in the lower troposphere. In contrast, the 'conventional' upper-level warm core during TC intensification via mechanisms such as WISHE is due to undiluted eyewall updraft and associated condensation heating.

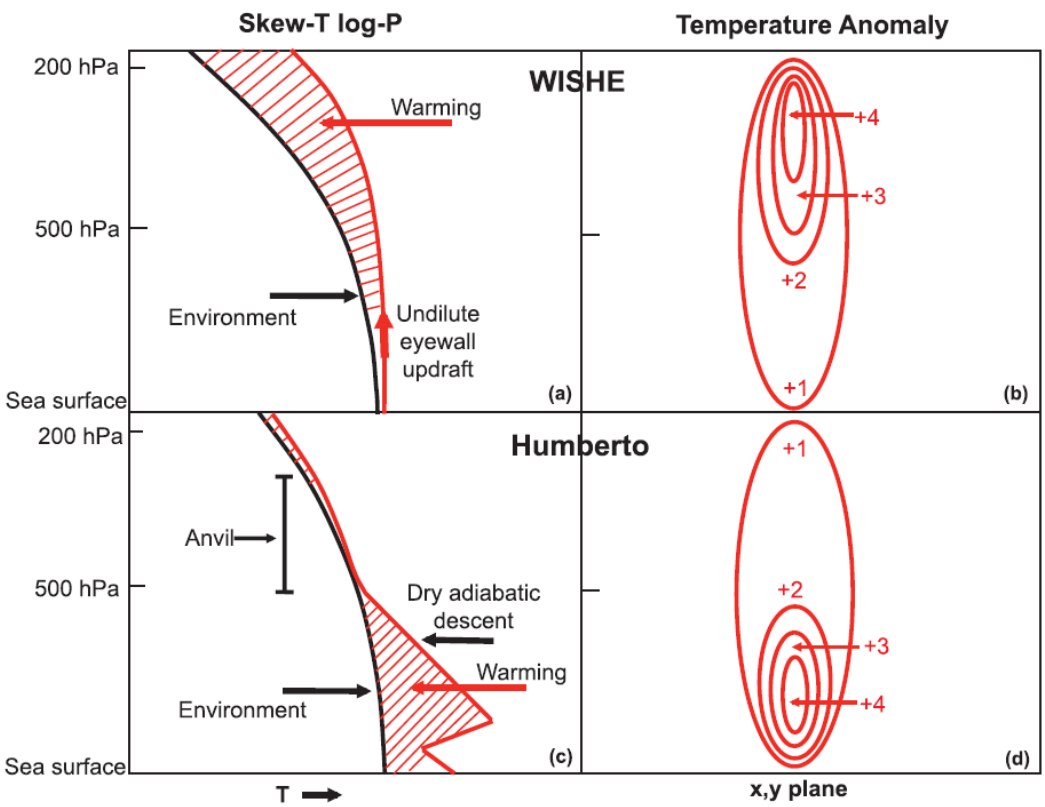

Fig. 1.7 Schematics of upper- (via WISHE) and lower-level (in Hurricane Humberto) warm core development and associated heating mechanisms (adapted from Dolling and Barnes 2012).

On the other hand, Ohno and Satoh (2015) analysed warm core formation near the tropopause through idealised numerical simulations. It was found that for the generation of such high-altitude warm core was likely due to tropospheric diabatic heating and the associated forced flow. Instead, upper-level subsidence at the lower stratosphere was enhanced when the vortex was tall enough. Accordingly, near-tropopause warm core may form in TCs with very intense convective bursts.

1.3 Thesis Objectives and Structure

In recent decades, weather forecasting heavily relies on applications of numerical weather prediction (NWP) models; however, the performance of NWP in the Tropics is still far behind that in the mid-latitudes especially for TC predictions. Although the performance of TC track forecasting has been improved significantly, forecasting of the formation and intensity of TCs still remains a challenging task (Jin et al., 2008).

The major objective of this dissertation is to reveal the mechanisms of TC formation processes and improve our understanding on these processes, which will lead to better skill in forecasting of TC early development. To attain this goal, data assimilation system is used to assimilate satellite observations such as satellite-derived winds and precipitable water into the boundary conditions and initial conditions of one of the best NWP models. There are two important aspects of TC formation: core structure formation and warm core formation. For the core structure formation, we study the roles of MCSs and convective-scale systems in the formation process. For convective-scale systems, we analyse the self-organization and vortex interaction aspect

of the positive and negative vorticity anomalies through the application of merger indices. The scale dependence of the development of solid body rotation in the TC core is analysed based on the normalised Okubo-Weiss (OWZ) parameter.

Further understanding on the contributions from MCSs to TC formation is obtained by investigating the contrasts between single MCS versus multiple MCSs development during the process of TC formation, and how these contrasts lead to different rates of TC early development. It is well known that diabatic heating due to condensation is critical to TC intensification. In particular, the locations of such diabatic heating modulate the inertial and static stabilities within the TC core, which in turn control the subsequent TC development. This study analyses the respective contributions from convective and stratiform heating associated with MCSs to TC formation, and how these centres of heating lead to the spin up of the TC core vortex as well the secondary transverse circulation in TC.

For the problem of warm core formation, satellite passive microwave data and associated temperature retrievals are examined to determine to what extent such datasets can reliably indicate the heights of TC warm cores, and the technical difficulties involved. Then the process of possible secondary warm core development at mid to low level is investigated through a case study. Since the TC case involves MCS development during its formation, the proposed mechanisms in Halverson et al. (2006) and Dolling and Barnes (2012) are verified and discussed.

Some of the specific research questions of this dissertation include:

- The surface vortex has to be enhanced to complete the TC formation. What are the relative contributions from midlevel MCVs and convective-scale system, and what is the temporal evolution between these factors?
- Is the deep convection within the last MCS the final "trigger" of TC formation? Or is the trigger with smaller scale such as the VHTs? What mechanisms are operating to organise the VHTs? How do they get organised to form the mesoscale core vorticity?
- How does heating associated with MCS aid in the formation of the dynamical and thermodynamic structure of TC?
- Do the number and spatial configuration of MCSs determine the rate of TC formation and early development, and to what extent?

The structure of the dissertation is as follows: Chapter 2 describes the numerical models applied, data sets used and methodologies. Chapter 3 addresses the issue of MCSs number and configuration, and their impact to the rate of TC development. Chapter 4 investigates the system dynamics of convective-scale systems during TC formation. Chapter 5 analyses the observational aspects of TC warm core and possible mechanisms leading to low-level warm core generation. Chapter 6 summarises the findings of this dissertation and discusses the remaining issues for future studies.

2 DATA SOURCES AND METHODOLOGY

2.1 Chapter Overview

This chapter explains the various data sources, the models used to performance the simulations and data assimilation, and the research methods applied to analyse the physical processes of TC formation and early development in this study. The theoretical concepts and computational algorithms of extracting convective and stratiform rain types that are associated with different profiles of condensation heating, the Eliassen-Palm (EP) flux and divergence to analyse vortex asymmetric dynamics, the merger index of vortices and the normalised Okubo-Weiss parameter for core vorticity analysis in TCs are introduced.

2.2 Data Sources

One of the most significant challenges to study TC development is the scarcity of data over the oceans. In this study, TCs formed over the western North Pacific are the focuses and thus remote-sensing data is essential to monitor their developments. For synoptic-scale analysis, the gridded U.S. National Centre for Environmental Prediction (NCEP) final (FNL) reanalysis data with $1^{o} \times 1^{o}$ latitude/longitude resolution is used to analyse the large-scale environment and also used as model input. Six-hourly sea surface temperature (SST) data combined with the NCEP atmospheric data provide the initial and lateral boundary condition for the numerical model. For data assimilation, Quick Scatterometer (QuikSCAT) oceanic surface winds from the National Aeronautics

and Space Administration (NASA) and the Special Sensor Microwave/Imager (SSM/I) oceanic wind speed and total precipitable water (TPW) from the Defense Meteorological Satellite Program satellite passive microwave radiometers are assimilated during the model simulations.

TC best tracks from the U.S. Navy's Joint Typhoon Warning Centre (JTWC) are applied. Infrared satellite images are examined to monitor convective activities and convective heating during the process of TC development. For Typhoon Ketsana (2003), hourly satellite images from the Geostationary Operational Environmental Satellite-9 (GOES-9) infrared channel-1 (IR-1) with wave length 10.3-11.3μm and 5-km resolution are used. For the earlier TCs such as Typhoon Dan (1999), images from the Japan Meteorological Agency (JMA) Geostationary Meteorological Satellite (GMS5) and Multi-functional Transport Satellites (MTSAT) are used. Synoptic analyses of these two typhoons will be presented in Chapter 3. Additional TC cases will be analysed for warm-core development in Chapter 5 and those cases will be presented in that chapter.

Since infrared satellite images are only able to analyse the general convection pattern and cloud-top temperature, microwave data is applied to examine temperatures at different heights and within TCs, which can be used to deduce the warm-core structures of the TCs. In particular, techniques exist in retrieving the brightness temperature from the Advanced Microwave Sounding Unit (AMSU) on board some of the satellites from the U.S. National Oceanic and Atmospheric Administration (NOAA). Details of the retrieval methods of brightness temperatures from AMSU and their limitations will be discussed in Chapter 5.

2.3 Numerical Model and Data Assimilation System

2.3.1 Description of the Weather Research and Forecasting Model (WRF)

In this research, WRF version 3.3.1 with the Advanced Research WRF (ARW) dynamical core, which was developed by the National Centre for Atmospheric Research (NCAR) (Skamarock et al. 2008), is employed to simulate the processes leading to cyclogenesis and early development of TCs including Typhoon Ketsana (2003) and Typhoon Dan (1999). The WRF model integrates the fully compressive non-hydrostatic Euler equations of motion in flux form on a Cartesian Arakawa C grid with hydrostatic option. Its vertical coordinate is a terrain-following sigma coordinate (Fig. 2.1).

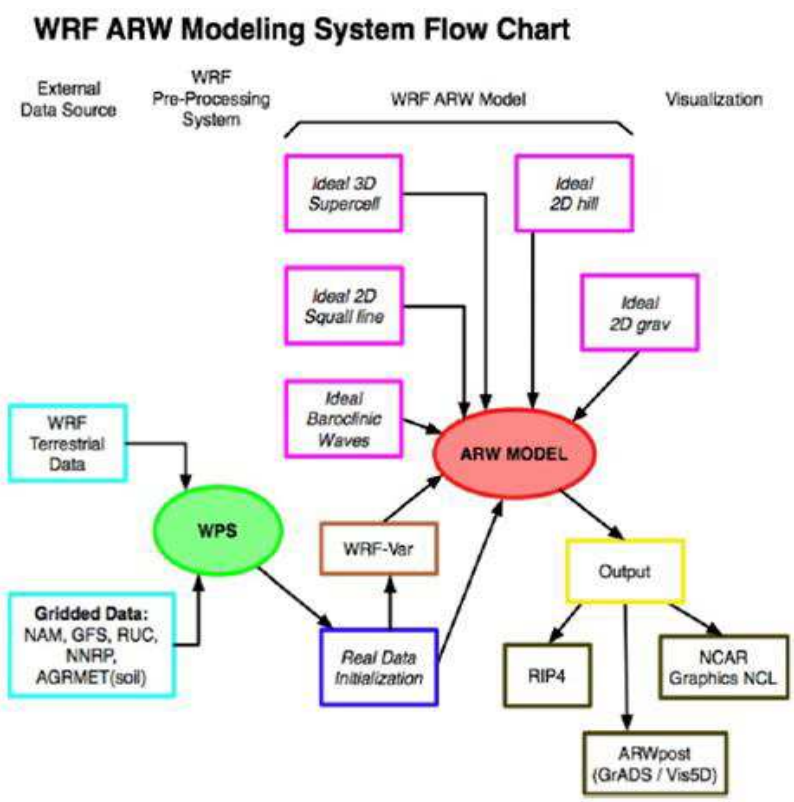

Fig. 2.1 The WRF model flowchart (adapted from http://www.wrf-model.org).

In the WRF simulations of Typhoon Ketsana (2003) and Typhoon Dan (1999), three nested domains are used with horizontal spatial resolutions of 27/9/3km with 2-way nest option, and the mesh sizes are set as 198×154 (D1), 295×232 (D2), 436×346 (D3) respectively. In the vertical direction, 35 layers are used with the model top at 50 hPa. The model physics schemes used in the simulations include the WRF single-moment 6-class microphysics scheme with graupel (WSM6; Hong et al. 2004) and the Yonsei University Planetary boundary layer (YSU-PBL) scheme (Noh et al. 2003). The modified version of Kain and Fritsch cumulus parameterization scheme (KF_Eta; Kain 2004) is used in the outer two domains (D1 and D2), while only explicit moisture calculation is used in D3. Radiation is treated using the RRTM long-wave scheme, a spectral-band radiative transfer model using the correlated K-method (Mlawer et al., 1997), while shortwave radiation was parameterised using the Dudhia (1989) shortwave scheme (MM5 shortwave scheme). At the surface, the NOAH land surface model (Ek et al., 2003) is used with the U. S. Geological Survey (USGS) land use data having 30 arc second resolutions (for domain D03).

2.3.2 Description of the WRF Variational Data Assimilation System (WRFDA)

Assimilation of available remote sensing data is a critical step for improving TC prediction. An important component in all assimilation models is the adjoint model, which computes the sensitivity of a certain forecast aspect with respect to another model parameter during the data assimilation process (Xiao et al. 2008). WRFDA version

3.3.1 includes an adjoint model developed by NCAR (Skamarock et al. 2008), and was built within the WRF software framework, for application in both research and operational environments.

The basic goal of variational data assimilation is to obtain a statistically optimal estimate of the true atmospheric state at a desired analysis time through an iterative minimization of the prescribed cost function J(x) (Ide et al. 1997):

$$J(x) = \frac{1}{2}(x - x_b)^T B^{-1}(x - x_b) + \frac{1}{2}(y - H(x))^T R^{-1}(y - H(x)) \qquad (1)$$

where x is the atmospheric state vector, x_b the background state (usually a short-range forecast), H the nonlinear observational operator, and y the observation vector. For satellite remote sensing, H is responsible for transferring model parameters comparable with observations. The B and R respectively are the background and observation error covariance matrices. They are directly associated with the data source (e.g., the party that provides the remote sensing data should also provide the corresponding R). If an iterative solution of x can be found by minimizing Eq. (1), the result represents a minimum variance estimate of the true atmospheric state, given the background x_b and observation y, as well as B and R (Lorenc 1986). In this proposed research, whenever an observed wind vector is available, a 3D-variational (3DVAR) analysis is performed in order to optimize the initial and boundary conditions and thereby permit forward predictions to be made based on the adjusted initial and boundary conditions. Specifically, the WRFDA 3DVAR system is used for the assimilation of the QuikSCAT oceanic wind vectors and SSM/I wind speed and TWP.

2.3.3 Procedure of Simulation and Data Assimilation

The 6-hour cycling forecast-analysis experiment is carried out for the TC cases in this study (Fig. 2.2). For example, for simulating Typhoon Ketsana (2003) the data assimilation period begins at 0000 UTC 16 Oct 2003 and the model is integrated 108 hours until 1200 UTC 20 Oct 2003. The background in the first analysis at 0600 UTC 16 Oct is provided by a forecast of WRF run that is initiated from NCEP FNL $1^{o} \times 1^{o}$ analysis at 0000 UTC 16 Oct 2003, with observed SST at the lower boundary. For the ensuing cycles, the background is the 6-hour WRF forecast from the previous cycle. The background error statistics are estimated using the method from Parrish and Derber (1992). In this study, data from within ±3 hour of analysis times are used and assumed to be valid at the reanalysis times.

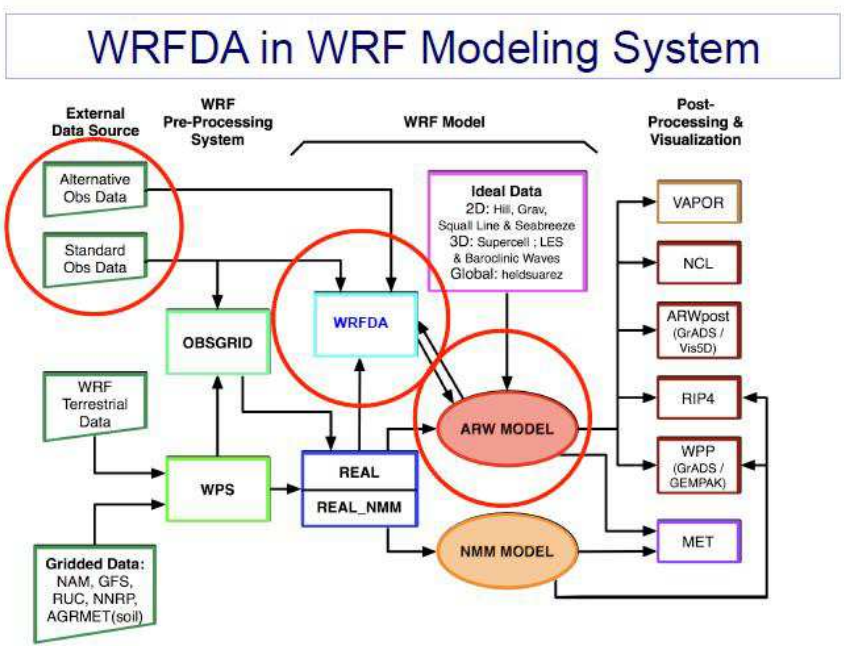

Fig. 2.2 WRF Modelling system flowchart (adapted from http://www.wrf-model.org).

2.4 Convective versus Stratiform Heating

In the spatial analysis of radar echoes, there are algorithms to extract information on the precipitation types. The radar structure and type of cloud systems are very important indicators for meteorologists to analyse the development of weather systems and their precipitation, especially the stratiform type and convective type precipitation. The microphysical difference between the convective and stratiform precipitation and their microphysical growth mechanisms were firstly shown by Houghton (1968). For the stratiform precipitation, it normally falls down from clouds in which temperature is lower than 0°C, and ice particles fall when vertical air motion speed is lower than the fall velocity of ice particle. Hobbs (1973) and Houze and Chuchill (1987) also showed that ice particles grew primarily by water vapour. On the contrary, the convective precipitation process, in which air motion speed equalled or was larger than the typical fall velocity. Matejka et al. (1980), Knight et al. (1982), Houze and Chuchill (1984) pointed out via observational study that the precipitation particles grew mainly through accumulation of liquid water. Houze (1989) and Johnson (1984) found out that diabatic heating processes were clearly different between convective and stratiform precipitation. For studying of TCs, separating the observed or simulated radar echoes into convective and stratiform type precipitation is able to infer TC development via their different thermodynamic processes.

To distinguish the two types of precipitation, Collier et al. (1980) used radar reflectivity brightness band but this method is very limited by the data area due to the radar beam width. Techniques have been developed according to storm structures

because the convective region and trailing stratiform area could be identified, however, this approach was still limited due to the large dependence on storm structures.

Houze (1973), Chuchill and Houze (1984) and Steiner and Houze (1993) developed a more practical approach to search for peaks of rain rate. If the grid point met the requirements of ratio of peak rain rate and surrounding rain rate, the peak and it surroundings were marked as convective. Steiner and Houze (1993) further developed this and adopted this using radar reflectivity (4.5 dBZ more than its surroundings). Due to the sensitivity to spatial resolution and over estimation of convective rain, Steiner et al. (1995) further modified this separation technique and revised the criteria based on intensity, peakedness and surrounding area. First, any grid point in radar reflectivity from and above 40 dBZ was automatically defined as convective centre; and if it exceeded the average intensity of surrounding background within 11 km of the grid point, it still was labelled as convective centre. However, rather than using a fixed reflectivity difference as criterion, such peakedness requirement depends on the background reflectivity nonlinearly up to 42.43 dBZ (Eq. 2 and Fig. 2.3):

$$\triangle Z = \begin{cases} 10, & Z_{bg} < 0 \\ 10 - {Z_{bg}^2}/{180}, & 0 \leq Z_{bg} < 42.43 \\ 0, & Z_{bg} \geq 42.43 \end{cases} \tag{2}$$

where ΔZ is the reflectivity difference, and Z_{bg} is the background reflectivity (Fig. 2.5). Then any grid points within an intensity-dependent convective radius around the grid point were identified as convective area (Fig. 2.4).

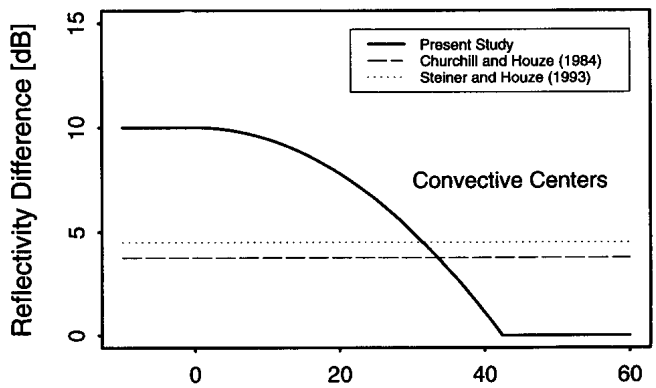

Fig. 2.3 The peakedness criterion (solid curve) is a function of the mean background reflectivity. Points along and above this curve are classified as convective centers. The constant peakedness criteria used by Churchill and Houze(1984) and Steiner and Houze(1993) are indicated by the dashed and dotted lines, respectively (adapted from Steiner et al. 1995).

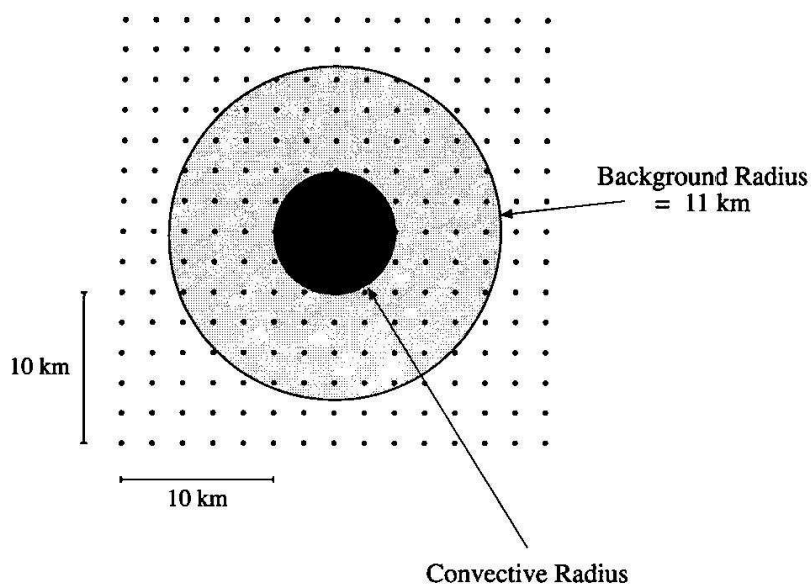

Fig. 2.4 Schematic diagram showing how convective grid points are identified. The lightly shaded circular area indicates the area within the background radius surrounding a given grid point (bold point in the centre). The darker-shaped area represents the area around the convective centre. The radius of this convective area is a function of the average reflectivity within the background radius (adapted from Steiner et al. 1995).

2.5 The Eliassen-Palm (EP) Flux and Divergence

Montgomery and Kallenbach (1997) introduced a hypothesis that the genesis of concentric eyewalls may take place via vortex axisymmetrization, and further pointed out that the critical radius represents a site for vortex Rossby wave-mean flow interaction and the vortex Rossby wave-mean flow dynamics may become a basic vortex spinup mechanism. Furthermore, many studies such as Reasor et al. (2000), Chen and Yau (2001) and Wang (2001, 2002a, b) found that the inner rainband of TCs have characteristics of Rossby waves. For quantitatively study the vortex Rossby wave in TCs, a useful diagnostic tool is the Eliassen_Palm (EP) flux and its divergence. In the paper of Eliassen and Palm (1960), the EP theory was creatively introduced to separate the flow into its zonal and deviations. Some later studies extended the use of this theory to the effect of humidity (e.g., Stone and Salustri 1984), however, these studies still applied the EP theory to large-scale circulation. Andrews et al. (1987) started to apply it on isentropic coordinates, and some studies such as Schubert (1985), Molinari et al. (1995, 1998), Chen et al. (2003), Chen and Yau (2003) and Martinez et al. (2011) have extended the application of EP theory to TC dynamics. The transformed Eulerian mean formulation was introduced to express the eddy heat and momentum fluxes in the form of the divergence of the EP flux to drive changes in the mean circulation (Andrews and McIntyre 1976). The EP flux and its divergence are also good indicators of the wave propagation and wave–mean flow interaction. The EP fluxes are associated with the flux of pseudomomentum; its divergence is interpreted as an eddy-induced force per unit mass and therefore provides a measure of the wave–mean flow interactions, and can

indicate where wave–mean flow interactions are taking place (Martinez et al. 2011).

In this study, we apply the version of the EP theorem in Molinari et al. (1995, 1998) for studying the heat transport, characteristics of vortex Rossby wave and wave-mean flow interaction. The formula to calculate EP flux and its time-mean divergence is from governing equations in isentropic cylindrical coordinates, and the EP flux divergence is given through the mean tangential wind budget equation:

$$\frac{\partial v_0}{\partial t} + \frac{u_0}{r}\frac{\partial (r v_0)}{\partial r} + u_0 f = \frac{1}{r\sigma_0}\nabla . F - \frac{1}{\sigma_0}\frac{\partial <\sigma' v'>}{\partial t} + D \quad (3)$$

where u, v denotes the radial and tangential wind component respectively, σ presents the isentropic density, f is the Coriolis parameter, D includes the diabatic heating and friction terms, and <.> denotes azimuthal average. F is the EP flux and $\nabla . F$ is EP flux divergence, A_0 is the mean and A' is the perturbation, so that the EP flux and its divergence can be expressed as follow:

$$F = -r\sigma_0 <u' v'> \hat{e}_r + <\frac{p'}{g}\frac{\partial \psi'}{\partial \lambda}> \hat{e}_\theta \quad (4)$$

$$\nabla . F = \frac{1}{r}\frac{\partial(-r^2 \sigma_0 <u' v'>)}{\partial r} + \frac{\partial <\frac{p'}{g}\frac{\partial \psi'}{\partial \lambda}>}{\partial \theta} \quad (5)$$

where λ is the azimuthal angle, Ψ is Montgomery streamfuction.

For interpretation, the radial component of the EP flux represents the eddy angular momentum flux, while the vertical component is the eddy heat flux. Parallel to the wave group velocity, the EP flux vectors illustrate the wave energy propagation.

2.6 Measure of Vortex Interaction

The large-scale environment, mesoscale convective vortices (MCVs) and convective-scale systems are all involved in the TC formation process, but the interaction

process is still not well understood. Research from Simpson et al. (1997) , Ritchie and Holland (1997) and Karyampudi and Pierce (2002) observed many MCVs interacting to form a TC, and many other studies such as McWilliams (1984), Dritschel and Waugh (1992), and Ritchie and Holland (1993) concluded that vortices of any scale would interact when in close enough proximity. Venkatesh (2003) analysed this by carrying out a barotropic simulation of idealised vortex patches (Figs. 2.6, 2.7), and identified a critical distance below which the vortex patches would interact and eventually merge to become a larger vortex. It was found by Venkatesh (2003) that such critical distance depended on the number of vortices. When simulations up to 6 vortices at the beginning were performed, the critical distance scaled by the length scale (L) of the vortex size varied approximately linearly with the number of vortices (n). Thus, linear regression of this relationship resulted in a theoretical critical distance for the vortices to interact:

$$r_{cg}^{*}(n) = 1.85 + 0.275(n - 2) \tag{6}$$

Note that since r_{cg}* has already been scaled by L, the relationship not only applied to mesoscale vortices, as has been performed in the Venkatesh (2003) numerical experiments, but also vortices of convective scales.

Then a merger index μ was defined as

$$\mu = \frac{r_{cg}^{*}}{\left({}^{R_{cg}}/_{L}\right)} \tag{7}$$

where R_{cg} is the average distance of the vortices to their centroid, and L is the average radius of the systems. That is, if the average distance between the vortices is smaller than the critical distance, merging would occur and μ will be larger than a threhold.

In the case study of Typhoon Ketsana (2003) this merger index is applied to both

mesoscale and convective scale systems. Fourier analysis is firstly performed to separate the relative vorticity into convective scale (< 50 km) and mesoscale vortices (50-200 km) and then all vortex patches are identified with relative vorticity higher than a threshold. The number of patches is counted as n and with the location (xc_i, yc_i) and area Ai of each patch recorded. The centroid position is the weighed (by area) average of the individual patch locations:

$$x_{cg} = \frac{\sum_{i=1}^{n} xc_i A_i}{\sum_{i=1}^{n} A_i} \tag{8}$$

$$y_{cg} = \frac{\sum_{i=1}^{n} yc_i A_i}{\sum_{i=1}^{n} A_i} \tag{9}$$

R_{cg} is then the average distance of the vortex patches to their centroid.

$$R_{cg} = \frac{1}{n}\sum_{i=1}^{n}\sqrt{(xc_i - x_{cg})^2 + (yc_i - y_{cg})^2} \tag{10}$$

Following this, L is the average size of the vortices.

$$L = \frac{1}{n}\sum_{i=1}^{n}\sqrt{A_i/\pi} \tag{11}$$

Lastly the merger index μ is calculated according to (7).

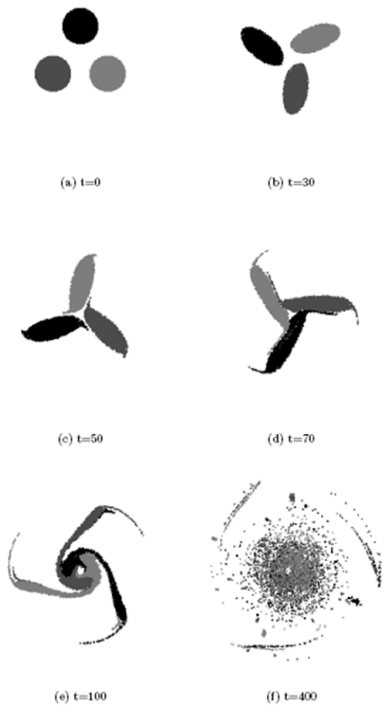

Fig. 2.6 Evolutions of three patches by blob method for distance=3.5 and vortex interaction (adapted from Venkatesh 2003).

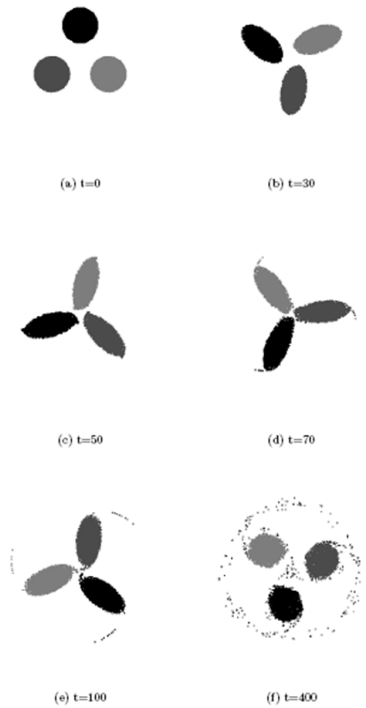

Fig. 2.7 Evolutions of three patches by blob method for distance=3.6 without vortex interaction (adapted from Venkatesh 2003).

2.7 The Normalised Okubo-Weiss (OWZ) Parameter

Over the past decades, operational TC track forecasts have steadily improved, but improvement on short-term intensity and formation predictions have been slow. A major challenge in the prediction of TC genesis is, among other things, searching for more effective TC genesis diagnosis parameters and predictors. Research (Gray 1979; Royer et al. 1998; Emanuel and Nolan 2004; Camargo et al. 2007; Tippett et al. 2011; Menkes et al. 2011) showed some parameters and predictors to pinpoint favourable regions within larger areas of enhanced vorticity. However, these genesis parameters and predictors mostly tried to identify directly the circulations that resembled TCs. Recent studies such as Dunkerton et al. (2009), Montgomery et al. (2010) and Raymond and Lopez Carrillo (2011) focused on the field of recirculating flow in quasi-closed circulations for the development of TCs in tropical waves, because the quasi-circulation contained an enhanced vortical environment that provided the background vorticity from which the TC vortex was constructed, and it also protected the pre-TC from the intrusion of dry air that might disrupt the developing circulation. Wang (2012) showed the thermodynamic transformation that occurred near the centre of the quasi-closed circulation, where there was strong rotation and weak deformation that favoured deep convection driving a large inward mass flux in the low- to mid-troposphere.

Okubo (1970) and Weiss (1991) developed the Okubo-Weiss parameter (OW), which was a measure of the relative amount of vorticity to deformation flow. OW could effectively distinguish the difference between vorticity with high flow curvature and vorticity dominated by shear. In another words, OW had greater potential for

identifying TC formation locations than vorticity only:

$$OW = \zeta^2 - (E^2 + F^2) \tag{12}$$

Here ζ is the vertical component of relative vorticity, E is the stretching deformation and F is the shearing deformation, which was expressed by Wang (2008) in Cartesian and cylindrical coordinates:

$$\zeta = \left[\frac{\partial v}{\partial x} - \frac{\partial u}{\partial y}\right] = \left[\frac{\partial V}{\partial r} + \frac{V}{r} - \frac{1}{r}\frac{\partial U}{\partial \lambda}\right] \tag{13}$$

$$E = \left[\frac{\partial u}{\partial x} - \frac{\partial v}{\partial x}\right] = \left[\frac{\partial U}{\partial r} - \frac{U}{r} - \frac{1}{r}\frac{\partial U}{\partial \lambda}\right] \tag{14}$$

$$F = \left[\frac{\partial y}{\partial x} + \frac{\partial y}{\partial x}\right] = \left[\frac{\partial V}{\partial r} - \frac{V}{r} + \frac{1}{r}\frac{\partial U}{\partial \lambda}\right] \tag{15}$$

where u and v are the zonal and meridional wind components, x and y are the zonal and meridional coordinate directions, U and V are the radial and tangential wind components, and r and λ are the radial and azimuthal coordinates.

Tory et al. (2013) further developed OW to the Normalised OW (OW_{norm}), which yielded a parameter that had a maximum value of one for solid body rotation and could be used to identify zero deformation flow. It is interesting to note that in the axisymmetric, U=0 framework OW is not necessarily maximised for solid body rotation, whereas OW_{norm} is. This difference between OW and OW_{norm} becomes apparent when the shear vorticity is expressed as a deviation from solid body rotation.

$$OW_{norm} = \frac{\zeta^2 - (E^2 + F^2)}{\zeta^2} \tag{16}$$

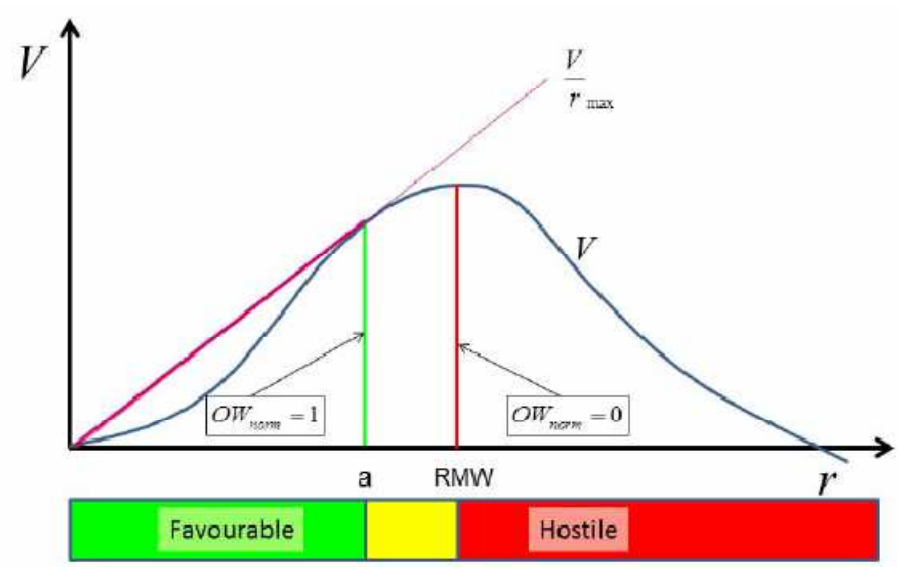

Fig. 2.8 Schematic representation of a hypothetical wind (V) profile (blue curve) with radius(r). The green line at r=a depicts the radius of maximum V/r, which is defined by the slope of the purple curve. At r = a, V/r =$\frac{\partial V}{\partial R}$, the flow is in solid body rotation and OW_{norm} = 1. Inside r = a, the area-averaged vorticity is maximised, which is deemed to be the most favourable region for TC formation. The red line depicts the radius of maximum wind (RMW) where OW_{norm} = 0, beyond which deformation exceeds vorticity and the environment is deemed to be TC formation. a is where the V-curve gradient first becomes less than the line of maximum V/r_{max} (adapted from Tory et al. 2013).

The area-averaged V/r is greatest inside the maximum V/r streamline for solid body rotation, Fig. 2.8 schematically shows that the most favourable region for TC formation (resides inside the largest radius of maximum V/r), the OW and OW_{norm} are rewritten to below by expressing the shear vorticity as a deviation (δ) from solid body rotation ($\frac{\partial V}{\partial r} = \frac{V}{r} + \delta$):

$$OW = 4\frac{V}{r}\frac{\partial V}{\partial r} = 4\frac{V}{r}(\frac{V}{r} + \delta) \tag{17}$$

$$OW_{norm} = \frac{OW}{OW+\delta^2} \tag{18}$$

only OW_{norm} is maximised for solid body rotation (δ=0). Due to its long-recognised importance for TC formation, the absolute vorticity (η) with positive values of OW_{norm} is

chosen as weight to get a quantity that reflected the solid body component of cyclonic absolute vorticity. The quantity is labelled as OWZ, in recognition of the dominant contributions of the OW parameter and the vertical component of relative vorticity (ζ) to the quantity, i.e.

$$OWZ = max(OW_{norm}, 0) \times \eta \times sign(f) \tag{19}$$

Here the parameter is multiplied by the sign of *f* to ensure OWZ is positive and negative for cyclonic and anti-cyclonic flow curvature, respectively in both hemispheres. It is clear from Eq. (17) that OWZ has the same magnitude as η for solid body rotation, and is zero for flows with zero curvature vorticity or flows in which the deformation exceeds the vorticity. By the comparison in Fig. 2.9, the importance of Coriolis component in OWZ is schematically shown, OWZ is a better detector of TC formation than OW.

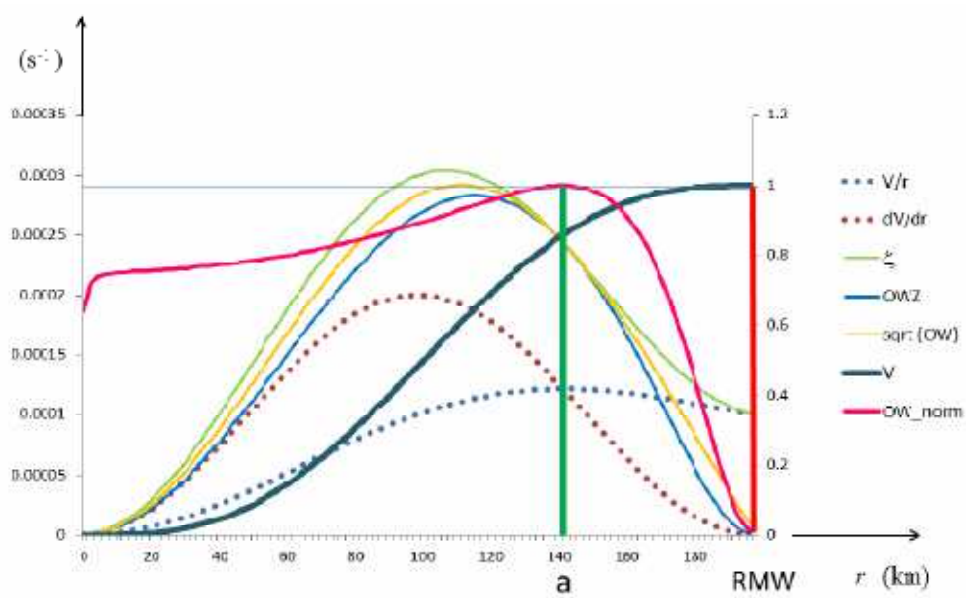

Fig. 2.9 Comparison of performance to predict TC genesis using OW, OWZ with 0 Coliolis, OW_{norm}, η, V, ζ, V/r and dV/dr (adapted from Tory et al. 2013).

Tory et al. (2013) tested this theory with the 20-year ERA-interim reanalysis data produced by the European Centre for Medium-Range Weather Forecasts (ECMWF), about 90% of TCs identified showed that the above dynamic conditions were satisfied for at least 24h prior to the TC declaration. OWZ parameter (OWZP) accurately distinguishes between developing and non-developing TCs. They drew a conclusion that enhanced OWZ pinpointed where the enhanced vorticity was likely to be associated with low deformation recirculating flow, and was thus considerably more specific in identifying favourable environments for TC formation. They further suggested that on the whole, the OWZP did capture the necessary ingredients for genesis, and the requirement that the ingredients be present for a gestation period, perhaps brought us closer to the identification of sufficient conditions.

3 MCSs DEVELOPMENT AND RATE OF TC FORMATION

3.1 Chapter Overview

This chapter studies two TC cases, Typhoon Dan (1999) and Typhoon Ketsana (2003), and discusses their rates of formation and relationship with the mesoscale convective activities through examining the numerical simulations of the two cases. Many TCs originate from a single MCS or multiple MCSs, the physical processes under these two patterns are found to include dissipation of convection leading to new bursts of deep convection located near the edge of the dissipating convection core, ingestion of nearby convection, merging of multiple MCSs into one MCS, and merging of deep convection within the MCS associated with the aggregation of vorticity in early development stage on TCs. How these activities lead to the formation of Typhoon Ketsana has been diagnosed. The diabatic heating associated with these convective activities also help to form the TC warm core. The relationship between the rate of TC formation and early development and convection energy consumption is discussed.

3.2 Introduction

Over the recent decades, Research for the process that generates a surface vortex have focused on the observation that TC formation is associated with MCSs and their accompanying mesoscale convective vortices (MCVs). It was believed that the transition from MCS to a TC-like vortex required the generation of low-level cyclonic vorticity below the MCS, and Research for TC genesis mechanisms focus on what

provided this sub-MCS low-level cyclonic vorticity. It is common to observe MCS or MCSs involved in the formation process of TCs in the WNP. Over 63% of the studied TCs have the multiple MCSs convection appearing at the formation process, and 35% have the single MCS appearing at the beginning of formation process. About 90% of cases with a shorter time period of formation process (within 6 hours) have single MCS (Lee et al. 2008). The physical processes under the single MCS and multiple-MCS convection are found to include dissipation of convection leading to new eruptions of deep convection located near the edge of the dissipating convection core, ingestion of nearby convection, merging of multi-MCS into single MCS, and merging of deep convection within the MCS associated with the aggregation of vorticity in fast formation process.

MCS is organised convective cloud clusters, and TC formation process is due to increasing organization of MCS, which is caused by accumulation of mesoscale vorticity (A. Laing and J. Evans, 2011). Convective activities resulted from thermodynamic and/or dynamic effects that affect the evolution of early development of TCs (Zehr 1992; Gray 1998). They play critical roles in the formation process on TCs, furthermore, the local warming and diabatic heating associated with these convective activities also help to spin up the circulation and generate the warm core structure. How the pattern of MCS convection affects the rate of TC formation and early development is the focus in this Chapter. In the following, two TC cases are studied and their synopses are first provided before their rates of development are discussed. The model simulations of the two cases are validated in terms of synoptic development and convective episodes. The

convection types in the model are separated into convective and stratiform-type with their respective vertical heating profiles. Then the heating associated with the MCSs and its effect on TC development are analysed based on previous theories (Vigh and Schubert 2009) and through EP flux analysis. After that, the rates of development in the two TC cases are discussed based on the convective energy consumption point of view. In regard to this view, convection development and maintenance consumes CAPE in their local environment. Firstly, it gradually makes the local environment less conducive for further convection development, which may affect the temporal evolution of TC formation when the surface vorticity is still below the threshold for tropical storm. However, it humidifies the middle and upper troposphere, and then gradually re-builds up the value of CAPE again in the local environment until new deep convection bursts up.

3.3 Typhoon Cases and Numerical Simulations

The numerical experiments in this study include two case studies, TY Ketsana (2003) with development of multiple MCSs and Typhoon Dan (1999) with only one MCS involved during its formation. These experiments, which use the WRF model detailed in section 2.3, are then examined to study the difference of the formation time and energy consumption in the two cases. In the simulations for both typhoon cases the same set of nested domain settings is applied, and the same satellite datasets have been assimilated via the WRFDA system.

In the WRF simulation of Typhoon Ketsana, the model's initial and lateral conditions are taken from the NCEP FNL analysis data with the outermost lateral boundary

conditions updated every 6 hours, and the SST data are interpolated to update the sea surface boundary conditions. The WRF model is initialised at 0000 UTC 16 October 2003 and integrated for 108 hours until 1200 UTC 20 October. Within this model integration period, the WRFDA is used to assimilate QuikSCAT oceanic winds available at 0600 UTC 16 Oct and 0600 UTC 17 Oct 2003, and SSM/I oceanic surface wind speed and TPW available at 1200 UTC 17 Oct 2003 into the boundary conditions. These twice daily swaths of QuikSCAT and SSM/I data are extracted from the Remote Sensing System (RSS) data archive with 0.25^{o} latitude/longitude resolution.

The WRF simulation of Typhoon Dan (1999) is initialised at 0000 UTC 01 October 1999 and integrated for 120 hours until 0000 UTC 06 October. Similar to the case of Typhoon Ketsana, the WRFDA is used to assimilate QuikSCAT oceanic winds available at 0600 UTC 01 October and 0600 UTC 02 October, and SSM/I oceanic surface wind speed and TPW available at 1200 UTC 01 October and 1200 UTC 02 October into the boundary conditions.

3.4 Synopses of Typhoon Cases

3.4.1 Synopsis of Typhoon Ketsana (2003)

In the middle of October 2003, Typhoon Ketsana initially developed from a disturbance embedded in a reversed-oriented monsoon trough between Luzon and Guam (about 1296 km east of Luzon Island) on 15 Oct 2003 (Fig. 3.1a). The monsoon trough provided a favourable large-scale environment with high humidity (Fig. 3.1b) and abundant low-level cyclonic vorticity for TC formation. For several days, the system

remained disorganised while drifting to the west-northwest due to weak steering currents south of the subtropical ridge. The disturbance developed to a tropical depression at 1200 UTC 18 Oct (taken as formation time) and on October 19, the Japan Meteorological Agency (JMA) upgraded the depression to Tropical Storm, and by that time the storm had begun drifting to the northeast. Throughout the days of 20–21 October movement was slow with only weak north-easterly steering currents controlling Typhoon Ketsana, although the intensification was not so slow. With favourable outflow, Ketsana quickly intensified and was upgraded into a typhoon at 1200 UTC October 20. After an eye formed, the slow motion continued throughout the day as did intensification. By 1200 UTC October 21 the intensity had reached the lifetime peak intensity of 125 kts. Ketsana started weakening at 1800 UTC October 22 with the intensity falling to 115 kts.

At 0000 UTC October 23, Typhoon Ketsana moved slowly north-eastward but a weakening trend had set in and began to accelerate the next day, with evidence of a mass of stratocumulus cloud to the northwest of Ketsana, showing the presence of colder, drier and more stable air. At 0000 UTC October 24, Ketsana was beginning extratropical transition. Drier air had penetrated into the circulation and went north-eastward into the westerlies with doubled forward speed.

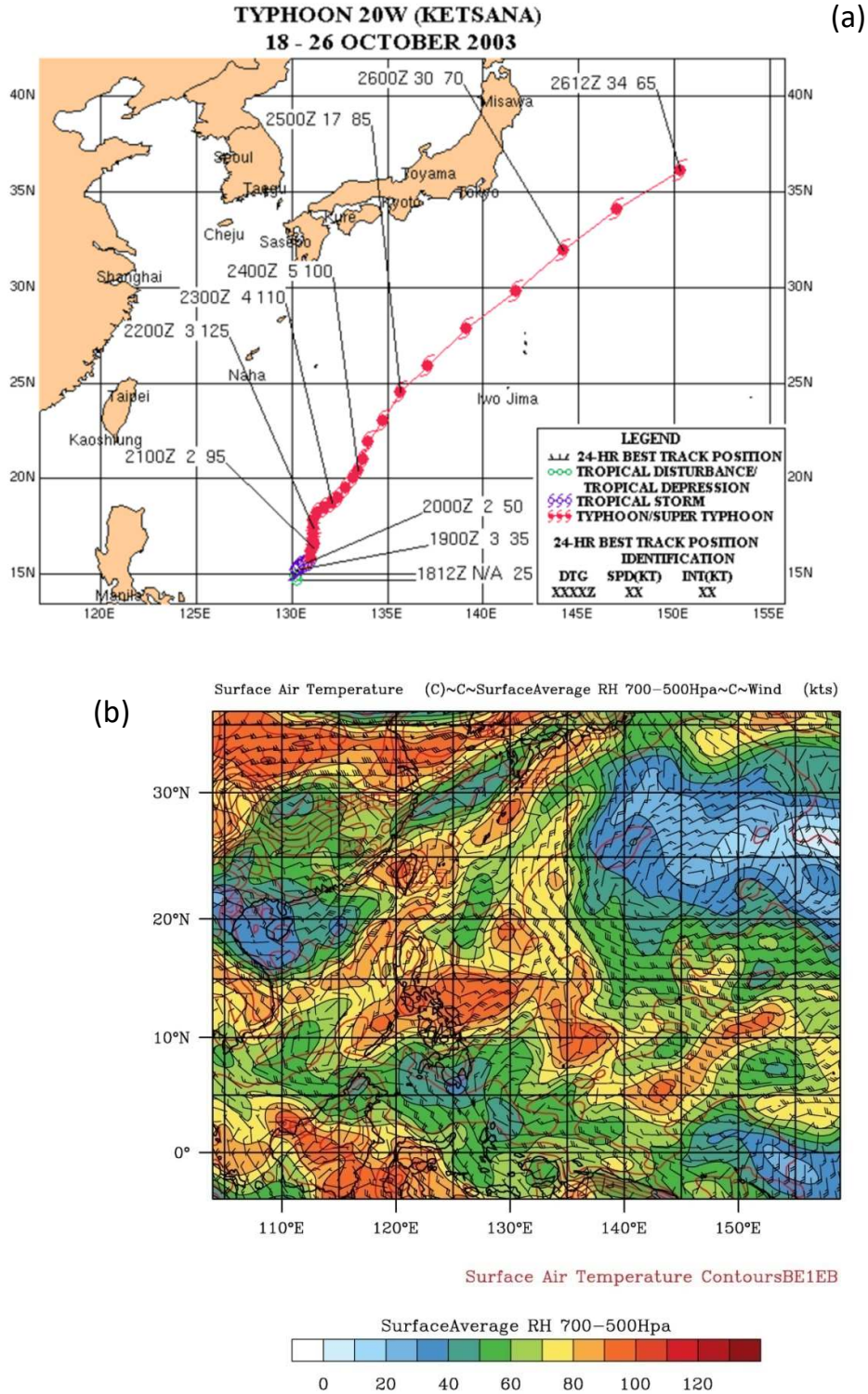

Fig. 3.1 (a) Best track of Typhoon Ketsana (2003) from the JTWC (adapted from ATCR 2003). (b) 500-700-hPa RH (Shade contour), 200-850-hPa VWS (vector) and surface temperature (contour) at 1200 UTC 02 Oct 1999.

3.4.2 Synopsis of Typhoon Dan (1999)

Typhoon Dan (1999) firstly developed over the Philippine Sea on 1200 UTC 01 October 1999 to the east of Island Luzon. The JTWC issued a TC formation alert at 0230 UTC 02 October. When deep convection was seen to build over the low-level circulation centre from the south near 1500 UTC 02 October, the first warning of the TC was issued by the JTWC. The system further developed into a tropical depression about 1140 km east-northeast of Manila on 03 October (taken as formation time at 1200 UTC 03 October 1999) and then moved westward (Fig. 3.2a). Dan intensified very fast to a tropical storm and then a typhoon the next day. It reached a peak intensity of 110 kts (56.9 m s^{-1}) when affecting the Northern Luzon coast on 05 October. TY Dan then moved over the South China Sea and weakened when it entered an increased vertical wind shear environment. It slowed down the next day and abruptly turned northwards on 07 October with slight re-intensification. It eventually made landfall near Xiamen, Fujian, China on 09 October and then weakened overland. Dan turned to the northeast and weakened to a tropical depression before it moved over the Yellow Sea later on 10 October.

Both Typhoon Ketsana (2003) and Dan (1999) developed in the monsoon trough environment with similarly high moisture availability (Figs. 3.1b and 3.2b). The low-to-mid-level RH associated with the development of these two TCs was above 80%. In terms of wind shear, both TCs developed in zones with moderate vertical wind shear(VWS) (130°E, 15°N for Ketsana and 130°E, 18°N for Dan), which was south of the high-VWS zone at the edge of the subtropical ridge. Thus, in the following focus

will be put to comparing the mesoscale convective patterns of these two cases.

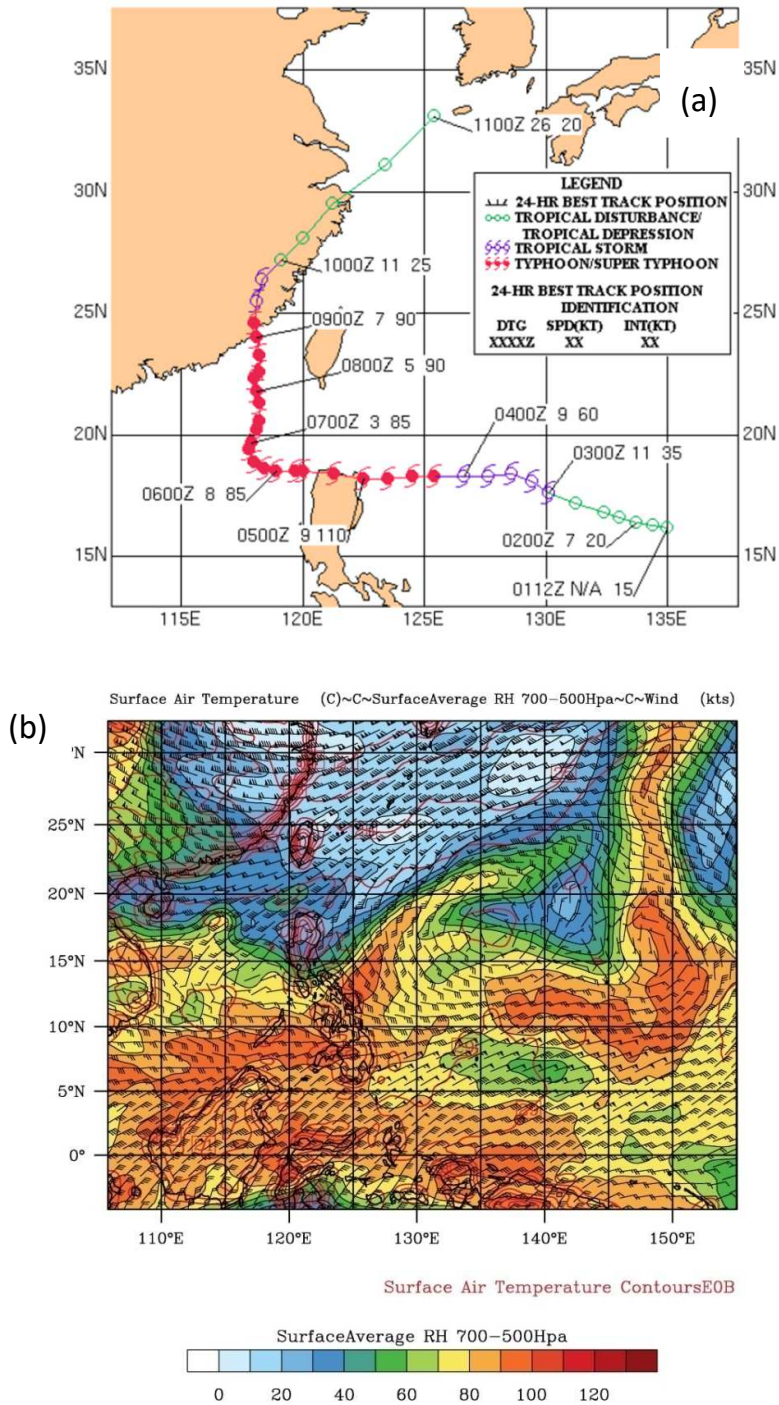

Fig. 3.2 (a) Best track of Typhoon Dan (1999) from the JTWC (adapted from ATCR 1999). (b) 500-700-hPa RH (Shade contour), 200-850-hPa VWS (vector) and surface temperature (contour) at 1800 UTC 17 Oct 2003.

3.5 MCSs Analysis

One of the characteristics of TC formation in the monsoon trough is frequent development of MCSs due to low-level convergence that enhances convection. The definition of MCS in Riosalido et al. (1998) (i.e., area > 1000 km^2 within the brightness isotherm -52°C) is applied. During the 48 h (1200 UTC 16-18 October) prior to Typhoon Ketsana's formation, five MCSs are observed. The first two developed on 16 and early 17 October respectively. Later, MCS3 and MCS4 developed almost simultaneous near 1500 UTC 17 October but then dissipated (Fig. 3.3). The fifth MCS5 developed at 0600 UTC 18 Oct near the low-level circulation centre, and led to formation of the Typhoon 6 hours later.

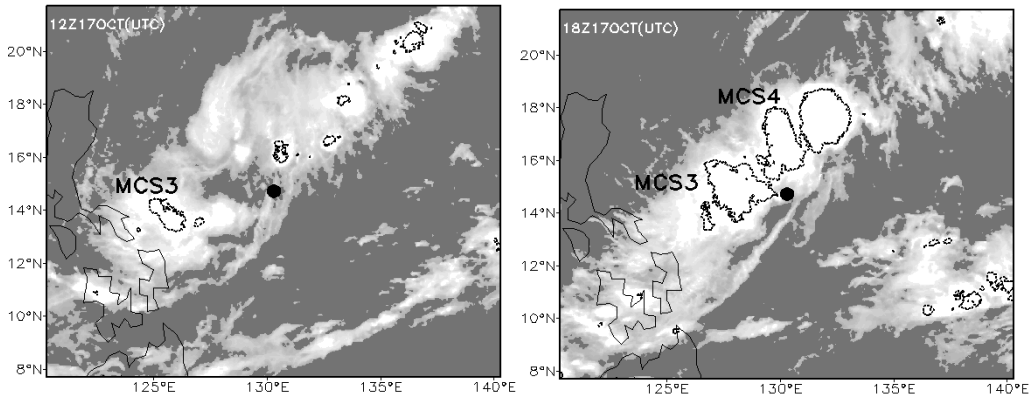

Fig. 3.3 Six-hourly IR1 satellite images from 1200 UTC 17 Oct 2003 to 1800 UTC 18 Oct 2003. The contour is TB of -75°C and the black dot is the best-track location of Ketsana's formation (adapted from Lu et al. 2012).

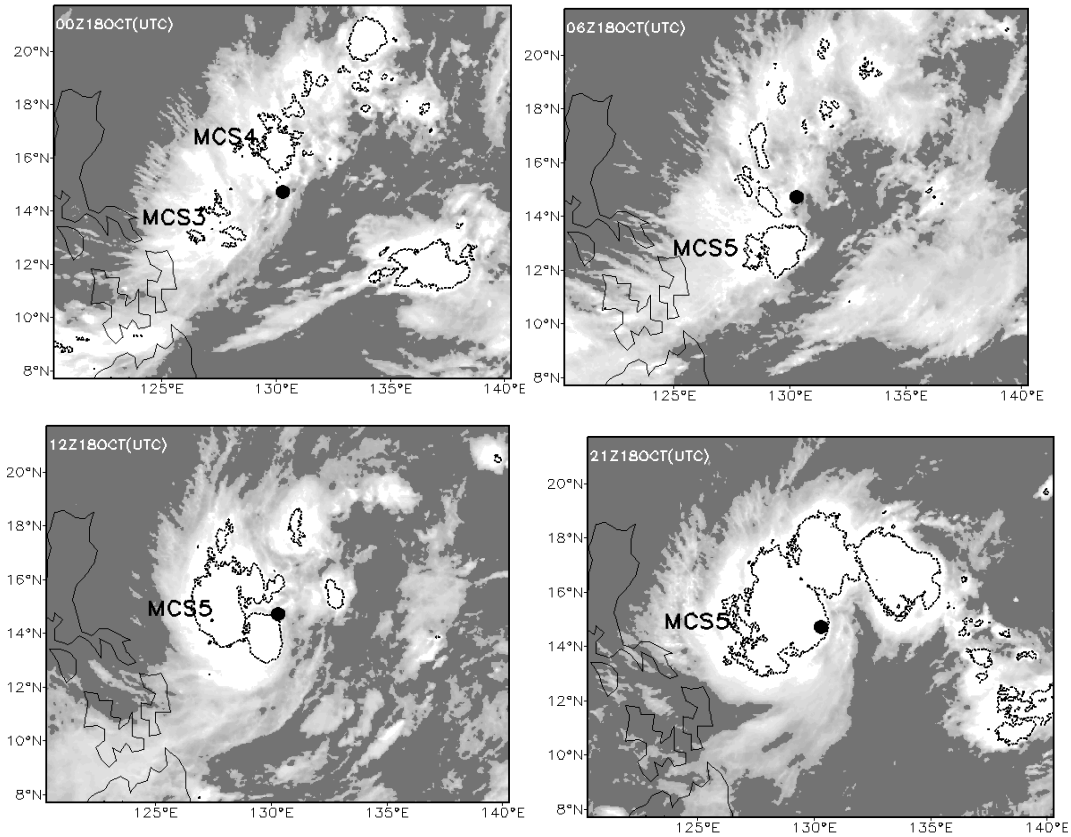

Fig. 3.3 (cont.)

Fig. 3.4 shows the development process of the formation of Typhoon Dan. Since 1 October 1999, there were many weak tropical convective clusters formed and maintained. On 1200 UTC 2 October one of the cloud clusters started to develop and kept expanding to form a MCS at 0000 UTC 03 October and then further developed to a tropical depression at 1200 UTC the same day. In contrast to Typhoon ketsana, there was only one MCS that occurred during the formation process of Dan. While Lee et al. (2008) identified that many of the TC cases with single MCS during formation were associated with easterly wave, filtered low-level winds (based on a simple running mean technique with similar low-pass effect of 3-8 days as in Fu et al. 2007) do not reveal wave activity

during the formation of Typhoon Dan. Thus, Typhoon Dan is also classified as a typical monsoon trough formation. The focus here is the single-MCS configuration associated with Typhoon Dan's formation in contrast to that of Typhoon Ketsana, with both cases embedded in similar environmental setting.

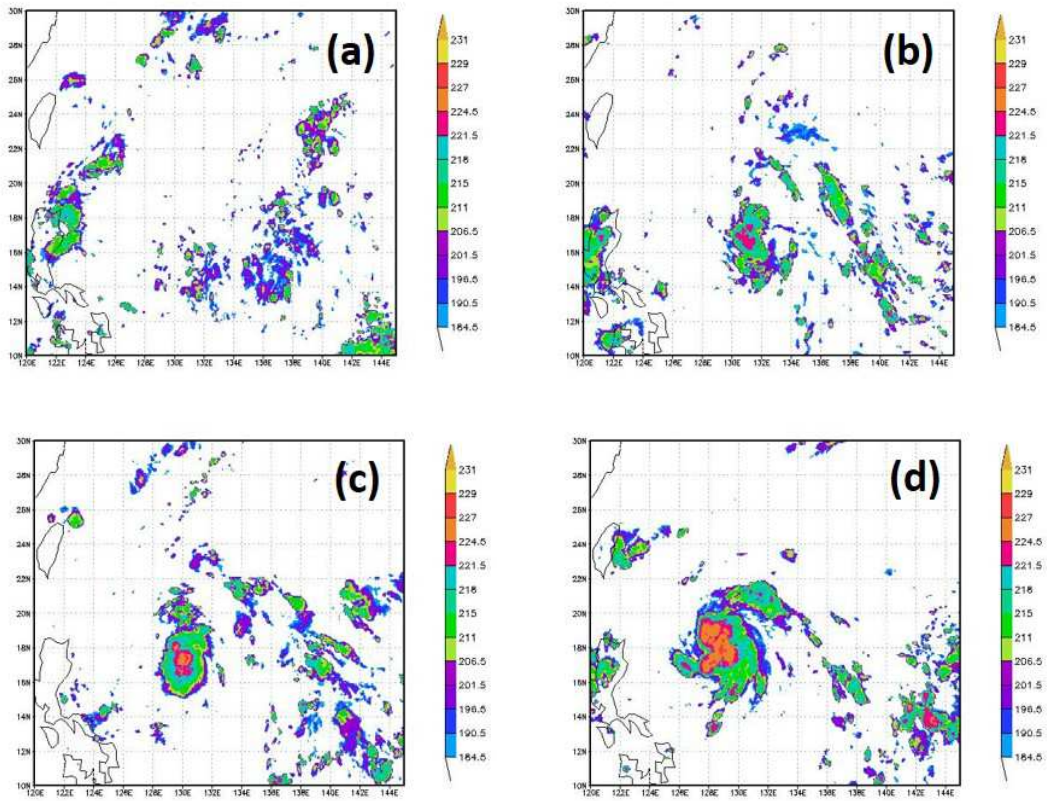

Fig. 3.4 MCSs involved in the formation process of Typhoon Dan at (a) 0500 UTC 01 October, (b) 1200 UTC 02 October, (c) 0000 UTC 03 October and (d) 1200 UTC 03 October 1999. Raw pixel values have been shown. (Source: JMA GMS5 infrared channel-1 data).

3.6 Model Validation for Typhoon Dan

3.6.1 Synoptic Flow

When comparing the NCEP FNL (final) operational analysis data with the WRF simulation of Typhoon Dan in the large domain, it can be seen that the large-scale circulation has been simulated well. In the FNL analysis there are two cyclonic regions at about 130°E and 140°E (Figs. 3.5). The WRF model mainly developed the incipient vortex circulation at 130°E that eventually became Typhoon Dan. Such consistency with the analysis at the low and mid (not shown) levels provides the conditions for the right timing of TC formation in the model. At the upper level, the simulated subtropical high is located north of where Typhoon Dan is developing, with the maximum high pressure centre east of the Taiwan island. This is well verified by the FNL analysis (Fig. 3.6) and the system provides good outflow for the formation of Typhoon Dan during its development. The simulated formation position (based on identified near-surface circulation centre) and early westward motion of Typhoon Dan match with the best track very well (Fig. 3.7), with the formation only a small distance east of the actual position.

The model validation for Typhoon Ketsana has been presented in detail in Lu et al. (2012), and thus not repeated here. The WRF model applied here is the same version that used in Lu et al. (2012). The simulation of Typhoon Ketsana in this study well reproduced the reversed-oriented monsoon trough in October 2003 as well as the convection episodes of all MCSs associated with Typhoon Ketsana's formation. The simulated formation position of Ketsana is southwest of the best-track position (Fig. 3.7), however, the weak steering flow during the early development has been well simulated.

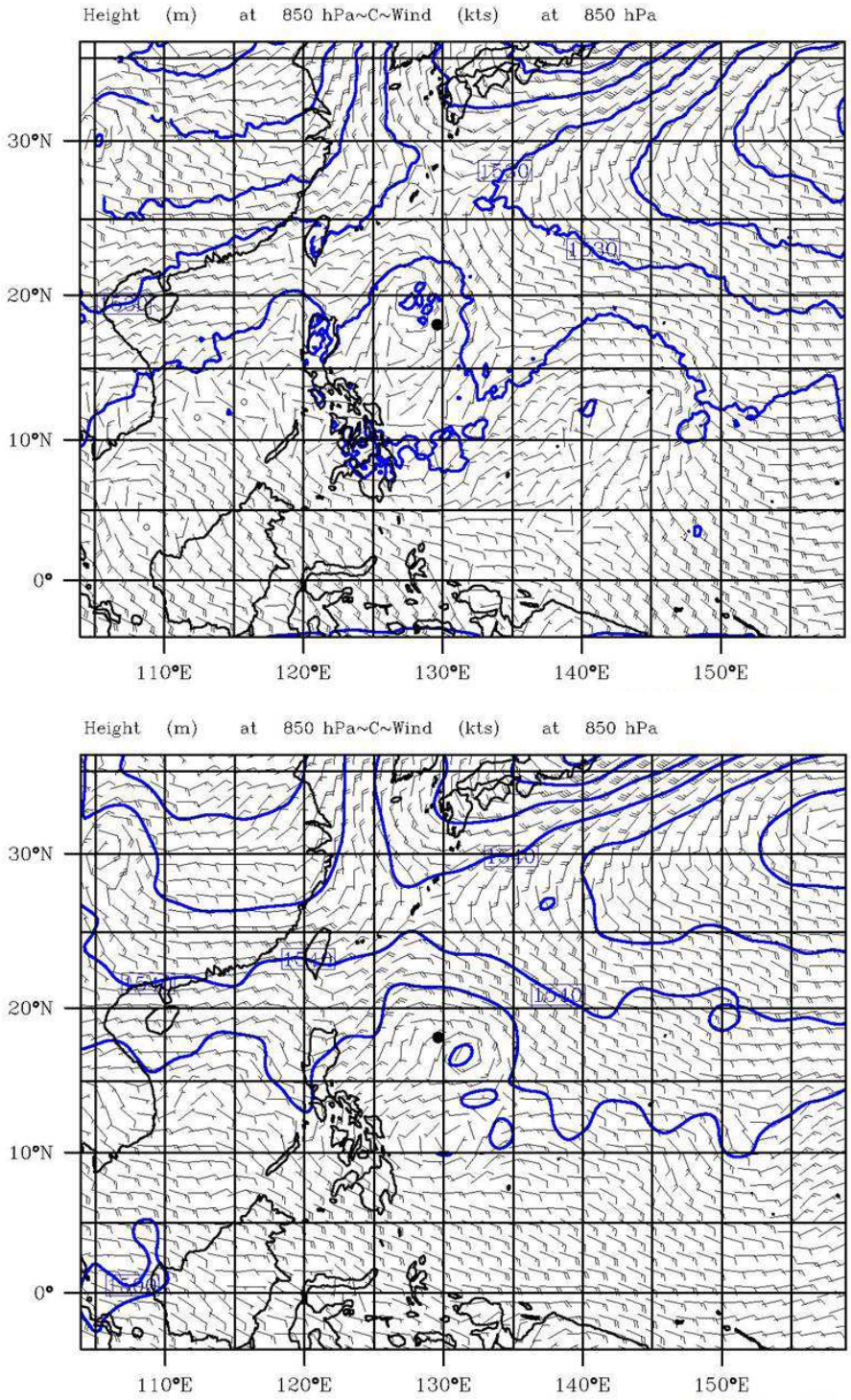

Fig. 3.5 Simulated (upper) and FNL analysis (lower) 850-hPa geopotential height and wind barbs at 2000 UTC 3 October 1999.

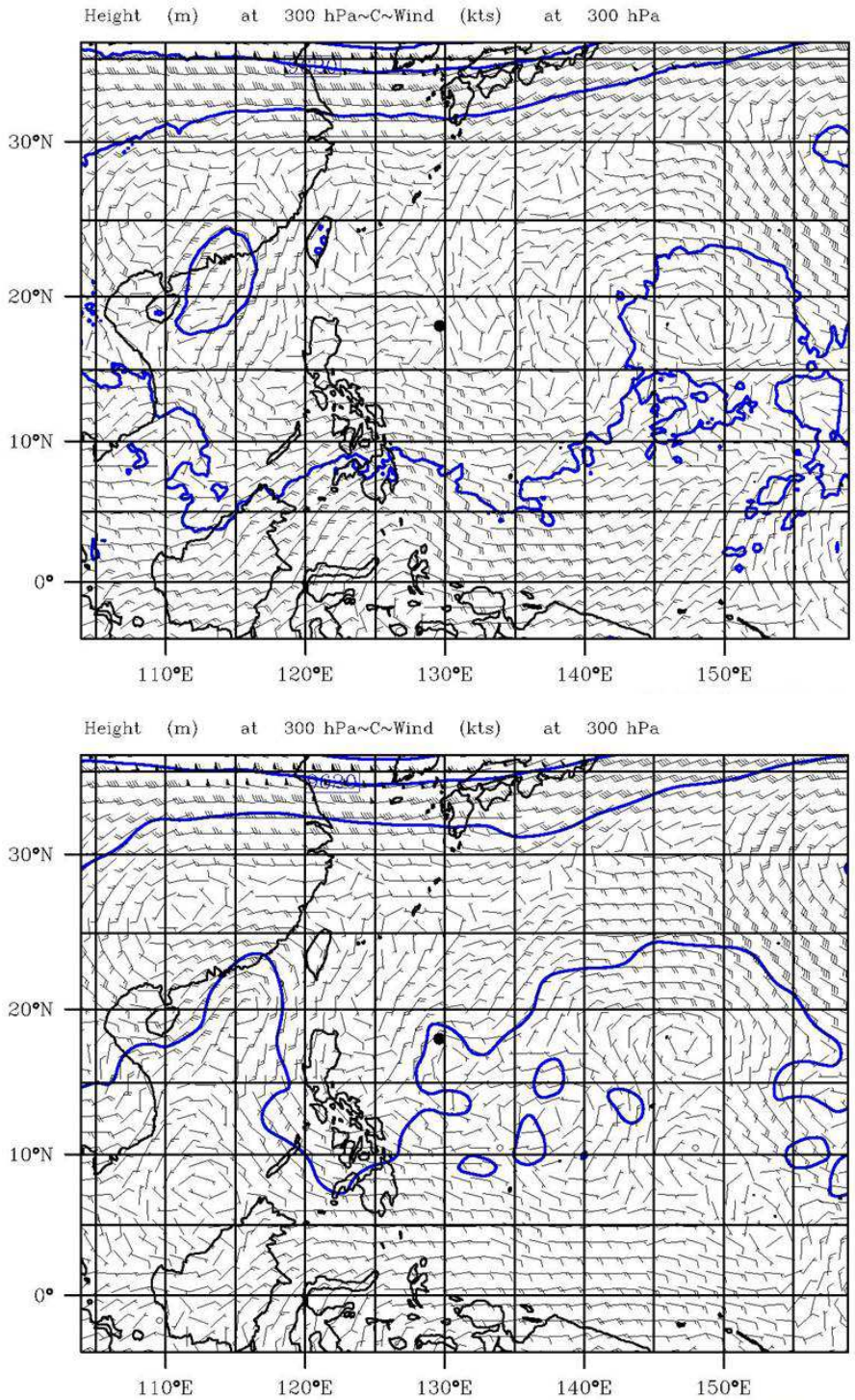

Fig. 3.6 As in Fig. 3.5 except at 300 hPa.

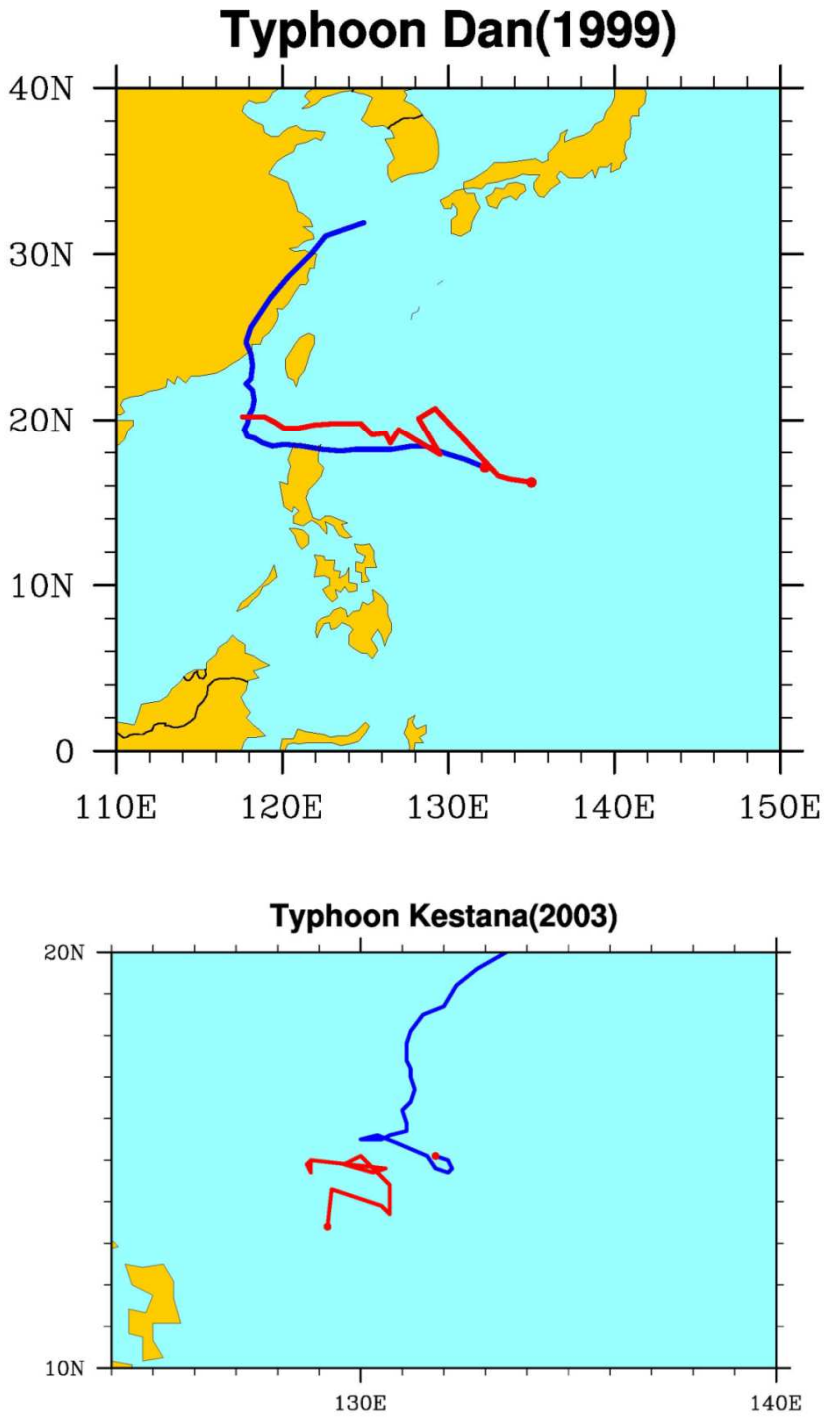

Fig 3.7 Simulated (red) and JMA best track (blue) of Typhoon Dan (upper) and Ketsana (lower) during 0000 UTC 3-6 October 1999 and 1200 UTC 17-20 October 2003 (best track has been extended after 20 October 2003 for Ketsana).

3.6.2 Evolution of MCS and Intensity

In Lu et al. (2012), the area average observed TB from satellite images shows a minimum at around 2100 UTC 17 October 2003 that is associated with MCS3 and MCS4, and then there is another major decrease before formation associated with MCS5 (Fig. 5b of Lu et al. 2012). Simulated radar reflectivity is used to examine convection activity in the model. The time series of simulated radar reflectivity has a local maximum at the same time of occurrence of MCS3 and MCS4. It then increases rapidly 6 h before Ketsana's formation, which is due to convective bursts within MCS5 and is consistent with the observed variation of the area-average TB. The simulated positions of these 3 MCSs also match with those in satellite images: MCS3 was east of the low-level circulation centre and later MCS5 developed at similar position (Fig. 3.8). In terms of intensity, it can be seen that the simulated storm intensifies at the similar rate as observation before formation, however, it becomes too intense in the rest of simulation (Fig. 3.9).

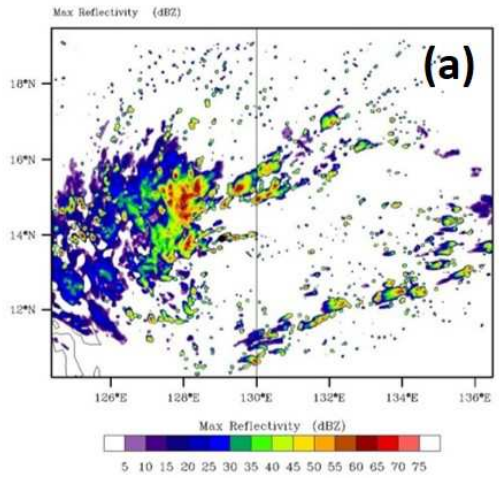

Fig. 3.8 Simulated radar reflectivity (dbZ) of Typhoon Ketsana at (a) 1500 UTC 17 October and (b) 0600 UTC 18 October 2003.

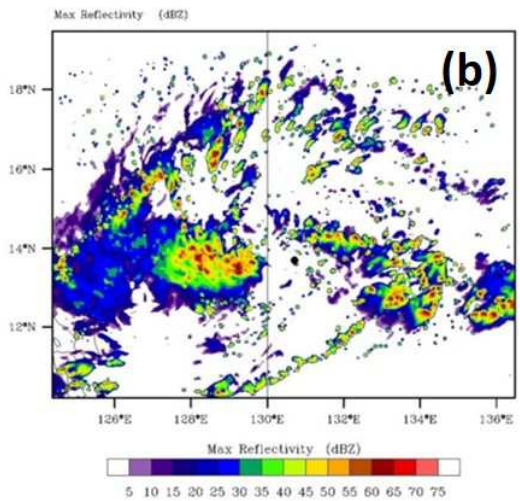

Fig. 3.8 (cont.)

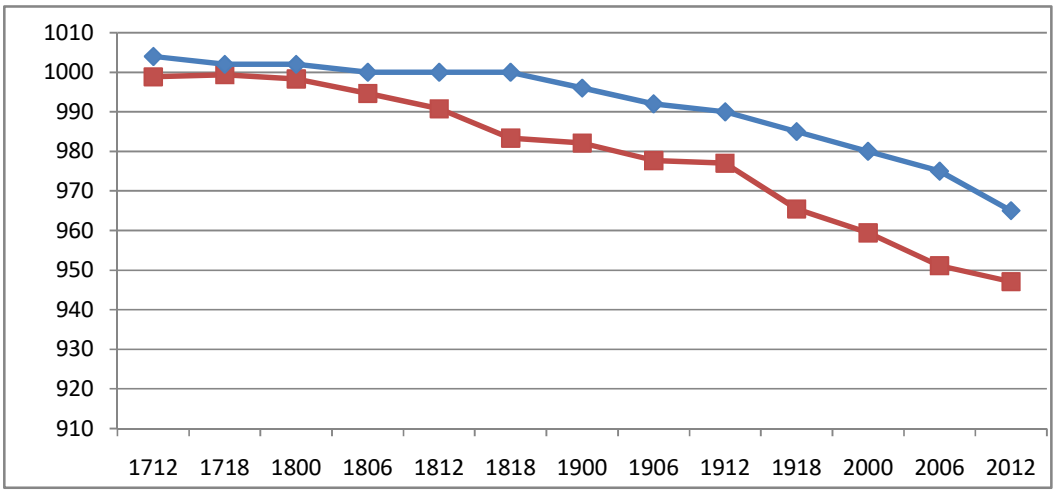

Fig. 3.9 Simulated (red) and JMA best-track minimum surface pressure (hPa) of Typhoon Ketsana during 0000 UTC 17-20 October 2003.

The simulated MCS activity of Typhoon Dan is also examined via the simulated radar reflectivity. In early 02 October 1999, the model simulated patches of convection on the eastern side of the broad cyclonic circulation within the monsoon trough (Fig.

3.10). A few hours later, the convection organised into a MCS northeast of the circulation centre. Such convection persisted when the incipient vortex moved north-westward and intensified. At the beginning of formation, there were still some weak convective cloud clusters that developed slowly until the only MCS formed. In the early formation stage, the model has not captured the initial rate of intensification very well. In the simulation, the surface pressure only started to drop from about 0000 UTC 03 October (Fig. 3.11). Nevertheless, the convection pattern that developed from the single MCS has been reproduced well in the model. From 03 October, the simulated intensification rate was similar to that in the best track, and by the end of simulation the TC was more intense than that Typhoon Dan actually attained.

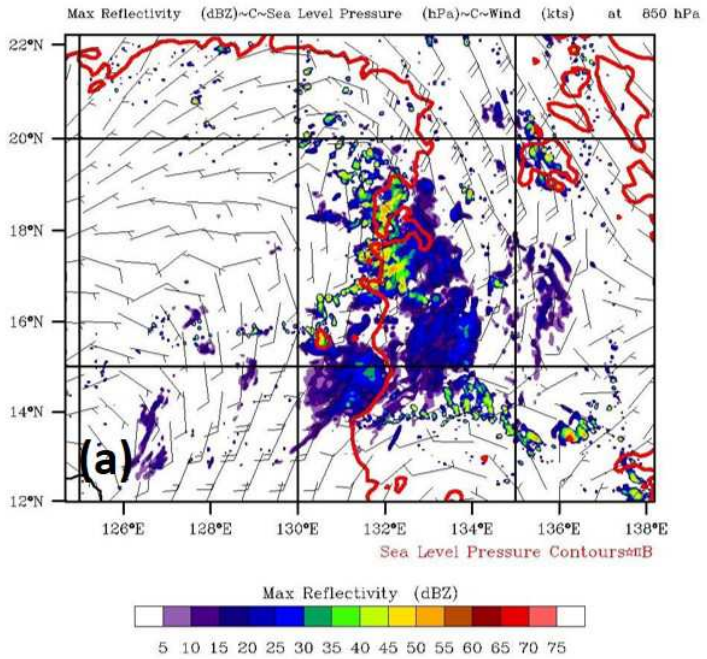

Fig. 3.10 Simulated mean sea-level pressure, 850-hPa wind barbs and maximum radar reflectivity at (a) 0300 UTC 02 October and (b) 0700 UTC 02 October 1999 (lower).

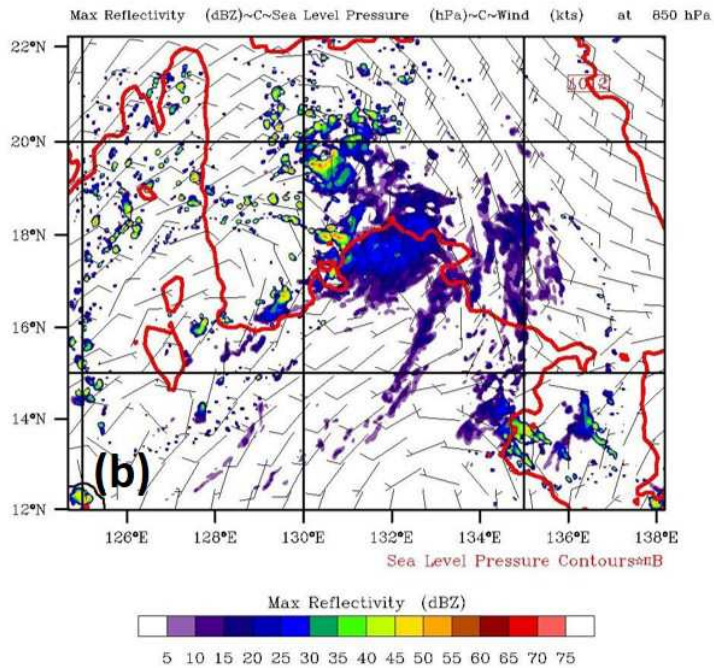

Fig. 3.10 (cont.)

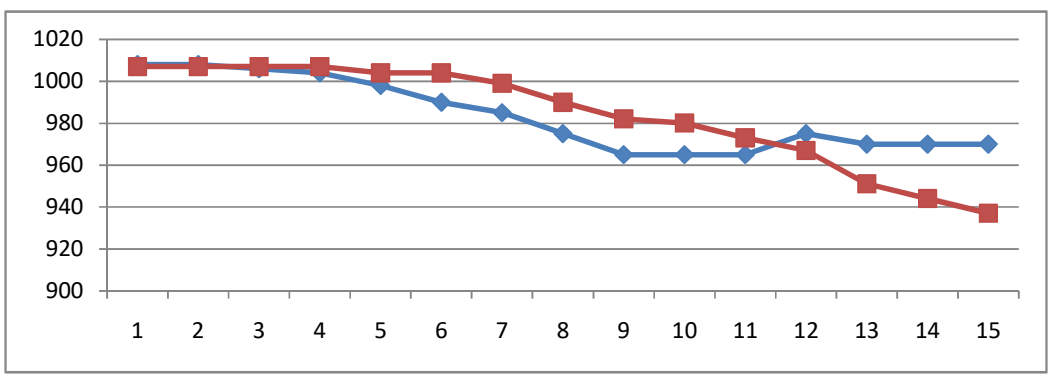

Fig. 3.11 Six-hourly time series of simulated (red) MSLP and that in JMA best track (blue) from 1200 UTC 02 October 1999.

3.7 Mesoscale Heating and TC Development in Typhoon Ketsana

3.7.1 Axisymmetric structure

It can be seen from the synopsis and model validation of Typhoon Ketsana that the

MCS developments during its formation were highly spatially asymmetric with respect to the low-level circulation centre. These MCSs would impose vorticity enhancement and heating effect to the system-scale vortex. Before such responses are analysed, the axisymmetric structure in the simulation is first examined through the azimuthal mean of tangential and radial wind. The system centre is taken as the surface circulation centre.

During 17 October, the axisymmetric structure of the simulated Typhoon Ketsana shows a broad low-level cyclonic circulation (Fig. 3.12a). The maximum tangential wind is below 850 hPa and located between 150 km to 200 km from the centre. This broad circulation is consistent with the early MCS activities during that day when the first four MCSs developed more than 100 km away from the centre. There was only a small region of inflow below 950 hPa, and thus the secondary circulation has not been setup in this stage.

On the 18th October when MCS5 developed near the system centre, strong low-level tangential winds started to move inward within 50 km and at the same time extended to the midlevels (Fig. 3.12b, c). The radial winds also reveal the secondary circulation of inflow below about 800 hPa and outflow above 150 hPa.

Less than a day after the formation time, a mature axisymmetric structure is observed in the simulation. The most intense tangential winds concentrated at about 850 hPa and have been extended from 100 km to 200 km from the centre (Fig. 3.12d). The eyewall structure is clear and the eye has been enlarged.

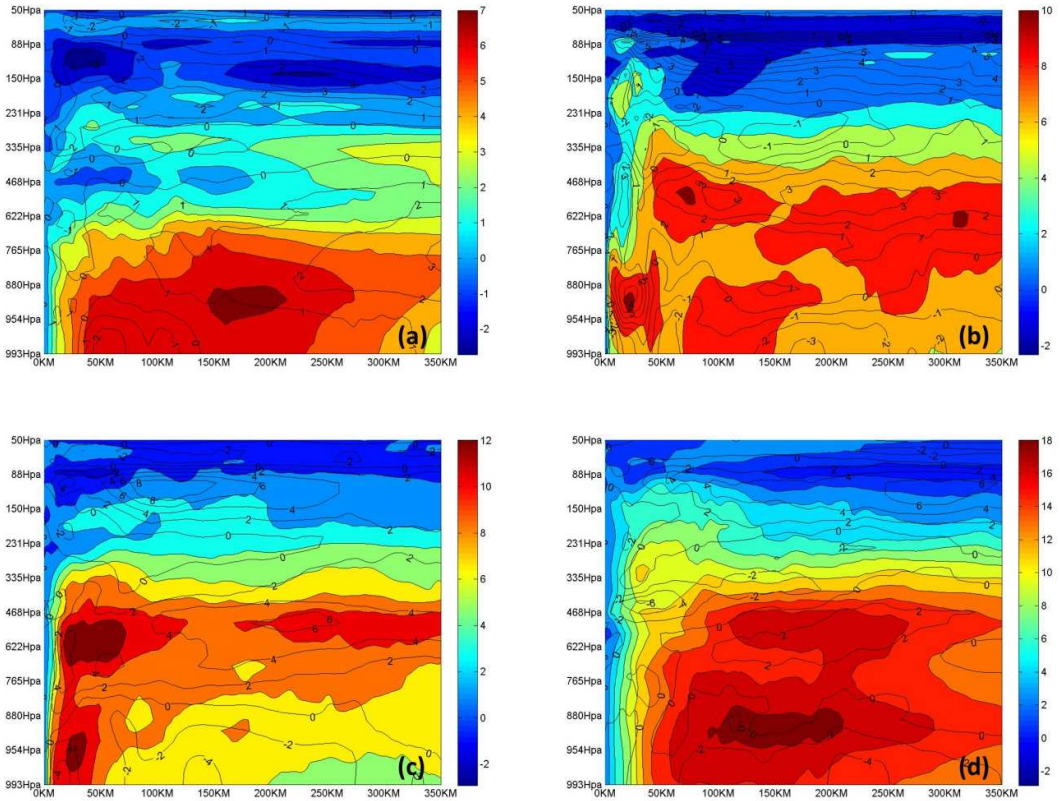

Fig. 3.12 Azimuthal average of tangential (shaded) and radial (contour) wind (m s^{-1}) at (a) 1500 UTC 17 October, (b) 0800 UTC 18 October, (c) 1000 UTC 18 October and (d) 0600 UTC 19 October 2003.

3.7.2 Diabatic heating associated with MCSs

It is well known that convective-type and stratiform-type rain, besides their respectively unique microphysical nature, are associated with different diabatic heating profiles (Johnson 1984; Houze 1989). The latter is important to the process of vorticity enhancement and warm core during TC development. Convection is associated with deep tropospheric heating, while stratiform rain is associated with upper-level heating but possibly low-level cooling due to evaporation.

The method in Steiner and Houze (1993) and Steiner et al. (1995) is used to separate

the two types of rain in Typhoon Ketsana based on the simulated radar reflectivity. The identification of the convective rainfall has further confirmed the MCS activities during the typhoon's development. During 17 October 2003, among the larger stratiform rain patches the convective rain concentrated first to the west of the low-level circulation centre (which was near 130°E, 14°N) and a few hours later to the north and northeast (Figs. 3.13a, b). This is consistent with the temporal evolution of the deep convection from MCS3 to MCS4.

In early 18 October 2003, deep convection occurred again but much closer to the low-level circulation centre, which is associated with MCS5. The deep convection persisted until the formation of the cyclone (Figs. 3.13c, d). On the other hand, the stratiform rain areas are much larger than the convective areas at all times, which is similar to the partition of other TC cases based on observed rainfall (Wang et al. 2010).

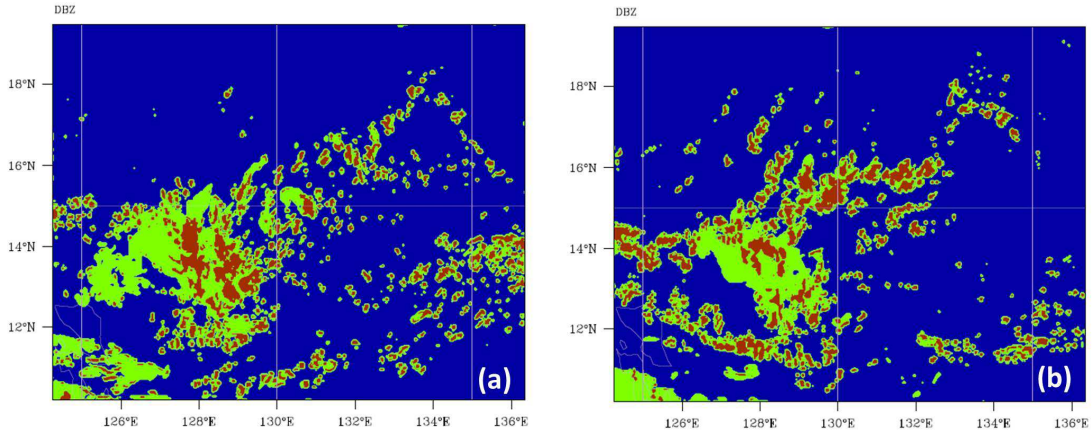

Fig. 3.13 Convective (red) and stratifiform (green) rainfall in simulated Typhoon Ketsana at (a) 1200 UTC 17 October, (b) 1500 UTC 17 October, (c) 0800 UTC 18 October and (d) 1200 UTC 18 October 2003.

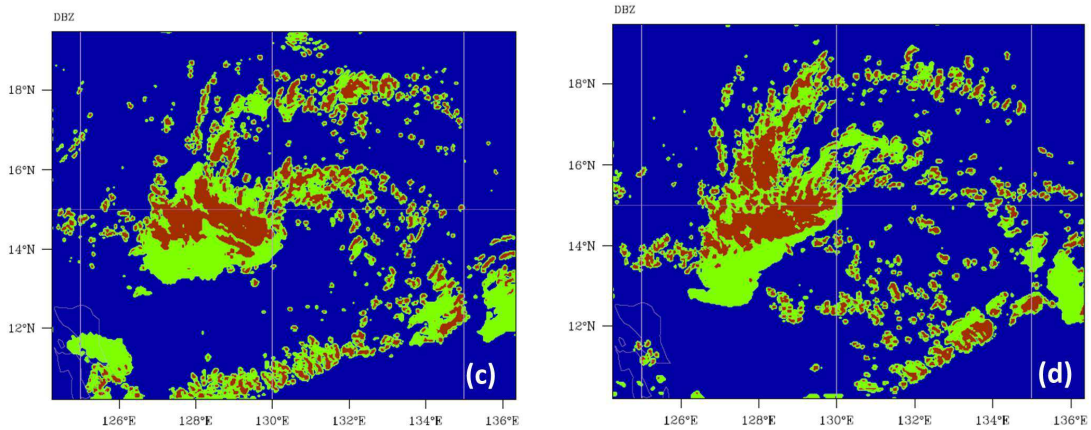

Fig. 3.13 (cont.)

When the simulated diabatic heating in WRF is examined, the maximum heating is identified to locate around midlevel with extension from about 850 hPa up to 200 hPa. The spatial distribution of maximum heating is confined to specific locations and thus attributed to the deep convection episodes. For example, the azimuthal average of diabatic heating during 17 October shows tropospheric heating positions mostly outside radius of 50 km, which are likely due to the early MCS activities (Figs. 3.14a, b). The maximum heating of these early episodes is of the order 10^{-3} K s^{-1}.

In early 18 October, it can be seen that maximum heating occurs within 50 km that is associated with the last convection episode before the formation of Ketsana (Fig. 3.14c). The heating location further moves inward to the circulation centre and increases in magnitude about an order higher than the previous episodes (Fig. 3.14d).

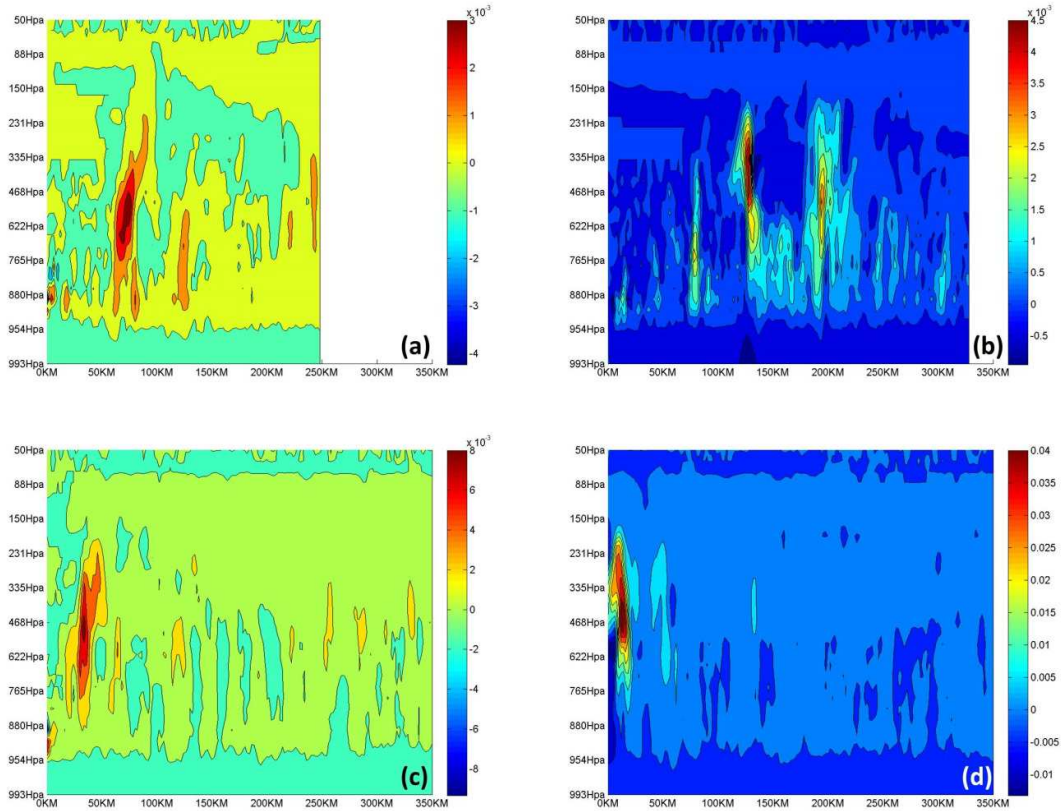

Fig. 3.14 Azimuthally average diabatic heating(Ks^{-1}) in simulated Typhoon Ketsana at (a) 1600 UTC 17 October, (b) 2300 UTC 17 October, (c) 0500 UTC 18 October and (d) 0800 UTC 18 October 2003. Note the changes in scales.

3.7.3 Responses to diabatic heating

Vigh and Schubert (2009) analysed the responses of a weak TC vortex to diabatic heating based on analytical solution of the balanced vortex model, which leads to rapid development toward the steady state with a mature warm-core thermal structure. It was found that the responses depend on the radial location of the diabatic heating. In particular, three factors of static stability, baroclinity and inertial stability are involved in critical in formulating the responses, especially the inertial stability that usually varies substantial with radius in a TC vortex. Diabatic heating would be most effective when it

is located within the high inertial stability region, which is inside the radius of maximum wind. When the heating position is outside the radius of maximum wind, rapid development is not likely. Thus based on these theoretical results, the convection episodes associated with the MCSs in the case of Typhoon Ketsana are increasing in heating efficiency for forming the TC. The diabatic heating in the earlier MCSs are outside the inner core with high inertial stability, which is mostly inside radius of 50 km (Fig. 3.15a). This is consistent in the simulated TC that shows only slowly intensifying low-level winds in the outer region. During early 18 October when the TC incipient vortex is becoming more intense, the high inertial stability region expands slightly (Fig. 3.15b). When the last convection episode associated with MCS5 occurs, the heating sits mostly in that region and thus is able to spin up the inner-core winds rapidly (Fig. 3.12c) and lead to TC formation.

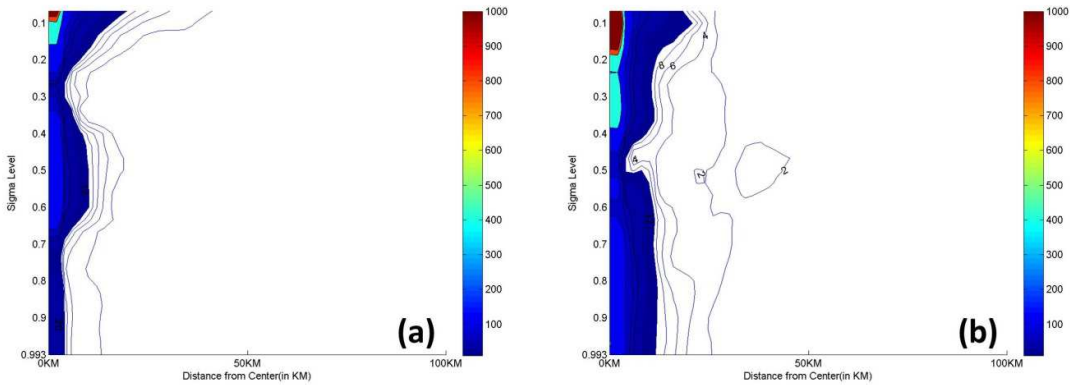

Fig. 3.15 Inertial stability in the simulated Typhoon Ketsana at (a) 0600 UTC 17 October and (b) 0800 UTC 18 October 2003, which correspond to Figs. 3.14a, d.

Another way to examine the effects of diabatic heating, especially that with

azimuthally asymmetric distribution and thus possessing eddy heat flux, is through the Eliassen-Palm (EP) fluxes (Molinari et al. 1995, 1998; Chen et al. 2003; Chen and Yau 2003; Martinez et al. 2011). The EP fluxes on isentropic coordinates are calculated and analysed for the simulated Typhoon Ketsana. The EP flux vector consists of the horizontal and vertical component, which corresponds to angular momentum flux and heat flux respectively. The divergence of the flux vector indicates the flux gradients.

During 17 October, it can be seen that the EP fluxes with large divergences are mostly scattered at the large radii outside 200 km and concentrated at the lower levels (Fig. 3.16a), which are associated with the heating of the earlier MCS convection episodes. The magnitudes of the low to midlevel flux vectors are larger outside 200 km compared with the inner core. The outward directions of these flux vectors indicate inward transport of angular momentum fluxes. There are also small upward components of these flux vectors, indicating inward heat fluxes.

The locations of the largest EP flux divergence remain in the outer region throughout 17 October, and then move inward during early 18 October. Sometimes the EP flux vector directions show outward transport of angular momentum in the outer low to midlevel region, which is likely due to spinning up of the outer winds. Right after the formation of the Typhoon, the EP flux divergence near the inner core is still strong (Fig. 3.16b). Outside radius of 100 km strong magnitudes of outward EP flux vectors indicated inward angular momentum transport again when the core vortex of the Typhoon develops rapidly.

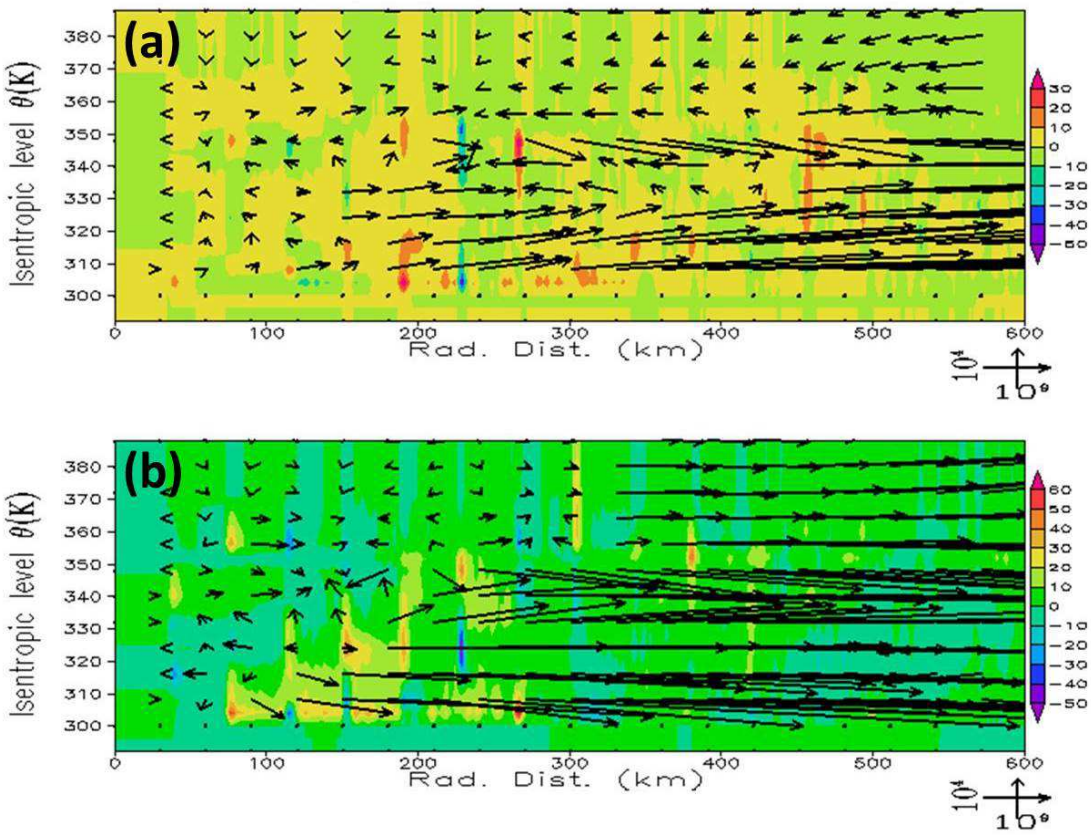

Fig. 3.16 Divergence (contour) of the EP flux vector (arrow) in simulated Typhoon Ketsana at (a) 1200 UTC 17 October and (b) 1800 UTC 18 October 2003.

3.8 CAPE and the Rate of TC Formation

While both Typhoons Dan (1999) and Ketsana (2003) formed in similar location of the WNP and the same month of year, their rates of formation were very different. Typhoon Dan developed from the disturbance to tropical depression in about one day, however, Typhoon Ketsana took two days to form from the initial MCS convection. What factors lead to these different rates of TC development? In this section, this question is examined through the CAPE consumption and recovery point of view.

When Typhoon Dan started to develop on 02 October 1999, the CAPE in the region

was quite low (Fig. 3.17a). The only source of high CAPE was from the southwest of the incipient circulation centre. This region of high CAPE persisted throughout the day of 02 October 1999 to support the convection development of the MCS (Fig. 3.17b). After the convection further developed near the circulation centre, the CAPE was lowered in the region (Fig. 3.17c). When the disturbance attained near tropical low intensity at 0000 UTC 03 October, the low-level circulation centre migrated to the northwest into a region still of quite low CAPE (Fig. 3.17d). In other words, throughout the early development of Typhoon Dan, the CAPE with high value in that area was enough to support the development of one MCS, which was close to the low-level circulation centre to establish the surface winds effectively. Thus, multiple MCSs development before formation has not been observed in this case. However, the CAPE recovered rapidly after the formation of Typhoon Dan (Figs. 3.17e, f), which was good to support further intensification of the storm. This can also be identified in the area average CAPE in Fig. 3.18 (the control experiment), which shows the CAPE consumption during 1200 UTC 02 October – 0000 UTC 03 October, and then the rapid increase thereafter.

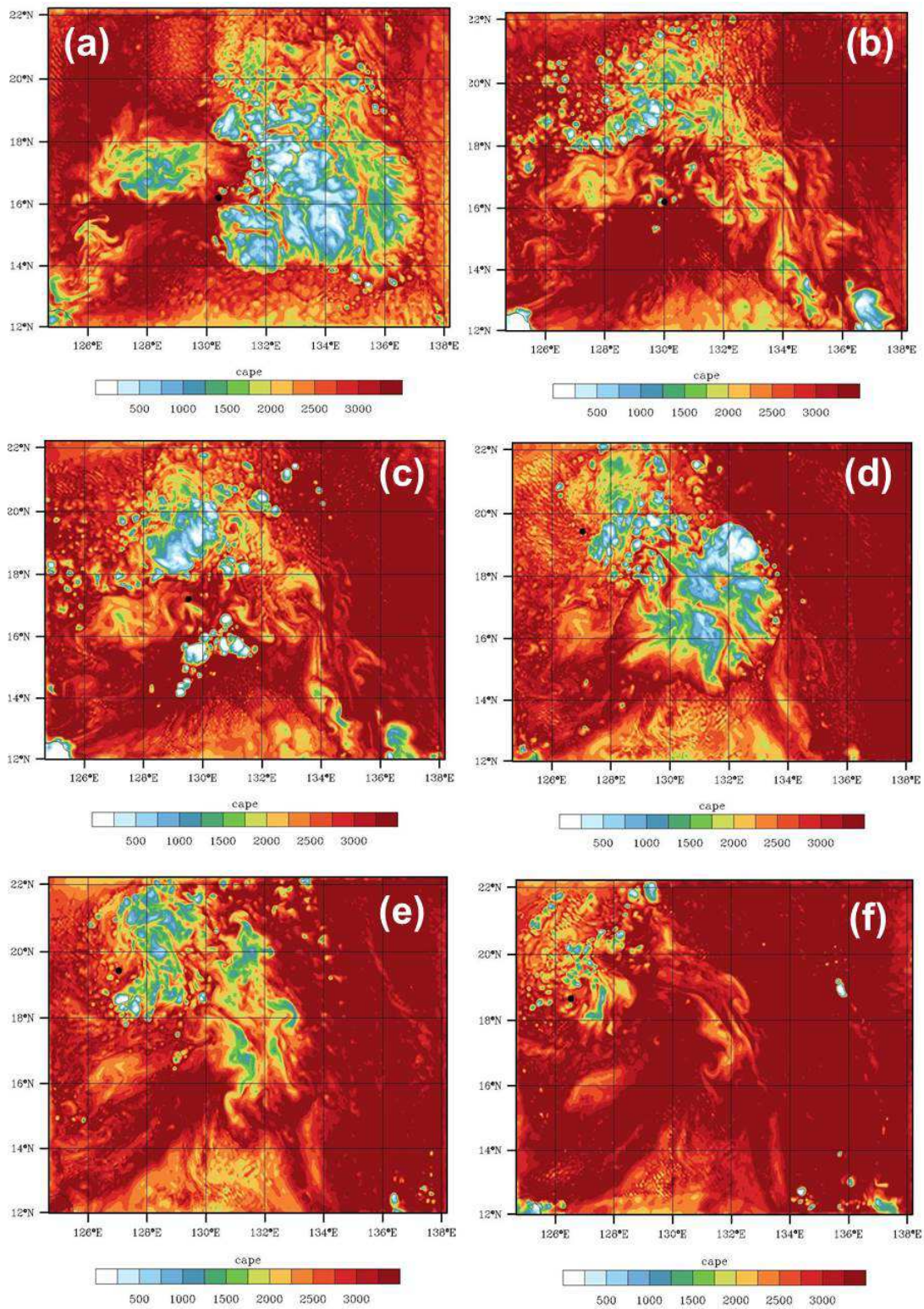

Fig. 3.17 Simulated Surface-based CAPE for Typhoon Dan at (a) 0300 UTC 02 October, (b) 1200 UTC 02 October, (c) 1500 UTC 02 October , (d) 0000 UTC 03 October (e)0600 UTC 03 October and (f)1200 UTC 03 October 1999.

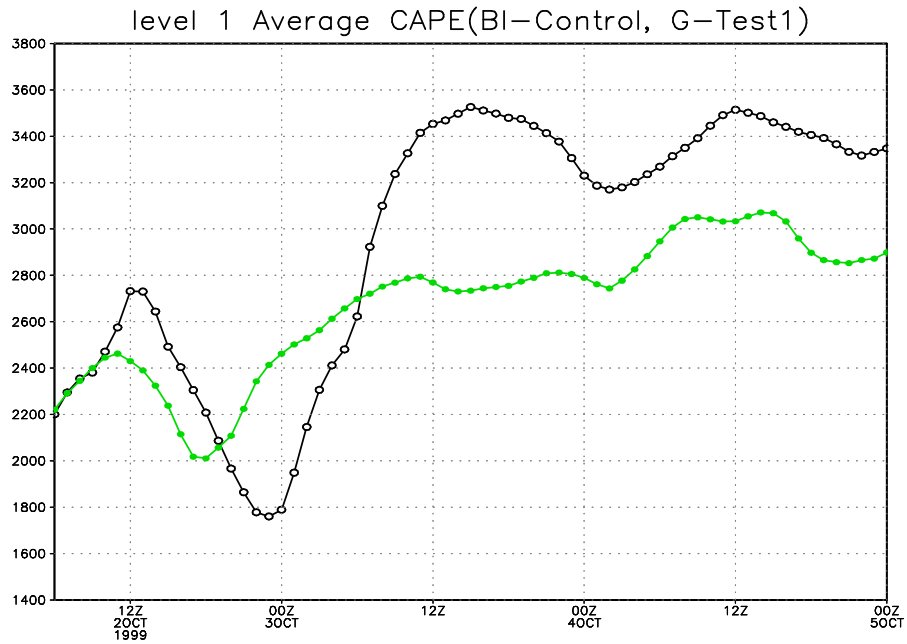

Fig. 3.18 Area-averaged (13-17°N, 127-132°E) surface-base CAPE during formation of Typhoon Dan in the control WRF experiment (black) and sensitivity test (green).

On the other hand, the formation of Typhoon Ketsana (2003) experienced multiple cycles of CAPE consumption and recovery associated with the MCS episodes of convection. After the first two MCSs dissipated in early 17 October, the CAPE on the western side of the incipient vortex was clearly lowered (Fig. 3.19a). The CAPE did not recover much and thus the two later MCSs on the same day actually developed out of only moderate values of CAPE. Their consumption of CAPE further lowered the values on the west and north side of circulation (Fig. 3.19b). At about 0600 UTC 18 October, high CAPE values entered the core region of the vortex, which supported the last (fifth) MCS to develop near the centre and led to the formation of Typhoon Ketsana at 1200

UTC 18 October (Figs. 3.19c, d). The last MCS dissipated near 0000 UTC 19 October (Fig. 3.19e) that remained low CAPE values in the core. After that the TC vortex sustained and high CAPE values reappeared associated with the eyewall convection (Fig. 3.19f).

Therefore, the development of Typhoon Ketsana during the two days before formation was much driven by convection and thus related to the variation of CAPE in the area of development. The convection episodes associated with the MCSs spun up the winds first at the periphery and then in the core, and led to formation of the typhoon, because the four early MCSs formed and developed in northwest of the core. This process was quite slow compared with the single-MCS development in Typhoon Dan.

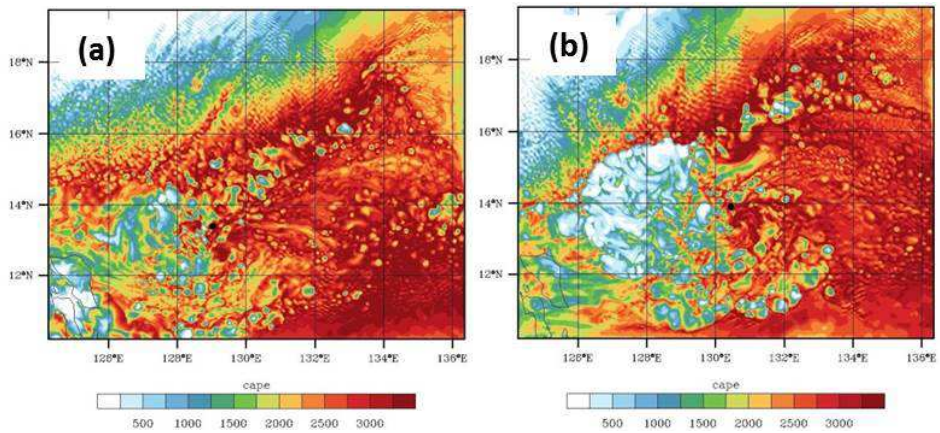

Fig. 3.19 As in Fig. 3.17 except for Typhoon Ketsana at (a) 1200 UTC 17 October, (b) 0000 UTC 18 October, (c) 0600 UTC 18 October, (d) 1200 UTC 18 October, (e) 0000 UTC 19 October and (f) 0700 UTC 19 October 2003.

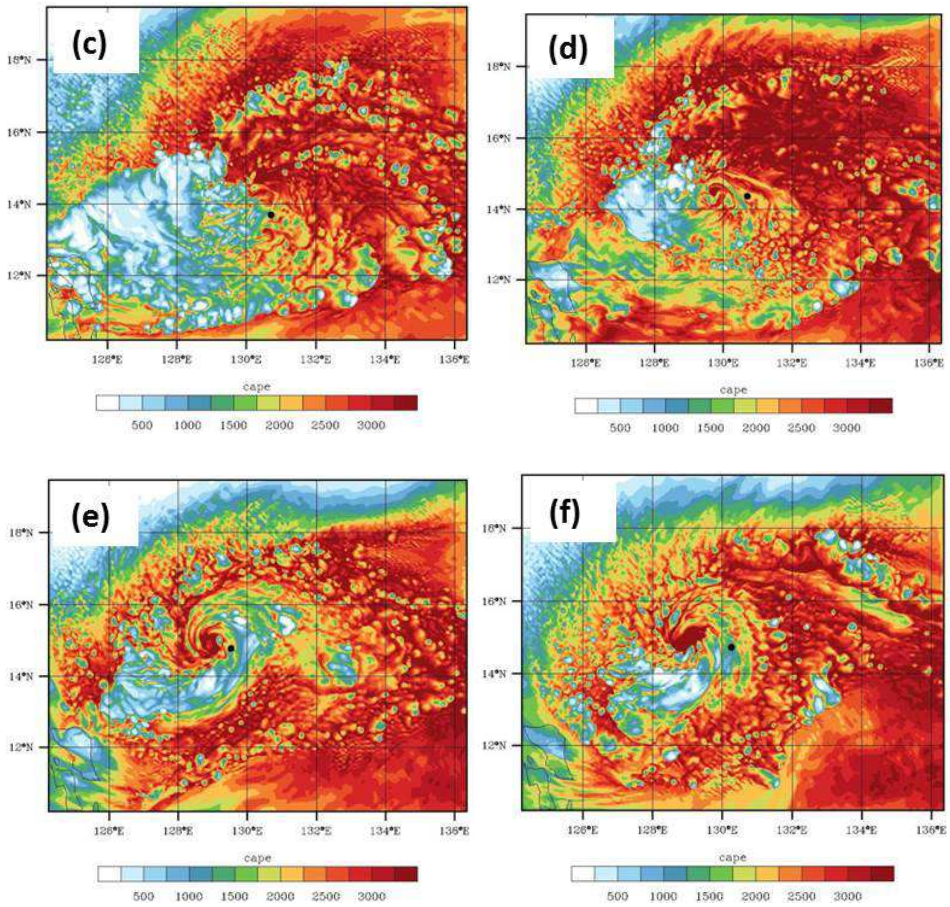

Fig. 3.19 (cont.)

Since the circulation associated with Typhoon Ketsana's formation did not move much, the area average CAPE time series also shows the consumption and recovery cycle on the day of 1200 UTC 17-18 October (Fig. 3.20 control experiment). In order to study the MCS activities of Ketsana, Lu et al. (2012) designed three sensitivity experiments on the impacts of MCSs to the early intensification rate. The same set of experiments is applied here to analyse the CAPE consumption and recovery cycles. Based on satellite images, the MCS3, MCS4, and MCS5 regions are identified as (12.8–15.8°N, 127.8–130.8°E), (15.8–18.8°N, 130.8–133.8°E), and (128–178°N, 127.8–130.8°E),

respectively. In the sensitivity experiment 1, the area-averaged relative humidity in the MCS3 region between 200 and 700 hPa at 1200 UTC 17 October 2003, which was higher than that around MCS4, is assimilated into the MCS4 region within the 6-h assimilation window (similarly for later experiments) in order to strengthen the intensity of MCS4. In experiment 2, MCS4 is weakened and only 60% of the 200–700-hPa relative humidity in the control experiment is retained and then assimilated at 1200 UTC 17 October 2003.

The sensitivity experiments in Fig. 3.20 show different CAPE consumption and recovery cycles of Typhoon Ketsana. When convection in the MCS4 is stronger (black line), the CAPE drops much more than in the control experiment during late 17 October. However, the recovery of CAPE is quite efficient after and by 0600 UTC 18 October the average CAPE value is not much lower than in the control experiment. The early intensification rate of Ketsana is actually faster than the control in this experiment. On the other hand, when convection in the MCS4 is weaker (yellow line), the average CAPE consumed is less initially, then building up slightly and going through another cycle before the TC formation. Although the CAPE level near formation time in this experiment is similar to that in the control, the weakened MCSs lead to a slower formation and early intensification rate.

Similar experiment as in the second sensitivity experiment of Typhoon Ketsana was performed for Typhoon Dan (green line in Fig. 3.18). With a weakened MCS, CAPE consumption before Dan's formation is much smaller than in the control. Due to the weaker convection, the early intensification rate of the simulated typhoon is also slower. After that, CAPE recovery is still quite efficient in the environment but has not increased

to the same level as in the control experiment. Therefore, from comparison of the two typhoon cases here it can be concluded that the rate of TC formation directly depends on how much each convection episode associated with MCS contributes to spinning up the low-level vorticity, which has been pointed out in previous studies. On the other hand, it can also be seen that how CAPE recovers in the developing TC depends on the earlier convection episodes but not only on the large-scale environment. The control by this factor on the pace of TC early development deserves more case studies.

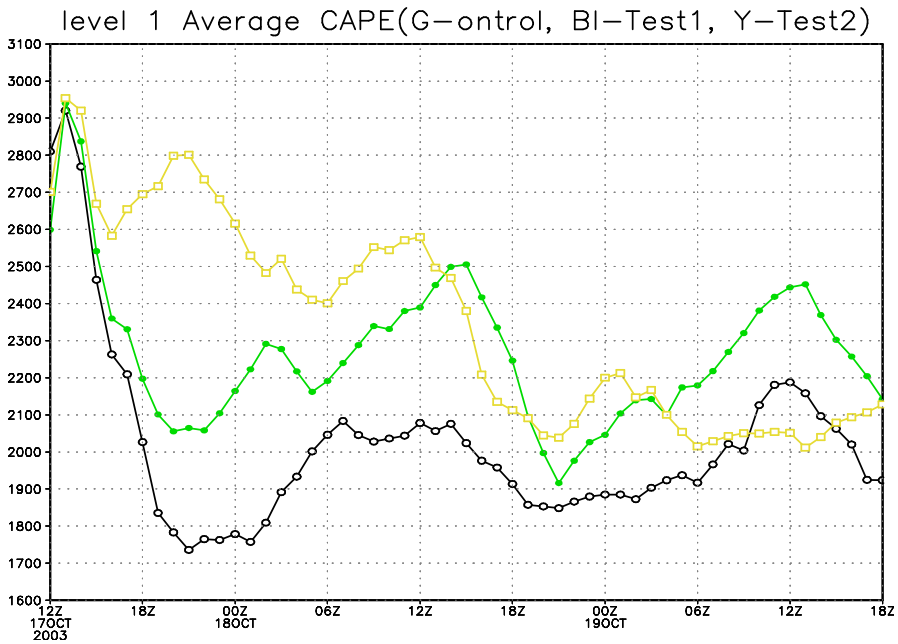

Fig. 3.20 Area-averaged (13-17°N, 127-132°E) surface-base CAPE during formation of Typhoon Ketsana in the control WRF experiment (green), sensitivity test with strengthened MCS4 (black) and weakened MCS4 (yellow).

3.9 Discussion

It has been observed that the times for tropical disturbances to develop to tropical storm vary with quite a large range, and are synoptic pattern dependent. For example, in analysing the MCS activities during TC formations in the WNP Lee et al. (2008) found that for easterly wave-type formations a single MCS usually develops and it takes an average of 13 h to form a TC. In contrast, for monsoon-trough-related formations, there are usually more than two MCSs and the average time to form a TC is about one day. Very often more than one MCS coexist at the same time within the monsoon trough. Whereas the recent studies on TC formations such as Fang and Zhang (2011), Lu et al. (2012) and Zhang et al. (2011) focused on contributions from convective-scale systems such as VHTs and CVAs (which will be discussed in Chapter 4), their interactions with mesoscale circulations and mechanisms to generate the core surface vortex, less discussion was on the relationship between convection patterns and development times of TCs. The numerical simulations of Typhoons Dan and Ketsana here illustrate that the pace of early development of a TC depends much on the convection configuration, namely, whether it is a single MCS or interacting multiple MCSs.

It might seem to be counter-intuitive that the multiple-MCS convection pattern is not speeding up the TC development process due to spinning up of larger relative vorticity within more areas in the TC, but rather slowing the process down compared with the single MCS pattern. Nevertheless, this phenomenon may be explained from the point of view of competing for convective resources. Whenever deep convection occurs, the environmental CAPE is consumed. Descent of cold and dry air left by heavy

precipitation is unfavourable for new convection development, which has to wait until the environmental CAPE increases again by heat and moisture fluxes from the ocean surface. When Fang and Zhang (2011) analysed the simulated formation of Hurricane Dolly (2008), similar processes were found under the TC system scale. Namely, there were episodes of deep convection during the development of Hurricane Dolly, but in between there was a period when the CAPE had a minimum. This interpretation is consistent with the simulation for Typhoon Ketsana especially during the development of MCS3 and MCS4. These two MCSs developed at about the same time with a large area of convection, but did not lead to TC formation right after. The reason may be that MCS4 to the east was consuming part of the CAPE within the TC area, making the MCS3 to the west less conducive to developing more deep convection and subsequent low-level vorticity generation. In fact, MCS3 dissipated first and the system intensification slowed down before another MCS developed in the core region.

It is interesting that this kind of CAPE argument is also applicable to the convective scales, as has been briefly discussed in Fang and Zhang (2011). Various convection processes such as waxes and wanes, merging and splitting within each MCS are common during TC early development. That is, these processes represent the variability of the convective-scale VHT and CVA activities of the MCS, which is likely also due to the consumption and recovery cycles of CAPE. One point to note is that since the single-MCS convection pattern has been identified as the most common one at the end of early development, i.e., for the TC to enter the intensification phase, the convection within that single MCS has to be long lasting enough for the system to intensify to a

sustainable level. In other words, there may be a hypothesis that the CAPE consumption and recovery cycles to sustain convection are more efficient under convective scales compared with mesoscales. This may be due to the fact that the areas for the surface fluxes to warm and moist the low-level atmosphere are simply much smaller, and/or that merging of the VTHs/CVAs is effective to sustain deep convection especially when these systems are moving toward the TC centre under the system-scale convergent flow. However, these assertions have to be verified by further investigations.

In the case that merging of MCSs occurs, the resulted mesoscale vortex may lead to faster system intensification rather than the retardation as obtained in the earlier simulations (Ritchie and Holland 1997; Simpson et al. 1997; Ritchie 2003). More numerical studies on TC cases with explicit MCS merging have to be conducted to validate such hypothesis.

4 CONVECTIVE-SCALE SYSTEM DYNAMICS

4.1 Chapter Overview

The signature of TC formation is the generation of near-surface relative vorticity that is large enough to form the intense cyclonic circulation. After the discussion on MCS activities and TC formation in Chapter 3, the focus is on the smaller convective-scale systems and the case of Typhoon Ketsana is used for illustration. Previous studies have demonstrated the contributions of such small systems in the process of TC formation from observational, modelling and theoretical approach. However, the system organization aspect of these systems has not been much emphasised. Therefore, in this chapter the simulated relative vorticity is first scale separated to examine its evolution under mesoscale and convective scale. Then, measures of the degree of aggregation of relative vorticity are applied, which include a vortices merger index and the normalised Okubo-Weiss parameter. The former emphasises the self-organizational aspect of vortices and the latter measures when the storm-scale vorticity necessary for TC formation has been obtained.

4.2 Introduction

As has been reviewed in Chapter 1, there are convective systems with different scales that are involved in the TC formation process. The focus in this Chapter is the small-scale (of order ~10 km) convective systems and how they organise to form the core relative vorticity in TC. In order to study the evolutions of these systems, spectral

decomposition as in Fang and Zhang (2011) and Lu et al. (2012) is applied to the WRF-simulated relative vorticity of Typhoon Ketsana (2003). The spectral decomposition separates the relative vorticity into meso-α (>250 km), meso-β (50-250km) and meso-γ (< 50 km) scales. The vortices with meso-γ scales are considered to reflect the activity of the VHTs or CVAs, while those with meso-α and meso-β scales reflect the storm system scale and MCVs, respectively. The scale separation performed in Lu et al. (2012) showed that the temporal activities of the meso-γ-scale systems correlate well with the development of the MCSs. These VHTs or CVAs have large values of positive relative vorticity induced by intense low-level convergence, and was suggested by Lu et al. (2012) to contribute substantially to the surface vortex necessary for TC formation besides the mesoscale processes.

One issue associated with CVAs is that large downdraft and associated negative relative vorticity is always accompanying the CVAs. It was discussed in Fang and Zhang (2011) that eventually both the negative and positive vorticity anomalies accumulate into a large single-sign vorticity region through larger-scale convergent (secondary or transverse) circulation that is driven by latent heating. The negative vorticity anomalies are weaker and shorter-lived compared with the positive ones, and are then absorbed. In this Chapter, the evolutions of the relative vorticity during the formation of Typhoon Ketsana (2003) after the aforementioned scale separation are first examined in more details especially on how the positive and negative vorticity change respectively. Then, a measure of self-organisation in vortex interaction is computed on how the CVAs aggregate, and how the up-scale energy cascade process of the CVAs

enables minimal impact from the negative vorticity anomalies. Finally, the scale dependence of a measure of the development of relative vorticity in TC formation, the normalised Okubo-Weiss parameter, is discussed based on the numerical simulation of Typhoon Ketsana.

4.3 Scale Separation

In the previous chapter, it has been discussed that there were four MCS convective episodes during the formation of Typhoon Ketsana. The first episode (associated with MCS1 and MCS2) occurred at 16 October, the second and third one (associated with MCS3 and MCS4) in the morning and afternoon of 17 October respectively, and the fourth one (associated with MCS5) occurred at around 1200 UTC 18 October. After the scale separation, the near-surface (level 6 in the model output that is located near 925 hPa) simulated relative vorticity shows quite interesting development (Fig. 4.1). The large-scale (meso-α) relative vorticity starts to increase since the first MCS development and continues to rise rapidly after 0000 UTC 17 October until the average value of 1.2×10^{-5} s^{-1} when the TC formed at 1200 UTC 18 October. However, the average meso-β-scale relative vorticity actually has negative value and decreasing trend in the broad area (4° latitude × 5° longitude) where the typhoon develops. This is because the average includes the areas with negative vorticity, and thus the trend implies that whereas the relative vorticity has been spun up in the MCS areas, the subsidence areas do have quite large negative vorticity values. The several negative peaks in the time series of the meso-β average vorticity also indicates that the negative vorticity is correlated with the

MCS convective episodes.

On the other hand, the trend of the convective-scale (meso-γ) average relative vorticity is similar to that for the storm scale. As has been examined in Lu et al. (2012), the frequency of VHTs is quite correlated with MCS activity, and this is consistent with the result here for the meso-γ trend. Namely, the net relative vorticity increases around 0000 UTC 17 October when the first few MCSs develop. This convective-scale vorticity then decreases shortly before the rapid increase that leads to the TC formation. As judged from the average magnitude, such convective-scale vorticity contributes substantially to the total when the TC forms and even after that during the intensification phase.

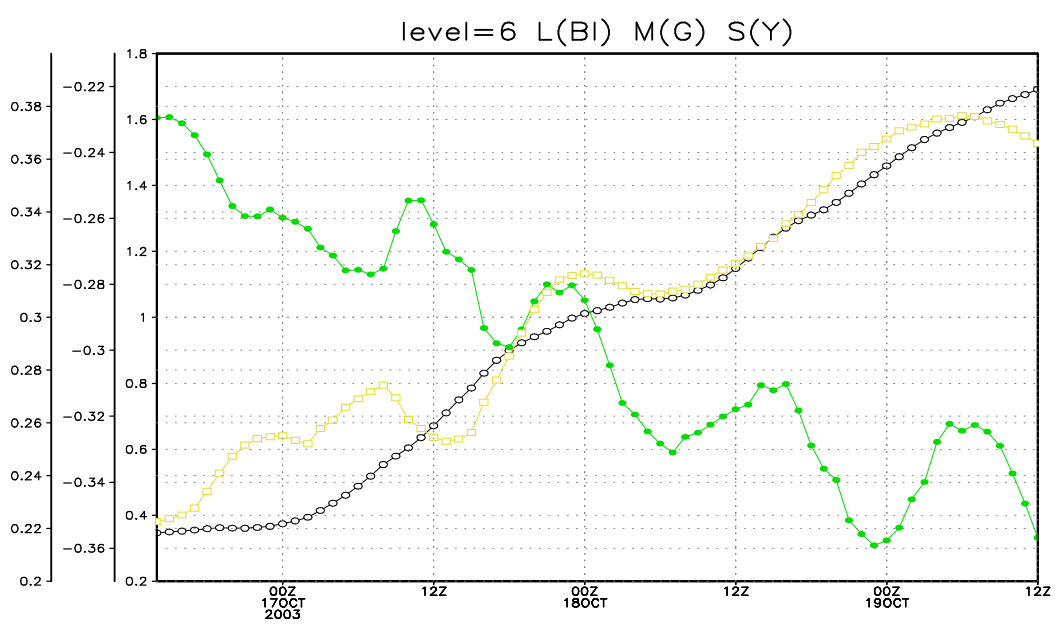

Fig 4.1 Smoothed area-averaged (13-17°N, 127-132°E) near-surface (~925 hPa) relative vorticity (10^{-5} s^{-1}) associated with meso-α (black, right scale), meso-β (green, middle negative scale) and meso-γ (yellow, left scale) spatial scale.

Fig. 4.2 confirms that there is always about the same magnitude of downdraft, which creates negative vorticity, accompanying the convective updrafts and associated positive vorticity for both the meso-β and meso-γ scale. These very similar time series for the positive (with the negative vorticity masked out and averaged over the positive areas) and negative vorticity (with the positive vorticity masked out and averaged over the negative areas) indicates that downdraft is associated with the development of the convection episodes on these scales. However, note that the areas of averaging are not the same in these two time series, and thus effectively they have been respectively weighed by the (reciprocal of) area with positive or negative vorticity. In other words, the mean of the positive and negative relative vorticity at any time in Fig. 4.2 does not equal to the average over the entire area (as in Fig. 4.1). Nevertheless, the same trends of the positive and negative vorticity, for both the meso-β and meso-γ scale, show that they are dynamically linked. The problem is how the centres of positive vorticity aggregate and eventually form the storm-scale cyclonic circulation.

The distributions of vertical velocities in the simulation are consistent with those of relative vorticity. Both mesoscale and convective-scale updrafts and downdrafts can be identified at various times (Fig. 4.3). During 17 October, there are more meso-β-scale vertical velocities associated with the early MCS activities. In early 18 October, very intense updrafts (and accompanied downdrafts) in the core region have been simulated, which are within the last MCS before formation and establish both the positive and negative relative vorticity as seen in Fig. 4.2.

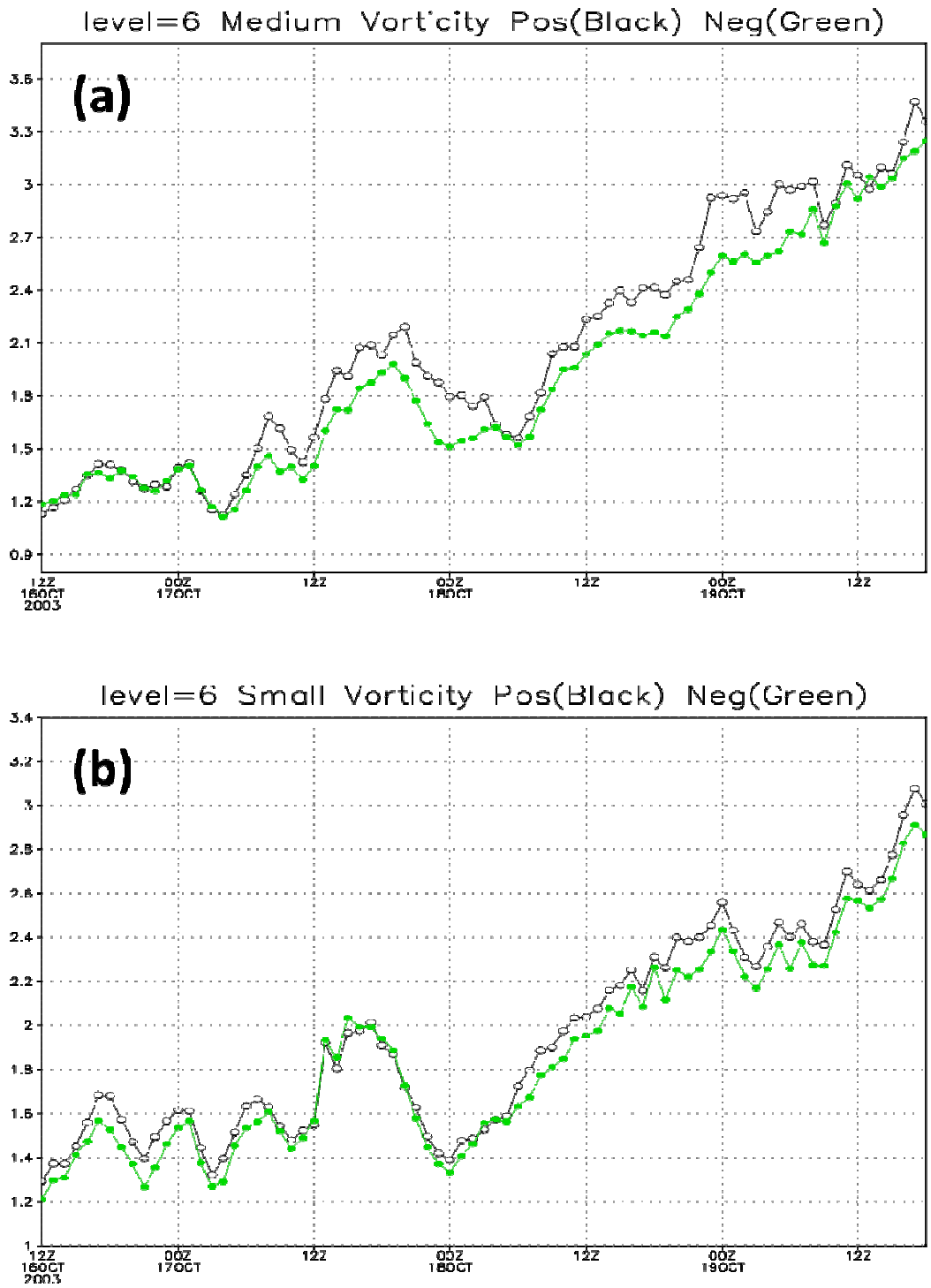

Fig. 4.2 Near-surface (~925 hPa) positive (black) and negative (green) relative vorticity average over their respective area within 13-17°N, 127-132°E at the (a) meso-β and (b) meso-γ scale.

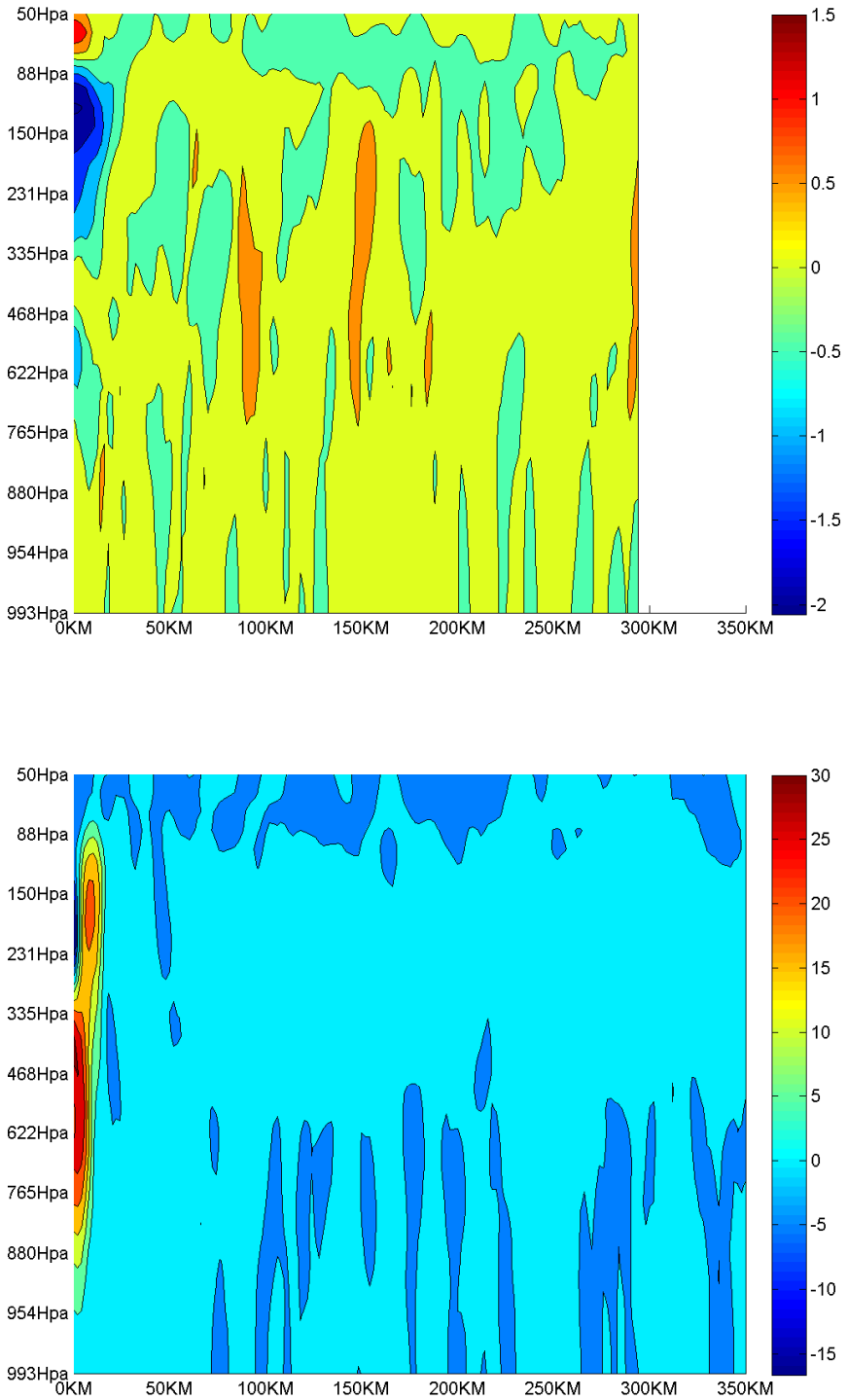

Fig. 4.3 Azimuthal average vertical velocity (m s^{-1}) with respect to low-level circulation centre in simulated Typhoon Ketsana.

When the spatial distributions of the meso-β and meso-γ relative vorticity are analysed, the development of the MCSs and convective systems involved in the formation process can be shown. On 16 October and early 17 October the meso-β vorticity is still noisy with a few large vorticity centres about 100 km from the surface circulation centre, which represent the early MCSs development (Fig. 4.4). Later on 17 October, there is an obvious upscale cascade of vorticity within the meso-β scale, and there are patches of large vorticity north of the circulation centre associated with MCS3 and MCS4. When the last MCS5 develops on 18 October near the low-level circulation centre, the core vorticity distribution is already circular in geometry and near storm scale. Certainly, there is also contribution from the up-scale energy cascade from the convective scale systems to this meso-β relative vorticity.

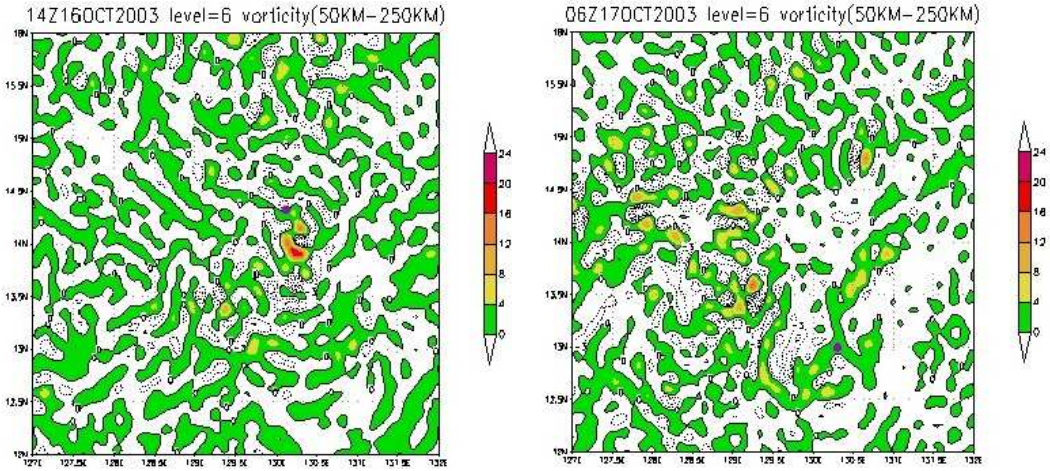

Fig 4.4 Meso-β-scale near-surface relative vorticity (10^{-5} s^{-1}) at 1400 UTC 16 Oct, 0600 UTC 17 October, 1800 UTC 17 October, 0600 UTC 18 October, 0900 UTC 18 October and 1200 UTC 18 October 2003 during the formation of Typhoon Ketsana. The purple dot represents the surface circulation centre.

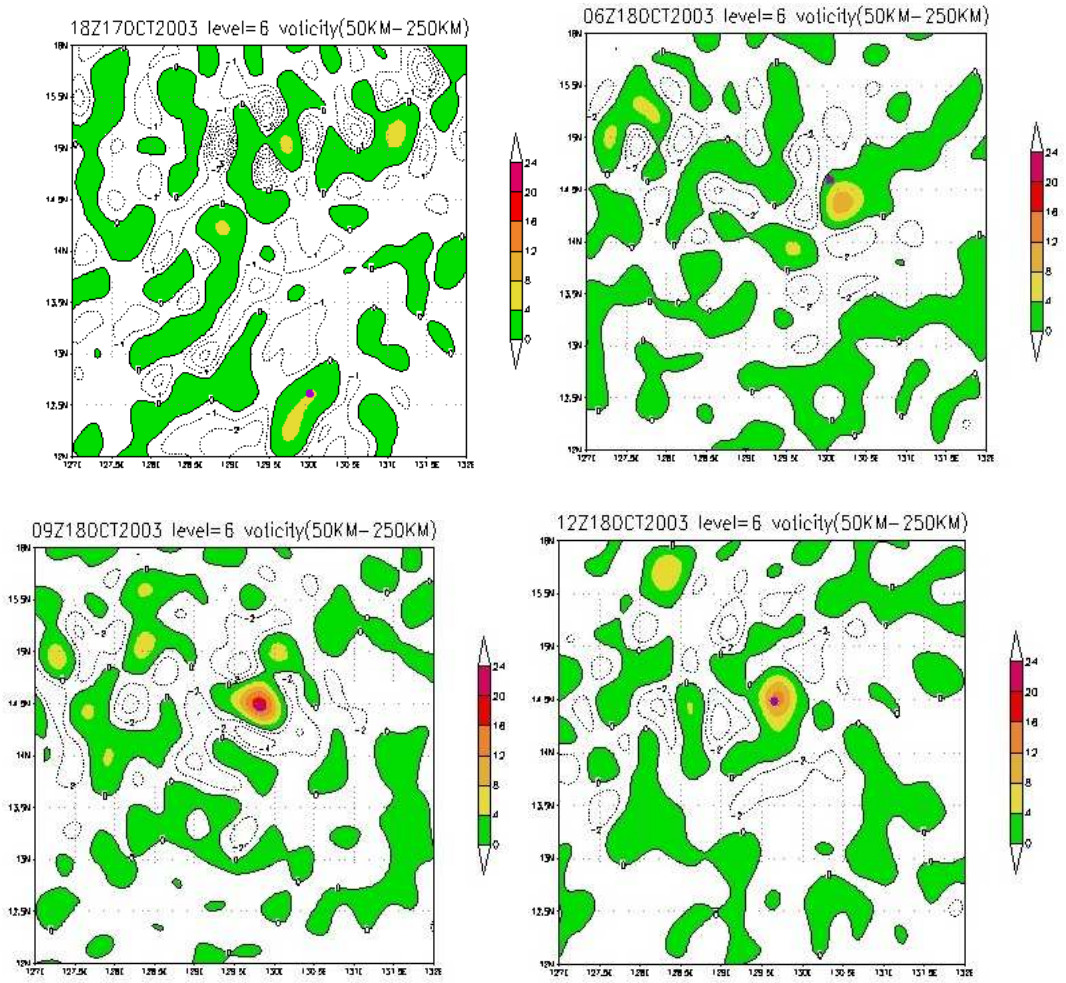

Fig 4.4 (cont.)

Fig. 4.5 shows the development of the meso-γ vorticity near the formation time. The positive vorticity centres associated with updraft and negative ones associated with downdraft always stagger together. According to studies such as Fang and Zhang (2011), the positive CVAs get closer to the centre through advection by the secondary circulation, while the negative CVAs get weaker. However, if there is persistent downdraft compensating the updraft, which is likely during convection, advection should

affect the negative vorticity centres too. Theoretically, early studies such as Schecter and Dubin (1999) has analysed vortex motion driven by a background vorticity gradient, which is similar to convective-scale vortices within TC circulation. By argument of vorticity mixing, it was shown that positive vorticity anomalies effectively move upstream the background vorticity gradient, while negative anomalies move downstream. That is, the positive vorticity would accumulate toward the centre but the negative vorticity would migrate outward. Fig. 4.6, which consists of the positive and negative vorticity averaged over fixed area, clearly shows this trend. While the updraft and downdraft activities are still highly correlated with each other, the average positive vorticity increases more than the negative one especially during the several MCS development episodes. In particular, the positive vorticity increases rapidly right after formation at 1200 UTC 18 October and overcomes the negative vorticity. Eventually, the core positive vorticity attains a magnitude necessary for TC formation. Indeed, in the simulation of Typhoon Ketsana the positive CVAs get centralised more than the negative CVAs during formation, such that the negative vorticity is expelled from centre, and the vorticity core is formed.

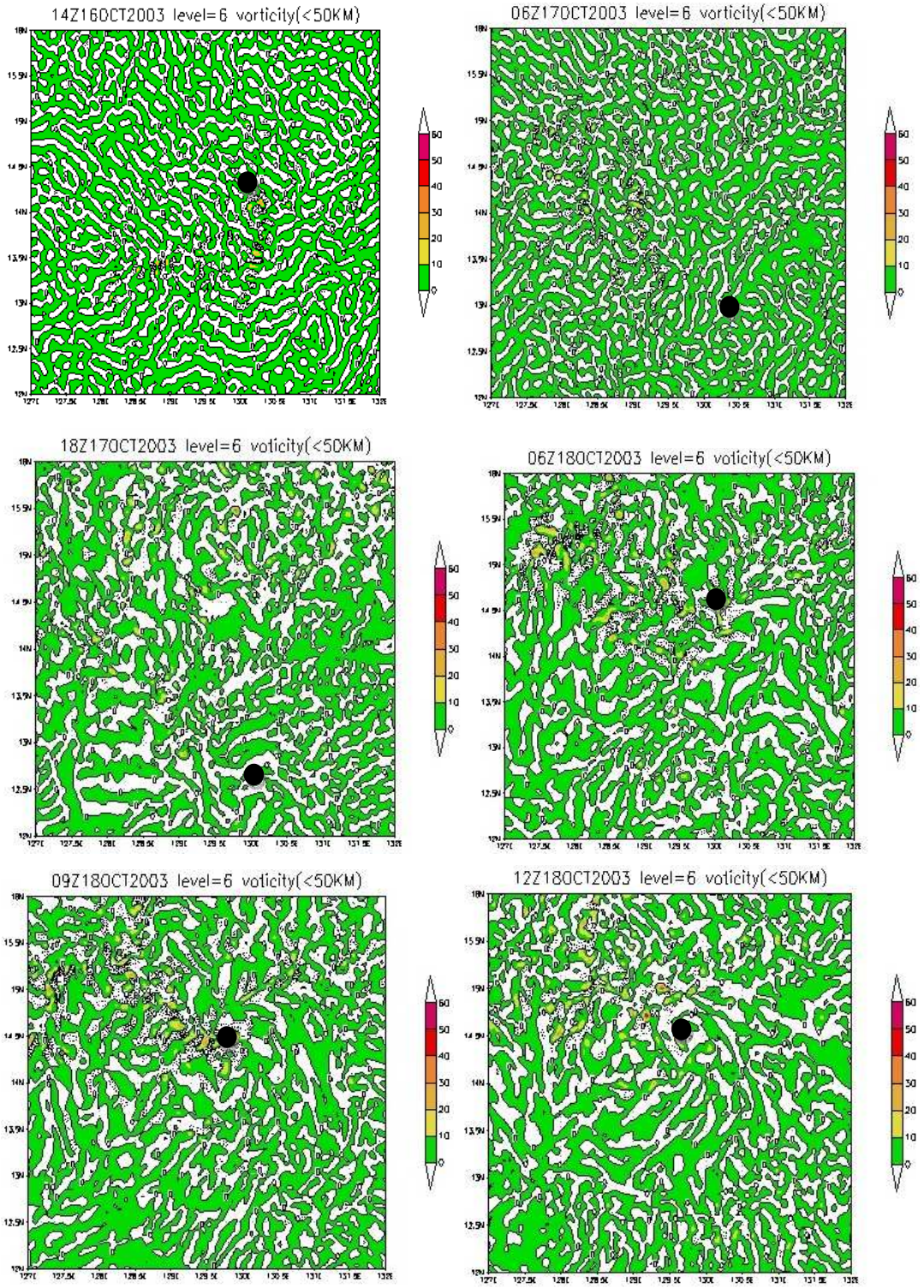

Fig. 4.5 Meso-γ-scale near-surface relative vorticity (10^{-5} s^{-1}) at the same times of Fig. 4.4 during the formation of Typhoon Ketsana. The black dot represents the surface circulation centre.

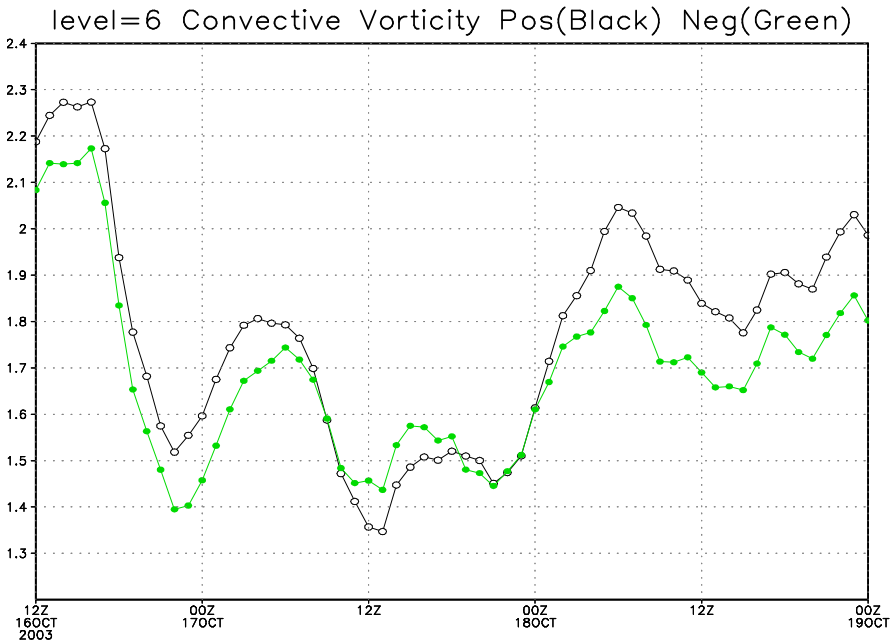

Fig. 4.6 Area-averaged (13-17°N, 127-132°E) positive (black) and negative (multiplied by (-1), green) relative vorticity at the meso-γ scale.

4.4 Merger Index in Vortex Interaction

Although there is a theoretical basis for the centralisation of the convective- or meso-γ-scale vorticity anomalies that leads to the core, storm-scale vorticity of the TC, another aspect of this organization is through vortex interaction. Even under barotropic dynamics and quiescent environment, vortex interaction will lead to interesting structure changes within a TC including the development of concentric eyewalls (Kuo et al. 2008). Vortex interaction is usually studied with simplified or full-physics numerical models. However, in such kind of studies the organization aspect of vortices has not been emphasised. In this section, a quantitative measure of the merger index developed in Venkatesh (2003) is applied. This merger index is essentially the ratio compared with a critical distance between two vortices under which they would interact and possibly

merge. Thus, this measure can be applied to examine whether the vortices during TC formation are aggregating. The original merger index in Venkatesh (2003) was designed for mesoscale vortices merging through statistical regression of idealised vortices at this scale, but theoretically the same idea applies also to convective-scale vortices. Here the same index is applied to both the mesoscale and convective-scale vortices after scale separation. By this, the magnitude of the merger index for the convective scale is not applicable for forecast purpose (as in the original design of it for the mesoscale), however, the trend of the index is still able to indicate the degree of aggregation of the vortices and the change over time when the TC forms.

Venkatesh (2003) designed the merger index with an increase trend before merging and an immediately decrease trend after merging. It can be identified from Fig. 4.7 that there is no merging of the mesoscale vortices. The index shows a stable trend without clear rise, which is consistent with the result when the spatial distributions of the meso-β vortices are visualised. While the evolutions of the vortices with positive and negative vorticity are highly correlated, the index does indicate higher values (closer to 1) during the developments of the MCSs in Typhoon Ketsana. Namely, the index has value up to 0.6 at the beginning of the time series when the early MCSs develop and then in the middle of the time series when the third and fourth MCSs develop. However, the merger index remains small before formation, indicating that the final vorticity enhancement is not due to merging of the mesocale vortices, but due to the core development of a MCS that leads to the intensification of the near surface vorticity. This is consistent with the conclusion in Lu et al. (2012).

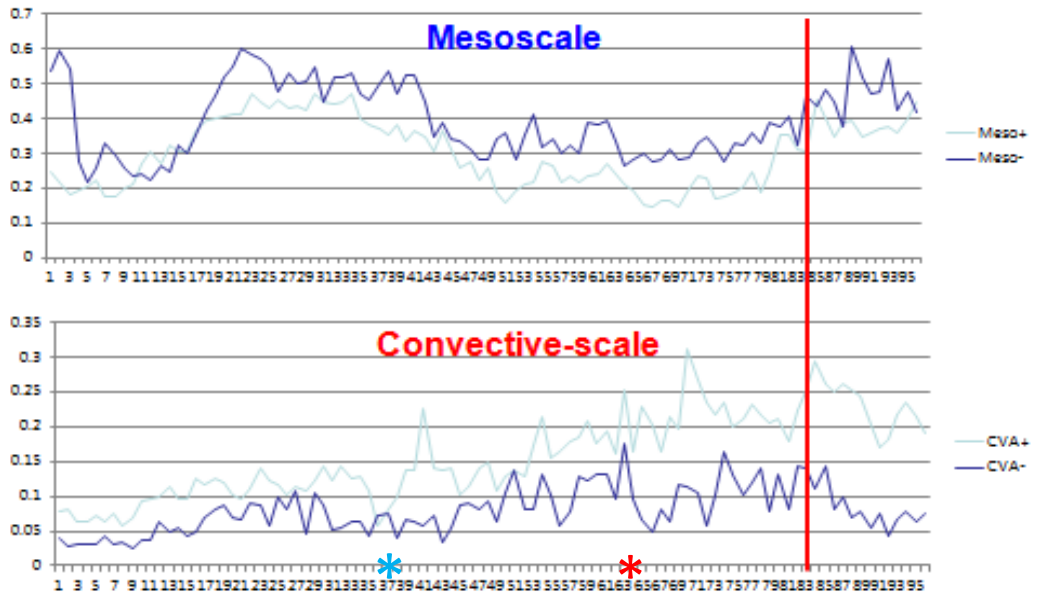

Fig. 4.7 Time series of the merger index for the mesoscale (upper) and convective scale (lower). The thick (line) line is for vortex with positive (negative) vorticity. The red vertical line is the formation time of Typhoon Ketsana. (Blue star is near the time of MCS3 & MCS4 development; Red star for MCS5)

For the convective-scale vortices, the aggregation process can be seen clearly and there is also distinction between the positive and negative vorticity patches. There has not been any previous study that tried to establish the threshold of index during merging of such small-scale vortices, and thus the values of merger index for the meso-β and meso-γ vortices are not according to the design of such merger index, the trend of the index does indicate aggregation. While the index for the negative (meso-γ) vorticity remains very low through the time series (i.e., no merging in Fig. 4.7, that for the positive vorticity has an increasing trend (i.e., with merging) from the early development of the MCSs until the TC forms. Although the magnitude of the index is not representative

under this scale, the index does attain a value as high as 0.3. This further confirms that the positive VHTs or CVAs do merge together to form the core vortex, on the other hand the negative ones either weaken or are expelled out of the core region.

4.5 Normalised Okubo-Weiss Parameter (OWZP) Analysis

Tory et al. (2013) modified the original OW parameter to the normalised OW_{norm}, and then the OWZ applicable to both Hemispheres to examine the formation time of TC in coarse-resolution reanalysis data such as the ERA Interim re-analysis. The development of an initial OWZ parameter with thresholds of 50 and 40 on the 850 and 500 hPa pressure levels were defined by Tory et al. (2013), respectively. When combining the OWZ with the low vertical shear requirement and troposphere relative humidity threshold to eliminate any obviously non-tropical flows (while being careful to avoid eliminating exceptional cases with potential for development), an imminent genesis parameter OWZP can be defined. Using 20 years of ERA Interim reanalysis data and the IBTrACS global TC database Tory et al. (2013) found that 95 % of TCs including, but not limited to, those forming in tropical waves are associated with enhanced level of OWZ at both 850 hPa and 500 hPa at the time of TC declaration, while 90 % show enhanced OWZ for at least 24 h prior to declaration. This result prompts the question of whether the pouch concept extends beyond wave-type formation to all TC formations worldwide.

The OWZ parameter includes only relatively large-scale fluid properties that are resolved by coarse grid model data (>150 km), and thus its purpose of design is mainly as

a TC detector for climate model applications. While it has been found out that the OWZP at both 500 hPa and 850 hPa is good indicator of TC formation, it is further said that it is also useful as a cyclogenesis diagnosis in higher resolution models such as real-time global forecast models. In this case study, we examine this parameter in our WRF fine-resolution domains when Typhoon Ketsana is simulated. The issue of interest is the scale dependence of the OWZP that indicates the core development of vorticity.

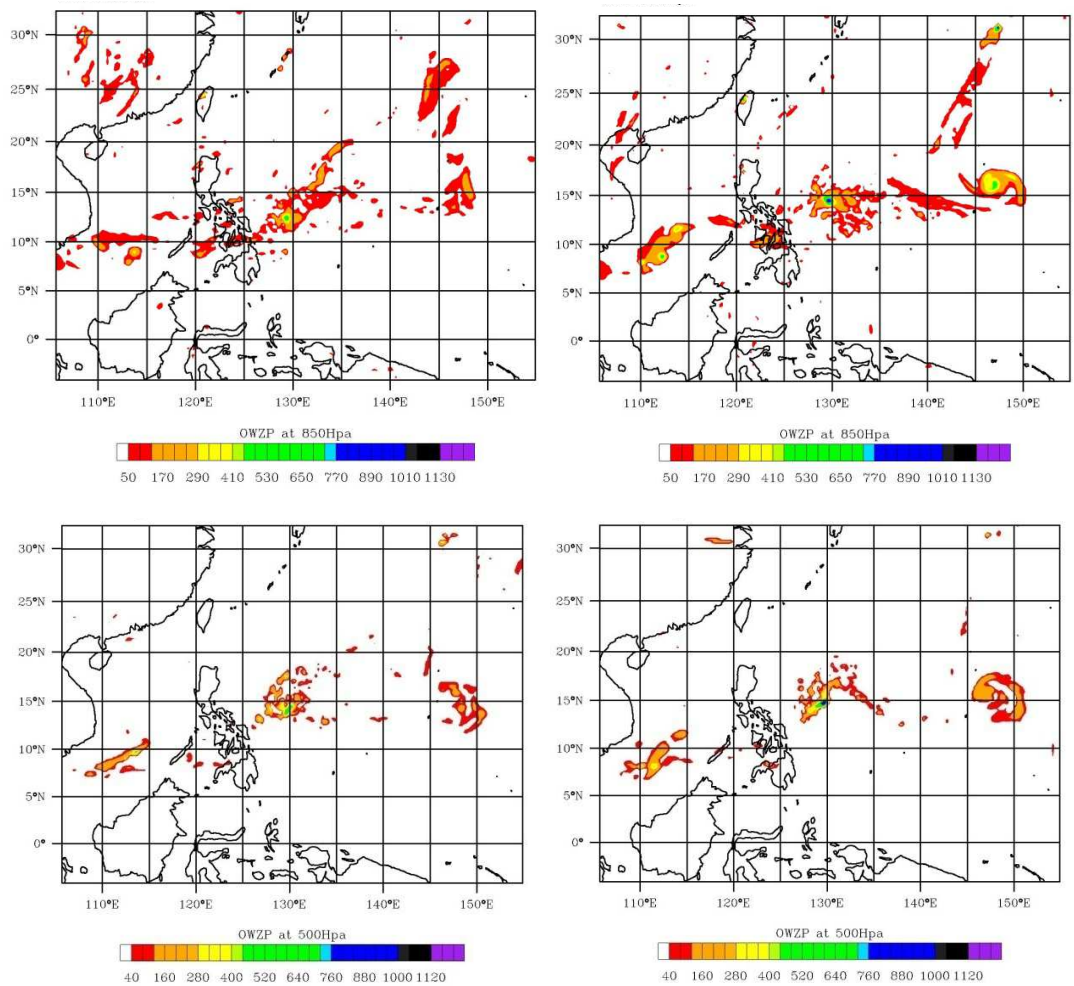

Fig. 4.8 Domain-1 850-hPa OWZP at 1500 UTC 17 October and 1200 UTC 18 October 2003 (upper panels); Domain-1 500-hPa OWZP at 0600 and 1200 UTC 18 October 2003 (lower panels).

For domain 1 with 27-km resolution, the OWZP starts to show value above 400 at 1500 UTC 17 October at 850 hPa and increases above 1000 at the formation time 1200 UTC 18 October (Fig. 4.8). However, the distribution of OWZP is quite noisy at this low level because the smaller-scale convective vortices do generate high values of the OWZP. At 500 hPa the distributions are clearer, which also show in the TC development area of values above 400 at 0600 UTC 18 October. Later at the formation time the 500-hPa OWZP well aligns with the low-level maximum and the value also increases up to 1000.

For domain 2 with 9-km resolution, the OWZP mostly indicates the vorticity patches (those with solid body rotation) associated with the convective-scale systems and thus the distribution of the parameter is much noisier than that in the coarse domain (Fig. 4.9). The maximum value at 0600 UTC 18 October still reaches the value of 1100. Both the maxima at 850 hPa and 500 hPa enlarge a few hours later near formation time. Again the maximum value of OWZP in the core is clearer at 500 hPa, that at 850 hPa is still recognisable among the other small-scale vortices. That is, with respect to this high-resolution simulation of TC of the order of 10 km, OWZP is a useful indicator and under forecast context a predictor of TC formation.

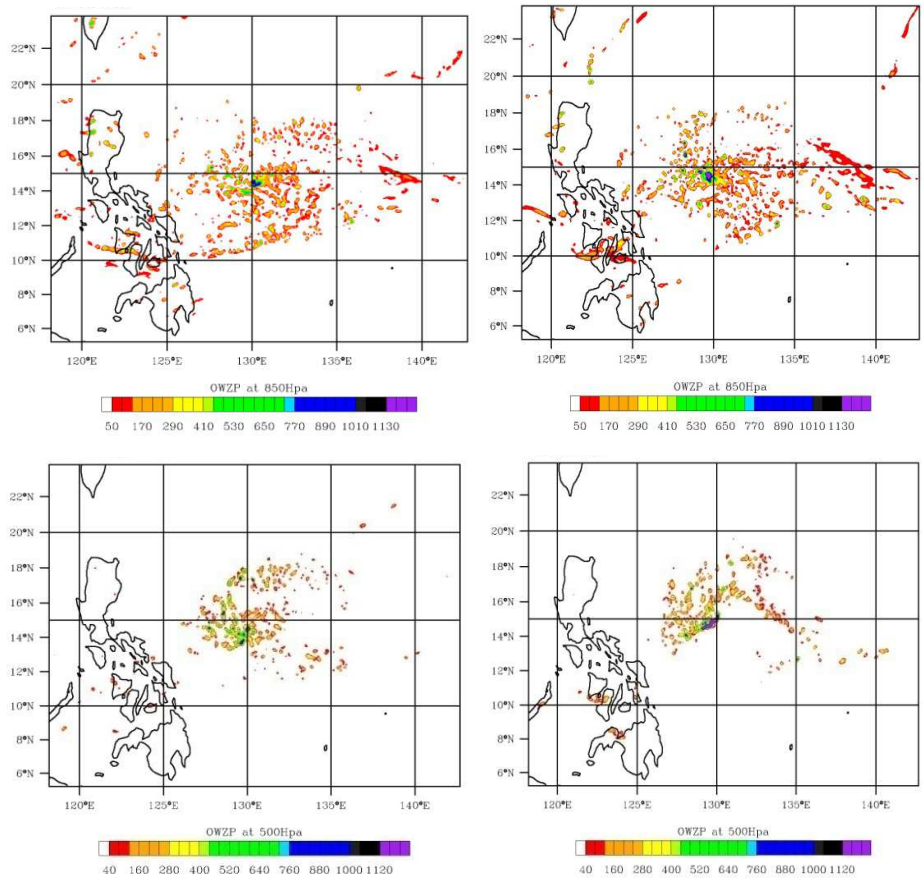

Fig. 4.9 Domain-2 850-hPa (upper panels) and 500-hPa (lower panels) OWZP at 0600 and 1200 UTC 18 October 2003 respectively.

As expected, the OWZP distribution in domain 3 with only 3 km resolution mostly indicates the scattered vorticity centres at both 850 hPa and 500 hPa (Fig. 4.10). There are indeed maximum values above 1000 but they remain scattered at the formation time. The likely reason is that while there is continuous aggregation process of the positive vorticity anomalies as indicated in the analysis of the merger index, the vorticity upscale cascade process enhances the vorticity in the meso-γ scale and results in the near storm-scale vortex. Within the domain 3, the dot vortices remain as shown in Fig. 4.10, and the OWZP does indicate the solid body rotation within these small vortices.

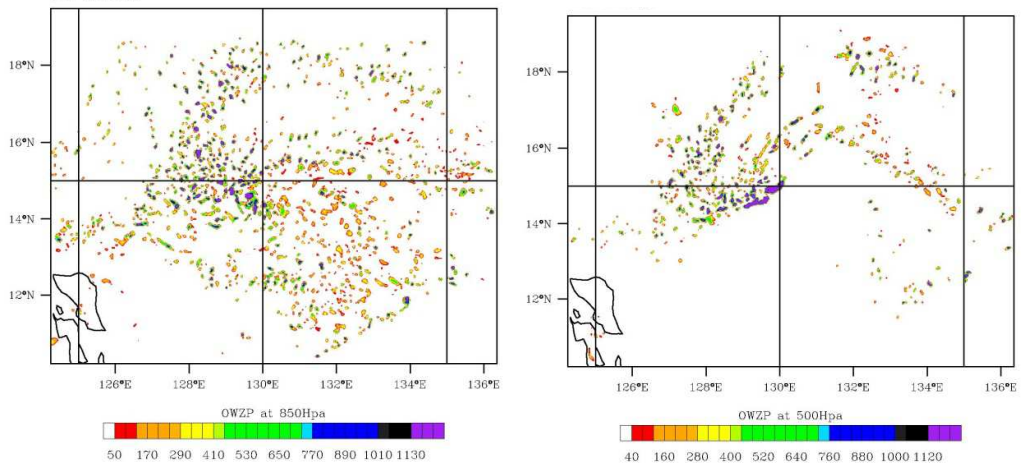

Fig. 4.10 Domain-3 850-hPa (left) and 500-hPa (right) OWZP at 1200 UTC 18 October 2003.

The OWZP has been designed to detect when a TC develops especially in coarse-resolution NWP and climate models. When applied to our high-resolution simulation of Typhoon Ketsana, it is still a good indicator of TC formation when the grid distance decreases to 27 km, but the threshold of the parameter has to increase to about 1000. When grid distance decreases to 9 km the OWZP starts to scatter, the maximum value at the vortex core to indicate the formation of TC can still be identified at both the low and mid levels. At 3-km resolution mostly the scattered convective-scale vorticity patches remain and there is little organization to indicate the TC formation. Thus, it can be concluded that 10 km seems to be the scale threshold of applying the OWZP concept to detect TC formation if the object under analysis is mainly direct numerical model outputs (e.g., for real-time forecast). Nevertheless, if the meso-γ vorticity is analysed, the OWZP should be a useful predictor of TC formation that utilises high-resolution numerical models.

Through examination of budget of the moist entropy (through surface and tropopause fluxes, temperature tendency due to radiative heating, and a term related to moisture input and gross moist instability), Raymond et al. (2011) argued that the column moist entropy tendency is likely positive during TC development. This is particularly the case when there are large bottom-heavy convective mass fluxes and subsequently the lateral moisture inflow would be large. With such large convective mass fluxes, low-level vorticity tendency would be positive as well, which is necessary in spinning up a TC.

Raymond et al. (2011) further examined the correlations between the column moist entropy and the midlevel OWZP and vorticity, respectively, for several tropical disturbances observed during the Tropical Cyclone Structure 2008 (TCS-08) field experiment in the western North Pacific. Indeed it was found that for the developing TCs with high OWZP values, the moist entropy tendencies are positive, while those non-developing disturbances have low OWZPs and negative moist entropy tendencies. Accordingly, quite high correlation exists between these two parameters, which was found by Raymond et al. (2011) to be even higher than that between the midlevel vorticity and OWZP. The latter is expected due to the definition of the OWZP as a measure of rotation.

When the correlation between moist entropy tendency and OWZP in the simulated Typhoon Ketsana is examined (i.e., showing the relationship during the evolution of the TC), it is found that the best relationship is shown in domain 1 of the simulation and the correlation at 500 hPa is better than that at 850 hPa (Fig. 4.11). In domain 2 and 3, the

average entropy tendencies are very small in values, which is likely due to the cancelling effect between the updrafts and downdrafts. This is consistent with the area average results presented in Raymond et al. (2011) with areas covering the tropical disturbances and coarse resolution of observations. While the potential utility of using the moist entropy tendency as a forecast parameter for TC formation has been emphasised in their study, the implication from our numerical simulation is that such relationship is best applied to the model results in which aggregation of vortices (as discussed associated with the merger index) is realised. Under the scale similar to the resolution of domain 1 of our simulation, both the entropy tendency and OWZP depict the system-scale development after the upscale processes from the fine domains have been taken into account, and thus showing a significant relationship between the two parameters. Such model-based application of using the moist entropy tendency to predict TC early development should be further explored based on extensive case studies.

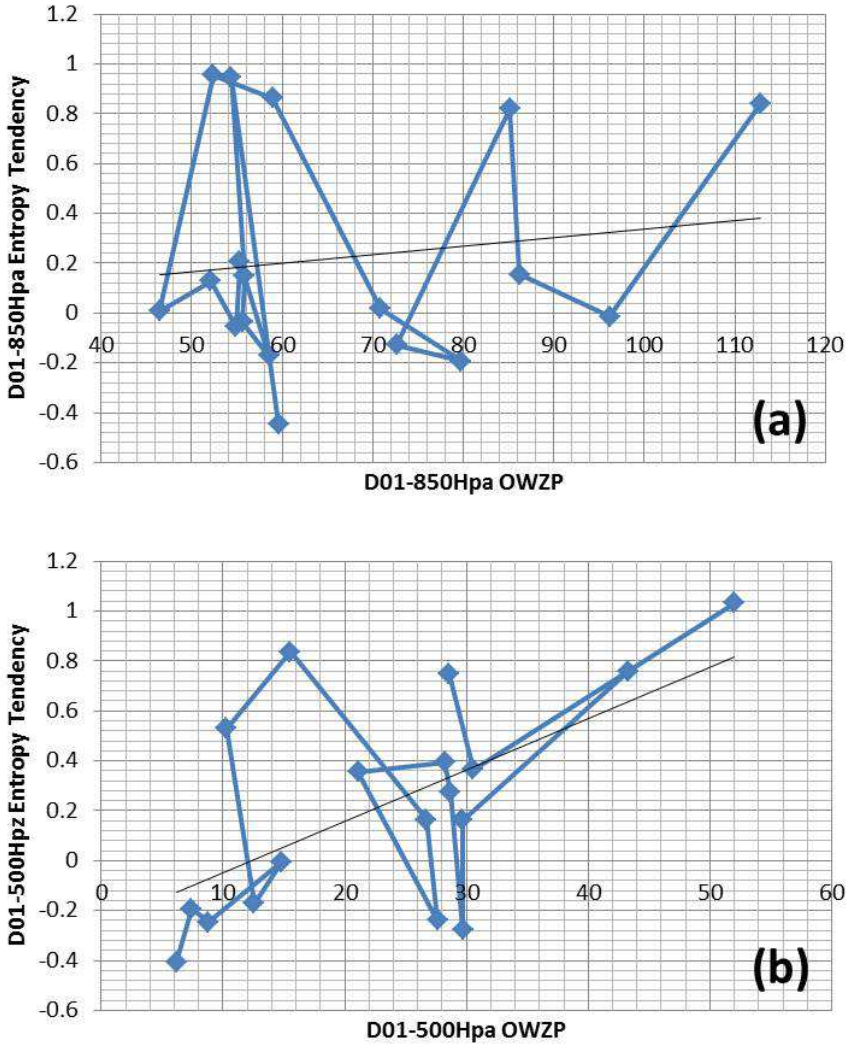

Fig. 4.11 500-hPa moist entropy tendency versus relative vorticity in the simulated Typhoon Ketsana. The data points are 3-hourly time series from 1200 UTC 16 October to 1500 UTC 18 October 2003.

Chapter 5 OBSERVED WARM CORE DEVELOPMENT AS REVEALED BY MICROWAVE SOUNDING DATA

5.1 Chapter overview

In this chapter, the warm core structures of 17 TCs that occurred in monsoon trough of WNP were analysed via examination of the AMSU-A brightness temperature data obtained from the NOAA-15, NOAA-16, NOAA-18 and METOP-2 satellites. Further, numerical simulation was carried out to analyse the warm core structure of a typhoon case. The simulations identify the secondary warm core development during early intensification, which cannot be illustrated by microwave data. Budget of the potential temperature tendency shows that vertical advection is the major mechanism of warming. While the upper-level warm core is more directly linked to diabatic heating, the low-level one after TC formation is associated with mesoscale decent of air, which is likely due to MCS activity leading to formation.

5.2 Introduction

The warm core of a tropical cyclone (TC) is one of its unique features that distinguishes it from other weather systems. However, since TCs spend most of their lifetimes over the oceans, the process of developing the warm core structures was never well observed except when there were aircraft surveillance observations. Such surveillance observations are only available over the Atlantic Ocean and occasionally WNP. Some recent studies emphasised that the process of warm core formation in TCs

has not been well studied (Stern and Nolan 2012; Dolling and Barnes 2012; Stern and Zhang 2013), and there are still a lot of unknowns on the associated mechanisms. Nevertheless, the generation of the warm core is a good indication of when an incipient vortex develops to a mature TC structure. Bessho et al. (2010) identified warm-core structures in organised cloud clusters by the Advanced Microwave Sounding Unit (AMSU). It was found that with a certain threshold of temperature anomaly the lead time from the detection of warm-core structure to TC formation can be more than one day. Moreover, most of the cloud clusters that did not have warm-core structure eventually dissipated and did not develop to TC. Thus, the detection of warm-core structure may improve the forecast of TC formation.

Stern and Nolan (2012) pointed out that the typical height of warm core development in the upper troposphere (> 10 km), which has been widely accepted, was likely due to the coarse resolution of satellite observations such as AMSU from which the conclusion was drawn. Stern and Nolan (2012) demonstrated this by performing an idealised, high-resolution simulation of TC development and then reduced the resolution of the simulated warm core by coarse graining. Further simulations with varied initial vortex and microphysics showed that warm core generally developed at 4-8 km, and sometimes there was a weaker, secondary warm core near 13-14 km. It was also argued that thermal wind balance does not restrict the location of the warm core to where maximum vertical shear of tangential wind or maximum radial temperature gradient is found.

In general, the development of the warm-core structure is due to the diabatic heating at the eyewall. When the inner-core temperature anomaly increases at the mid to upper

levels, the static stability increases and then the TC reaches a steady state. Consequently a dynamical balance is obtained between the TC circulation, especially the transverse circulation (e.g., Vigh and Schubert 2009), and the temperature field. However, depending on the synoptic environment there are possibly different mechanisms of developing the warm-core structure during the formation stage and early development stage. For example, Dolling and Barnes (2012) reported that during the development of Hurricane Humberto (2001) a pathway existed for a MCS accompanied by a MCV to evolve into the warm-core structure. The MCS develops an area with anvil stratiform cloud in the trailing edge of major convection. The mesoscale descent in that area induces dry adiabatic warming in the lower troposphere and subsequently an inversion layer that caps the boundary layer. When air in the boundary layer flows into the eye region, energy is released under the cap on the down shear side of warm core and generates cumulonimbi that become the eyewall. Note that this pathway is quite consistent with the possibility of warm core development in the lower troposphere.

In other scenarios of TC formation that develop from initially cold-core, low-level wave disturbances such as pre-Hurricane Felix (2007) as simulated by Wang et al. (2010), the sustained deep moist convection in the centre of the wave pouch played an important role in spinning up the deep-tropospheric cyclonic vortex. It was found that both convective and stratiform heating contributed to developing the warm-core structure. However, it was also identified that the temperature tendency in the moist inner core of pre-Hurricane Felix came from a small residual between convective heating and the cooling of adiabatic ascent. This result is quite consistent with a recent study of Stern

and Zhang (2013) that simulated an idealised TC. It was found by Stern and Zhang (2013) that during rapid intensification although advection of potential temperature was the significant term contributing to warming the eye, there was actually mean ascent in the region. Thus, advective tendency of temperature is cancelled by diabatic cooling to a certain degree, and subgrid-scale horizontal diffusion of potential temperature was identified to play an unexpectedly important role to maintain the warm-core structure.

Recently, Ohno and Satoh (2015) discussed another pathway to form an upper-level warm core in the lower stratosphere. It was found through their idealised numerical experiments that diabatic heating in the troposphere is not the primary reason for the upper-level warm core, but when the vortex is tall enough the lower stratosphere would respond by subsidence and thus heating. Dynamically, this process is by angular momentum transport into the lower stratosphere, which is likely due to convective bursts.

Techniques of temperature retrieval from remote-sensing data have been improving rapidly. Besides the fundamental limitation on spatial resolution, what are the other issues in applying such techniques to deduce the warm-core structure in TCs? Moreover, what factors determine the height of the warm core? Are there specific environmental conditions under which a secondary warm core forms? The objective of this study is to explore the possible answers to these questions through examination of satellite observations and numerical modelling. The organization of this Chapter is as follows. Section 5.3 documents the TC cases for analysis, data utilised and the processing procedure for the datasets. Section 5.4 focuses on the observed warm cores and interpretation of processes based on convective patterns of TC formation and limitations

in the datasets. With Typhoon Ketsana (2003) as the case study, section 5.5 compares the observed and simulated warm core in this typhoon, and discusses the potential pathways to different warm core configurations.

5.3 Data and Methodology

5.3.1 TC Cases for Analysis

The literature reviewed in the introduction shows that there is variability in the development of warm core, which may be due to the synoptic to mesoscale systems involved. While it is not feasible to analyse all the synoptic patterns and scenarios, this study focuses on the TCs that develop in the monsoon trough region of the WNP. A total of sixteen TCs over the WNP during 2007-2011 have been analysed, which include Sypertyphoon Manyi (2007), Megi (2010), Songda (2011), Muifa (2011), Nalgae (2011), Typhoon Fengshen (2008), Hagupit (2008), Jangmi (2008), Morakot (2009), Parma (2009), Lupit (2009), Kompasu (2010), Fanapi (2010), Chaba (2010), Roke (2011) and Nesat (2011). In addition, Typhoon Ketsana (2003) has been studied in details in Chapters 3 and 4 through numerical simulations, and it is a typical case of monsoon trough formation in the WNP with multiple MCSs during formation. Therefore, this case is applied again here to discuss the several pathways to warm core generation. Numerical simulation using the WRF model, with assimilation of the QuikSCAT oceanic winds and SSM/I surface wind speed and total precipitable water, is as depicted in Chapters 2 and 3 for Typhoon Ketsana.

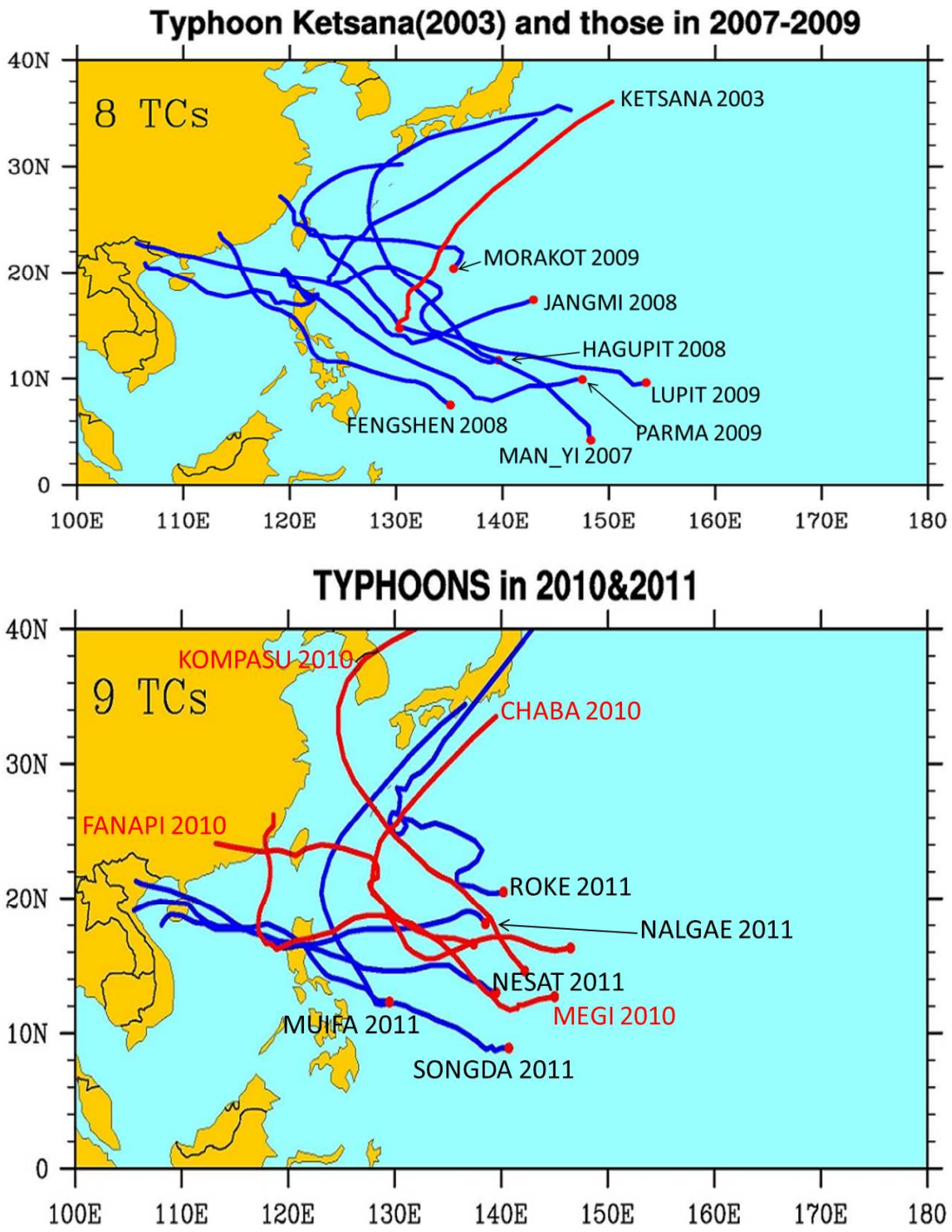

Fig. 5.1 Best tracks of the Typhoon Ketsana (2003) and sixteen other TCs during 2007-2011 for analysis in this study.

Except Supertyphoon Songda (2011) that developed in May, all the other cases developed in the peak season in the WNP from June to October. Similar to Typhoon Ketsana (2003), most of these sixteen TCs that have been selected originated from the monsoon trough at latitude around 15°N. Then they moved westward or northwestward during intensification (Fig. 5.1).

Best-track data from the U.S. Joint Typhoon Warning Centre (JTWC) for the selected typhoon in this study are used to indicate their formation times, motions and intensities. The JTWC best tracks usually start when the incipient disturbances reach an intensity of 20 kt (10.29 m s^{-1}) or 25 kt (12.86 m s^{-1}). The first warnings in these best tracks are considered the formation times of these typhoons, followed by the early development period. For examination of convection during the TC formations, images from the infrared channel with wavelength 11 μm from the Multi-functional Transport Satellites (MTSAT) are used, such as in the monitoring of MCS developments in the early stages of these TCs.

It is well known that the monsoon trough region is favourable for MCS development, and thus MCSs are quite common during the formation of TCs in the monsoon trough (Lee et al. 2008). It has been identified in Lee et al. (2008) that the percentage of TC cases in the monsoon trough with MCS occurrences at multiple times 48 h before formation is higher than 63%, and up to about 35% of cases have multiple MCSs at the same time. Similar situation applies to the sixteen TCs analysed herein. At least one MCS developed in each of these TCs and up to three MCSs are identified during the TCs' formation. Besides the dynamical effect of possible spinning up of a midlevel vortex,

MCS has its typical stratiform heating (vertical) profile.

5.3.2 Temperature Retrieval from Microwave Data

This study applies the AMSU-A brightness temperature (TB) data obtained from the NOAA-15, NOAA-16, NOAA-18 and METOP-2 satellites. The AMSU-A, which possesses 12 channels at the 55-GHz (oxygen absorption) frequency band, is a valuable instrument for observing atmospheric temperature profiles (Oyama 2014). These 12 channels have vertical weighting functions, which indicate the contribution of radiance from the respective atmospheric layers, with peaks from surface up to 2.5 hPa. Half of the channels have weighting functions that peak below 100 hPa and thus they are able to retrieve temperatures in the troposphere.

The AMSU-A instrument certainly has its own weaknesses. The primary one is that the instrument is affected by the variation of the atmospheric optical path length between the surface and top of the atmosphere along the scan line of the satellite. On the other hand, the AMSU-A data is limited in resolution, which is usually larger than 48 km and not quite enough to resolve detailed structures in TCs. The Field of View (FOV) size along the scan line of the AMSU instrument is not uniform, and the TB values' dependence on such FOV size has to be considered. A more serious issue about accurate temperature retrieval is the microwave scattering (i.e., Mie scattering) effect of ice particles, which would cause attenuation of the signal in cloudy areas such as the eyewall and spiral bands in TCs.

For this study, AMSU-A Level 1B data are obtained from the National Oceanic and

Atmospheric Administration (NOAA)/Comprehensive Large Array-data Stewardship System (CLASS) website (http://www.class.ncdc.noaa.gov/saa/products/welcome) and converted to Level 1C data, which is geo-referenced and calibrated TBs, by using ATOVS and AVHRR Pre-processing Package (AAPP) software (Atkinson, 2011). The limb adjustment technique is then applied to correct these Level-1C TBs from each AMSU-A channel (Goldberg et al., 2001; Demuth et al., 2004) to reduce the effect of the atmospheric optical length on the TB fields.

5.4 Observed Evolution of Warm Core Structure

Microwave data from the AMSU-A 55-GHz channels and the high-frequency 89-GHz (the C15) channel, together with IR satellite images are used to examine the warm core development in the typhoons during 2007-2011. It is found that the variability in the warm core development among the typhoon cases can be quite well monitored by these datasets with precautions in the limitations of the datasets. Several examples from 2011 are discussed here. Typhoon Songda developed from a MCS-like core convective area (Fig. 5.2) in late October 2011. At the formation time of 0600 UTC 20 October, the TBs from AMSU-A already showed an upper-level warm area at 200 hPa collocated with the core convection. However, at the slightly lower levels such as 350 hPa, negative TB anomaly is shown, which is consistent with the signal attenuation in the 89-GHz C15 channel. Although this channel 15 is sensitive to signals near the surface, its observations are also easily attenuated by rain particles, including ice, in all layers in the troposphere. Thus, the ice particles have likely affected the C15

signal on the eastern side of convective core developing into Typhoon Songda. If the TB anomalies west of this area are examined, the warm core has actually developed to the midlevels (Fig. 5.3).

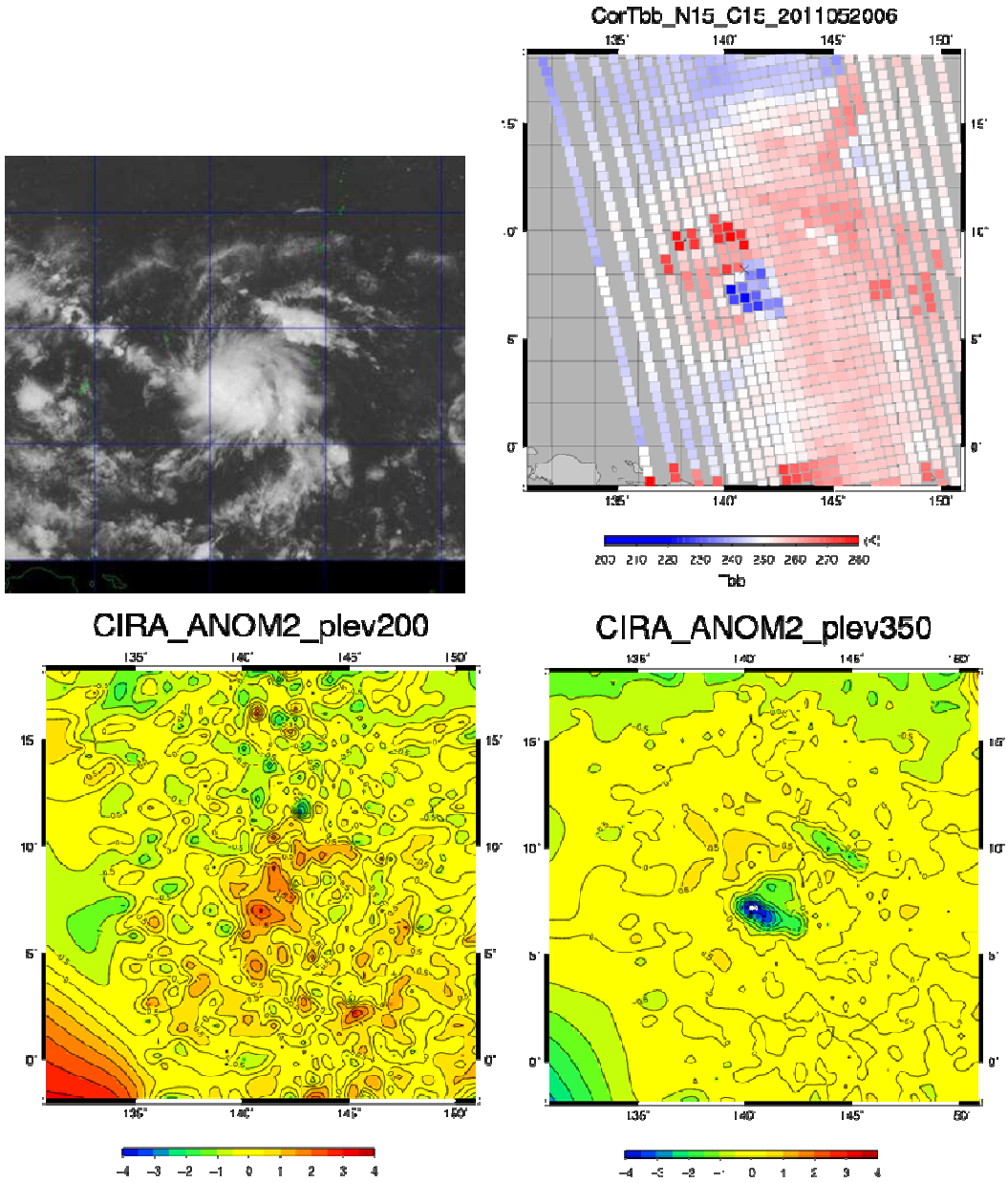

Fig. 5.2 Infrared satellite image (upper left), AMSU-A channel-15 (C15) TB at 0600 UTC 20 May 2011 (upper right) and TB anomaly from the 55-GHz channels at 200 and 350 hPa (lower) for Typhoon Songda.

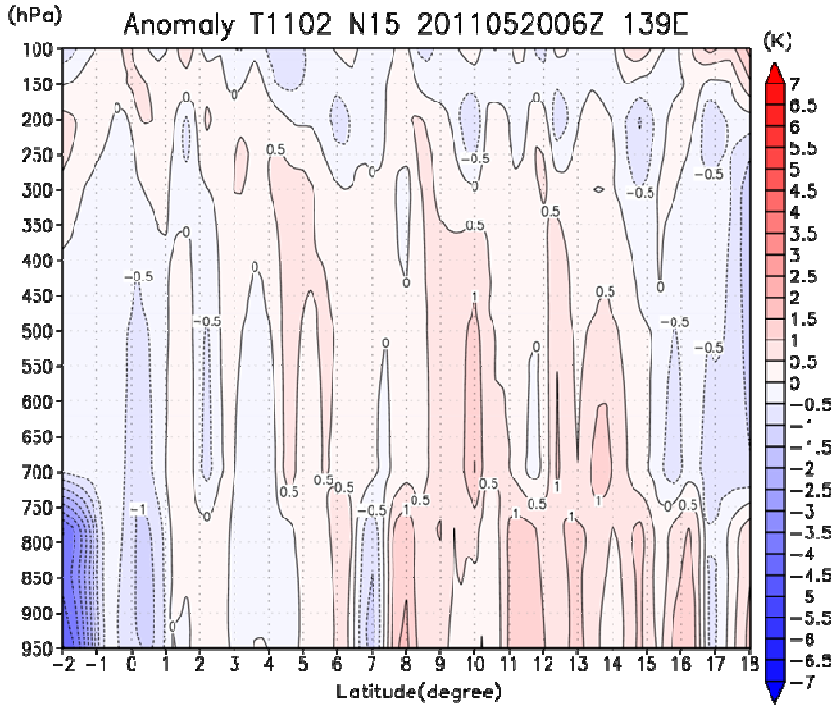

Fig. 5.3 Vertical cross section at 139°E of the channel-15 TB at 0600 UTC 20 May 2011 for Typhoon Songda, showing the midlevel warm core between 9-10°N.

A similar situation occurred for Typhoon Muifa that formed in July and also from an area of deep core convection (Fig. 5.4). For Muifa, the warm TB anomalies are as high as 4 °C in the centre of the core convection. Such anomalies are still clearly shown at 350 hPa with a small area of signal attenuation, which is consistent with the C15 observations.

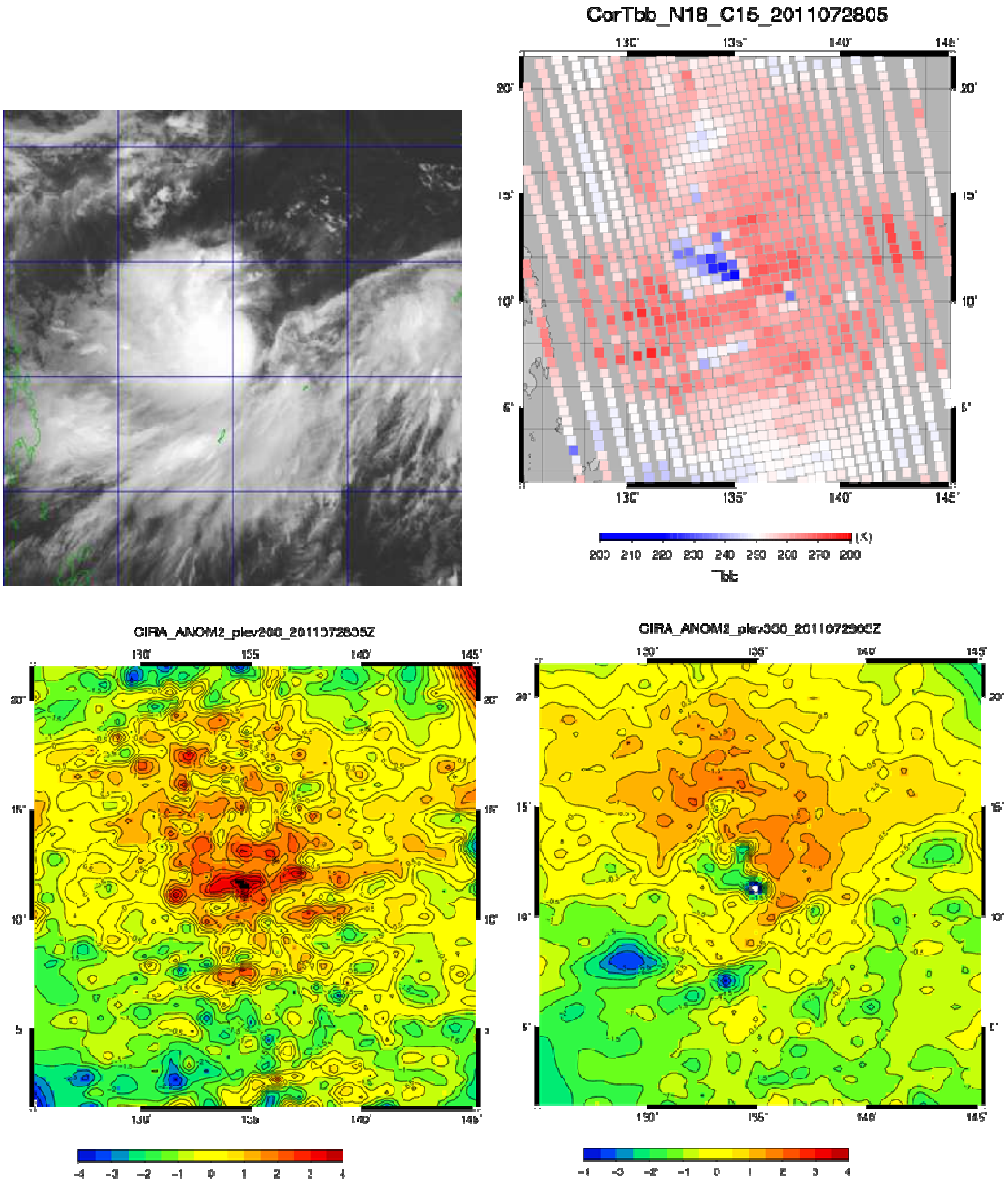

Fig. 5.4 As in Fig. 5.2 except at 0500 UTC 28 July 2011 for Typhoon Muifa.

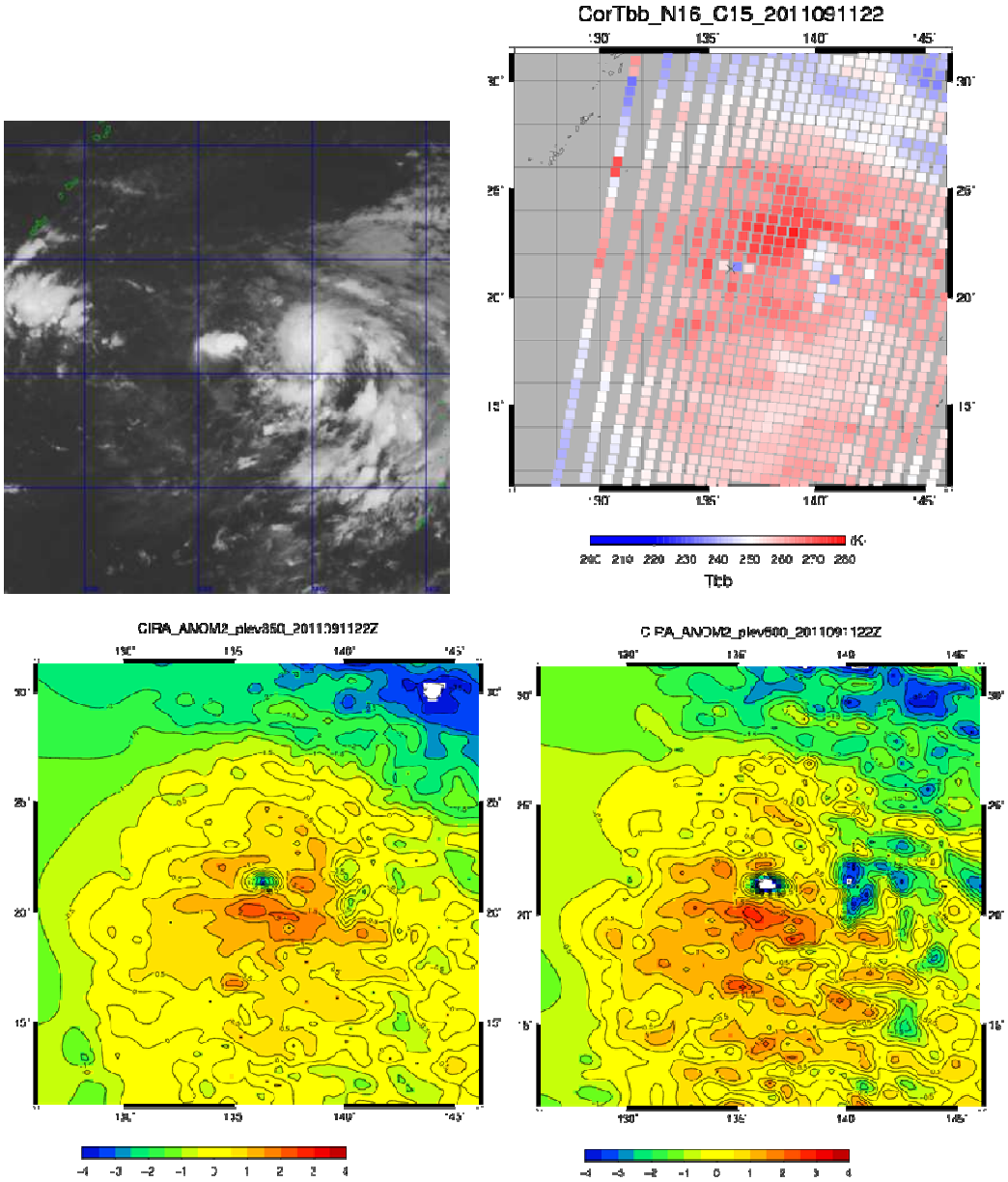

Fig. 5.5 As in Fig. 5.2 except at 2200 UTC 11 September 2011 for Typhoon Roke. The TB anomalies from the 55-GHz channels (lower panels) are at 350 and 500 hPa, respectively.

Typhoon Roke that developed in September 2011 formed within a tropical depression with cyclonic flow, and up to three MCSs are involved in the typhoon's formation (the IR satellite image in Fig. 5.5 shows one of them on the eastern side of circulation). By 2200 UTC 11 September, about ten hours after formation, the AMSU-A TBs show that warm anomaly has developed on the southern side of the broader-scale cyclonic circulation and down to at least the midlevels around 500 hPa (Fig. 5.5 lower panels). At the same time, the deep convection near the centre of circulation is indicated by negative TB anomaly in both the 55-GHz and C15 channel. In fact, this small area of negative TB is down to the surface at about 136°E, but to the east of this area, the warm core associated with Typhoon Roke is down to the low levels too (Fig. 5.6). Therefore, if the signal attenuation problem is interpreted according to the pattern of convection during TC formation, the warm core development process can be quite well monitored by utilizing information from the AMSU-A channels.

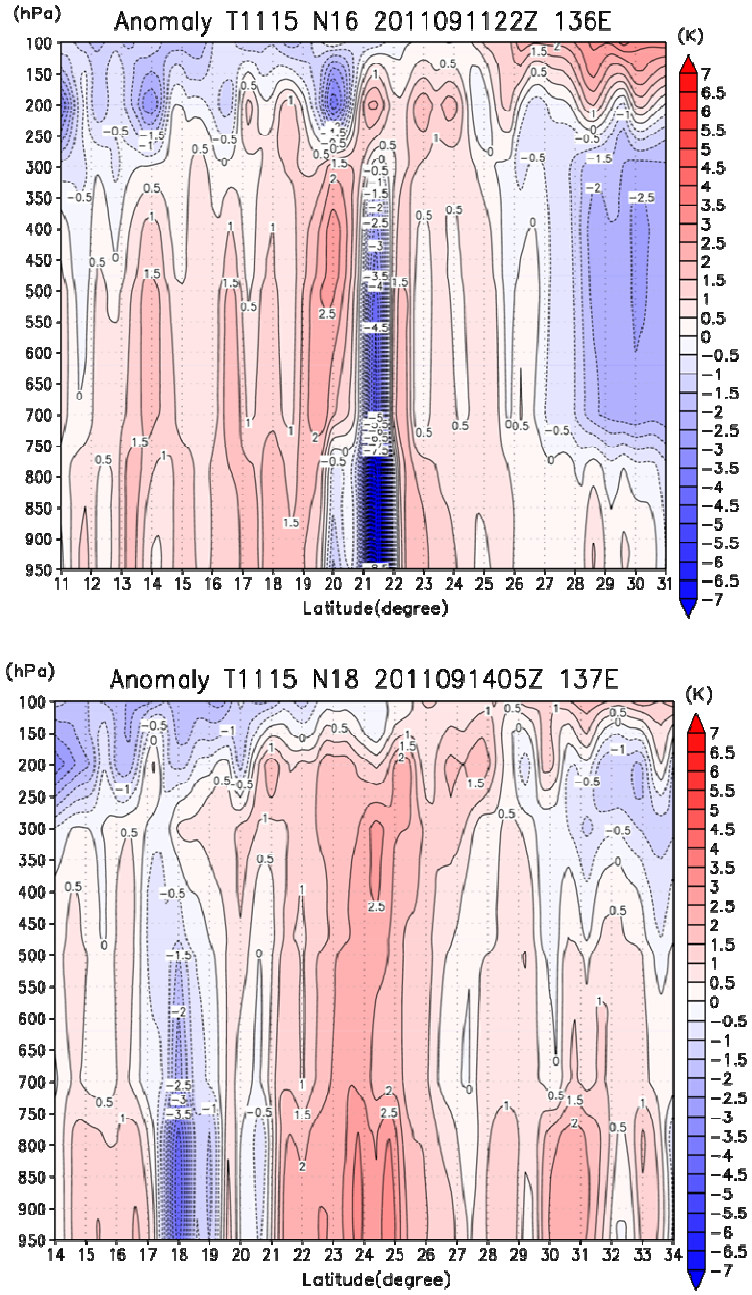

Fig. 5.6 As in Fig. 5.3 except with longitudes 136°E and 137°E at 2200 UTC 11 September 2011 for Typhoon Roke.

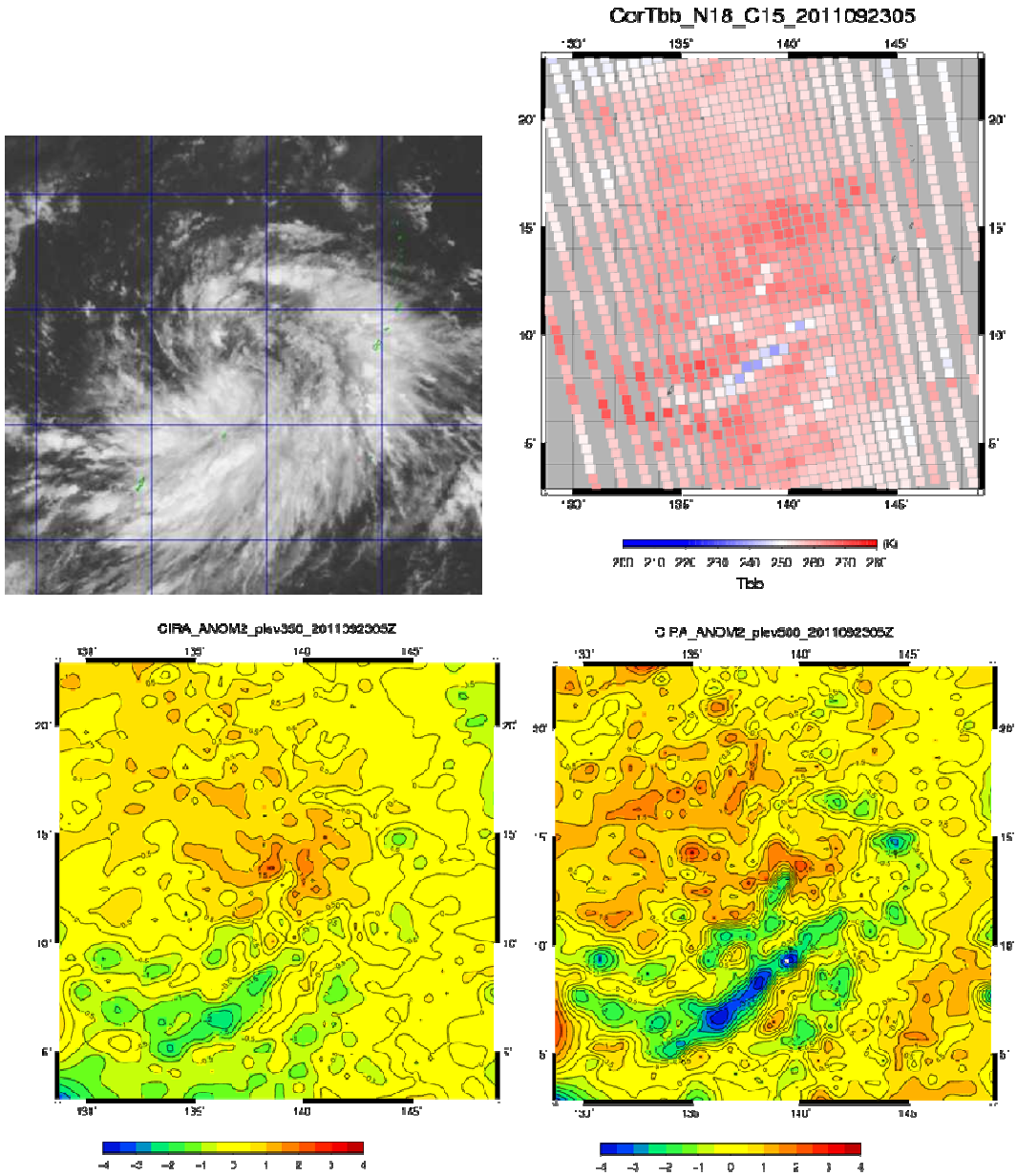

Fig. 5.7 As in Fig. 5.2 except at 0500 UTC 23 September 2011 for Typhoon Nesat.

To add two other examples to this discussion, Typhoon Nesat in September of the year also involved two MCSs during formation. At the time of its formation, rainband structure dominated and the rainbands were advected into the broad-scale tropical depression (Fig. 5.7). The deep convection in the two line-shape rainbands in this early

stage of Typhoon Nesat is clearly shown as a negative TB anomaly in the AMSU-A channels with much attenuation at the midlevels. However, the warm core is still clearly shown in the core part of TC circulation from the mid to upper levels.

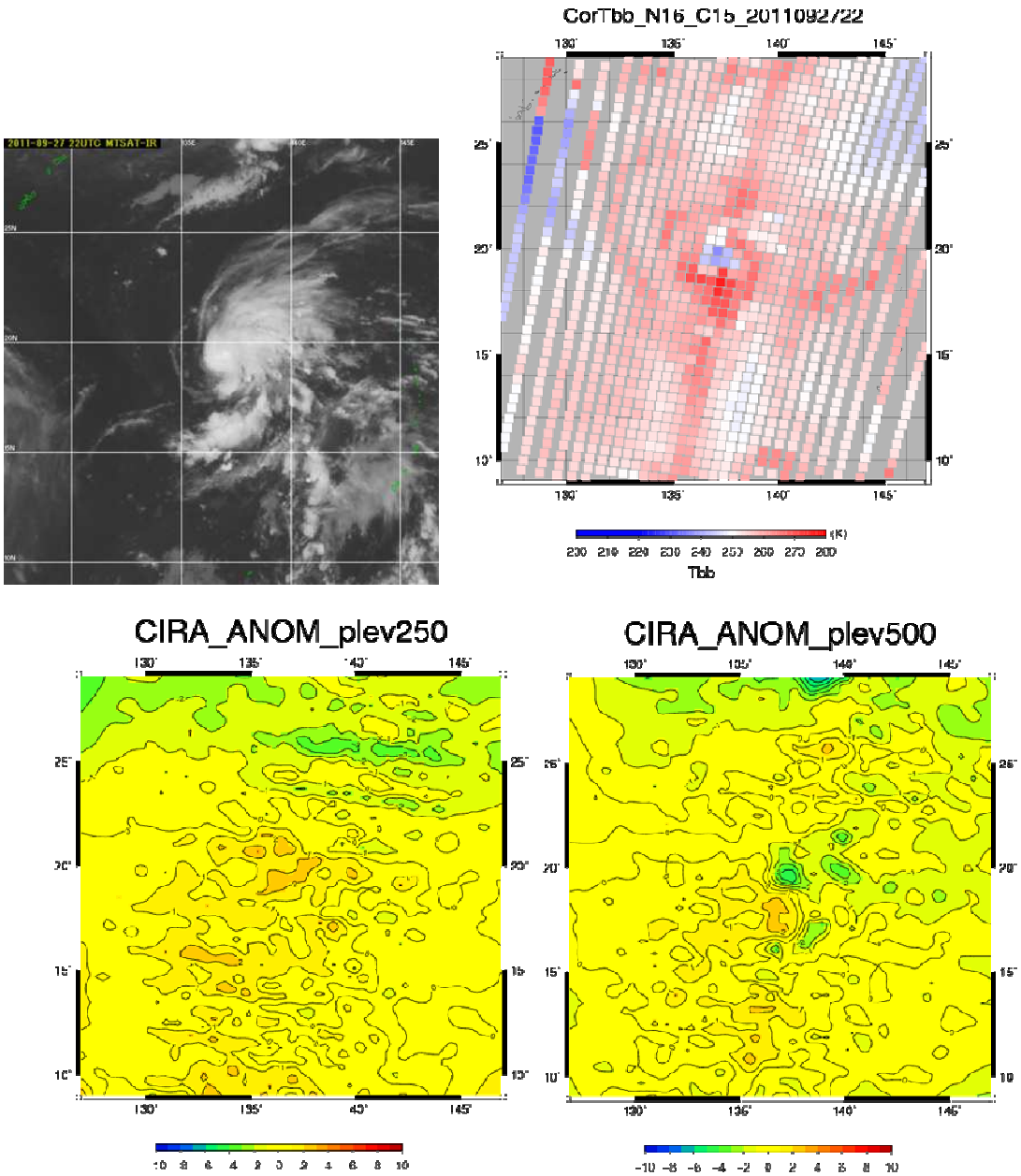

Fig. 5.8 As in Fig. 5.2 except at 2200 UTC 27 September 2011 for Typhoon Nalgae.

On the other hand, Typhoon Nalgae was a midget TC that involved only one MCS-like core convection (Fig. 5.8). Warm TB anomaly is shown at the upper levels but becomes negative near the midlevel. The five TCs that have been discussed here represent most of the sixteen samples with midlevel warm core development. Of the other eleven cases, only three have such development as depicted by AMSU data, which are Typhoon Morakot (2009), Typhoon Kompasu (2010) and Typhoon Chaba (2010). There is actually variability among these three cases when they approached their respective lifetime maximum intensity. Typhoon Morakot showed clear low-level heating and temperature anomaly; Typhoon Kompasu showed a clear upper-level warm core and a separate low-to-mid-level one; while Typhoon Chaba had its upper-level warm core extended to the midlevel (not shown). For the remaining eight TC cases, typical upper-level warm cores centred at about 200 hPa are observed, accompanied by cold anomalies underneath. As discussed in the introduction, such height estimation of the warm core may depend on the resolution of observational data. Nevertheless, since it has been demonstrated by the cases discussed here that AMSU data is capable to resolve the midlevel warm core development, indication of the typical upper-level warm anomaly should be quite robust.

In short summary, the utilization of the information from various channels of AMSU-A microwave data, with proper interpretation of the limitations on applications, is able to indicate the warm-core development processes in TCs well. This conclusion is based on examination of the warm core developments in the typical monsoon trough TC formations in the WNP. For many midget TC formations, the deep convection within a

small area (similar to a MCS or even smaller) contains dense rain water and ice particles that attenuate the microwave signal. However, outside such deep convection area, the warm core from upper level down to the midlevel can still be indicated by microwave data. For TC formations from broader-scale tropical depression, which are often embedded in monsoon trough, warm core develops within the centre of the depression due to dynamics adjustment between temperature and winds. If the major deep convection is in the outer rainbands, microwave signal attenuation in the core may not be significant and the TB anomaly is able to show the warm core development in the vertical direction clearly. As an application, the AMSU-A TB data can well be used to estimate cloud cluster organization and TC formation in advance, as has been demonstrated in Bessho et al. (2010). Note that these results do not contradict the conclusions from studies such as Barnes and Nolan (2012) that remote-sensing data mostly overestimates the height of TC warm core due to low spatial resolution and signal attenuation. Indeed, if areal average of the AMUS-A TB anomalies is computed at different levels and the three-dimensional structure of warm core is examined, the warm core height will be biased to the upper levels due to the low-level scattering problem and inclusion of the low TB anomalies in the computation. As has been demonstrated, if the evolution of convection pattern during TC formation is considered, the microwave-retrieved TB is a valuable resource to monitor the thermodynamic development in TC.

5.5 Typhoon Ketsana (2003)

5.5.1 Observed warm core

The formation process of Typhoon Ketsana (2003) has been studied in detail in the numerical modelling of Lu et al. (2012) as well as Chapters 3 and 4. This typhoon is a typical monsoon trough-related formation associated with multiple MCSs. It was found that both the mesoscale and convective-scale processes contributed to the spin-up process of Typhoon Ketsana by increasing the mid to near-surface relative vorticity, but without much attention paid to the warm core structure. The distribution of mesoscale heating (single versus multiple MCSs) has been identified to affect the development rate of the TC (Chapter 3), and system dynamics of the convective-scale systems have been analysed in Chapter 4. In the simulations of Lu et al. (2012) stratiform-type heating has been identified in the regions of the MCSs. Thus it will be beneficial to see whether satellite microwave data can monitor the development process of the warm core within Typhoon Ketsana.

The first episode of MCS development associated with Typhoon Ketsana's development occurred more than two days before its formation around 1200 UTC 16 October 2003. With more direct impact to the formation process, two other MCSs (MCS3 and MCS4 hereafter) developed at about the same time around 1800 UTC 17 October. The AMSU-A and C15 TBs available at 2200 UTC 17 October show that the warm centre already developed (Fig. 5.9). The warm core is clearly seen at the upper levels; however, examination of the vertical cross section in the meridional direction of the C15 data also indicates that warming occurred throughout the lower troposphere.

The latitudes of this warming at about 13-14°N collate with one of the major MCSs developing at that time. Next to this column of heating, cold TB anomalies are found to be due to rain evaporative cooling but signal attenuation problem due to low-level scattering, as discussed before, should contribute too.

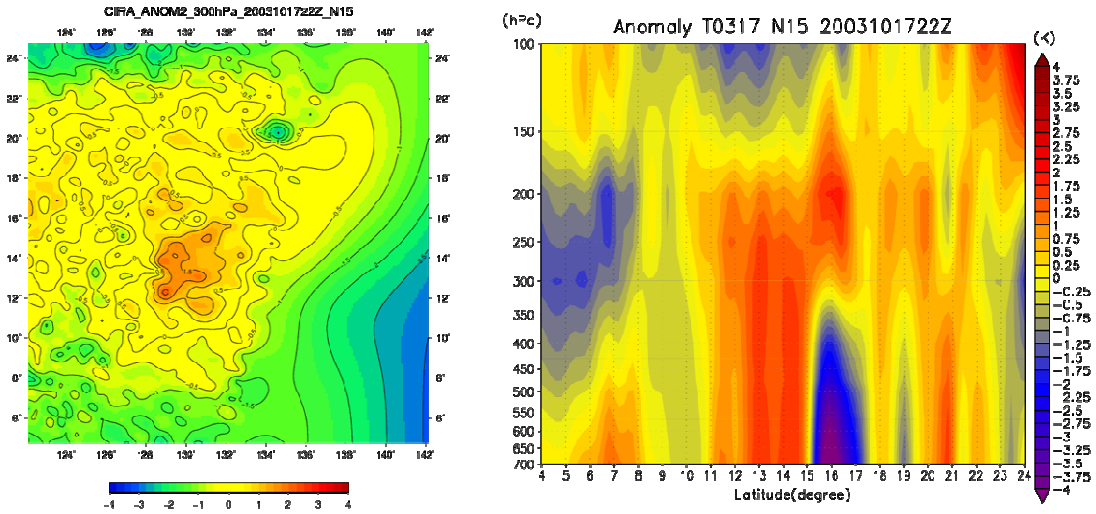

Fig. 5.9 Observed horizontal (left panel, 300 hPa) and vertical distribution (right panel) of TB anomaly at 2200 UTC 17 October 2003 for Typhoon Ketsana.

There was a MCS development (the fifth since two days before formation, MCS5 hereafter) near the core region of cyclonic circulation that directly led to the formation of Typhoon Ketsana at 1200 UTC 18 October. A few hours after this, the upper-level warm core is clearly identified in the AMSU-A TB (Fig. 5.10). Vertical cross section of the C15 data shows that the warm core centre is at about 250 hPa with warm anomaly of over 3°C. After the official time of formation, that last MCS actually dissipated and convective activity within the TC was lower temporarily. The dynamic warm core, on

the other hand, continues to strengthen at about the same vertical level the next day after formation (Fig. 5.11).

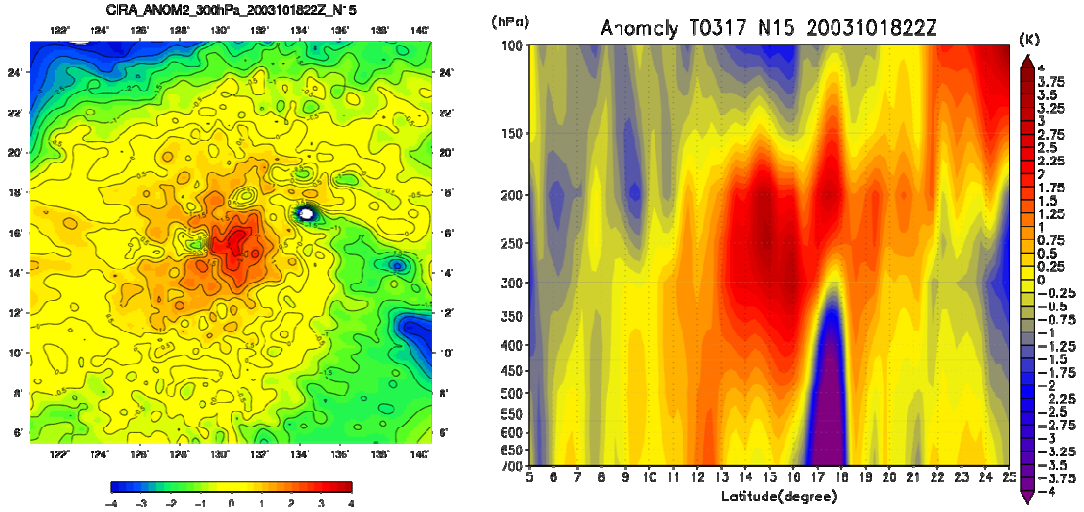

Fig. 5.10 As in Fig. 5.9 except at 2200 UTC 18 October 2003.

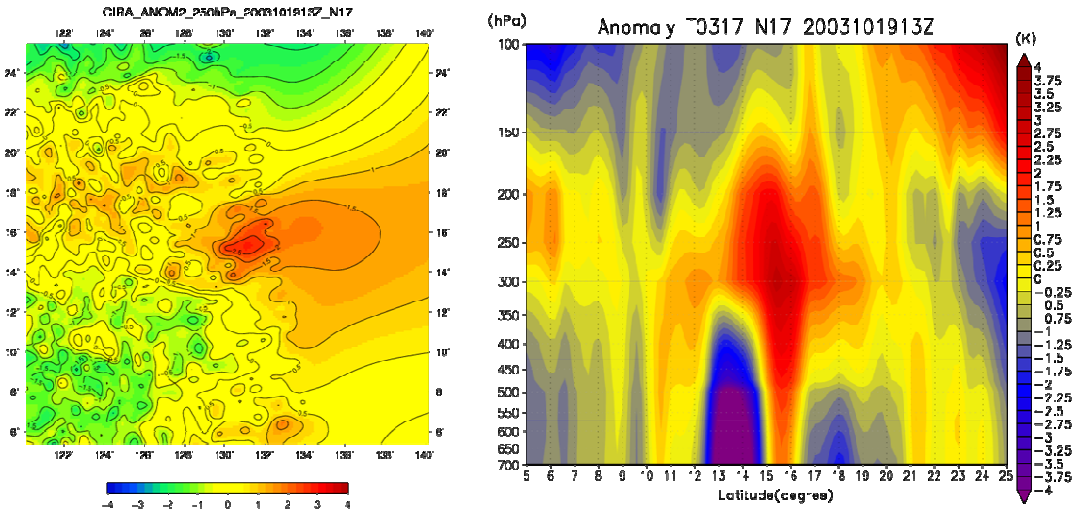

Fig. 5.11 As in Fig. 5.9 except at 2200 UTC 18 October 2003.

5.5.2 Simulated warm core

WRF simulations of the formation process of Typhoon Ketsana are carried out similar to the settings in Lu et al. (2012). It is identified in the WRF simulations that the evolution of the warm core in the typhoon is much more complex than as shown in the satellite microwave data. Every MCS is associated with strong mid- to upper-level heating as typically found in stratiform clouds. However, how these heating associated with the MCSs, especially the early ones, lead to the warm core when the TC forms has not been extensively discussed in previous studies, and will be one of the key questions to answer. The heating associated with MCS3 and MCS4 is northwest of the low-level circulation centre, which is consistent with these MCSs' location (Fig. 5.12 upper).

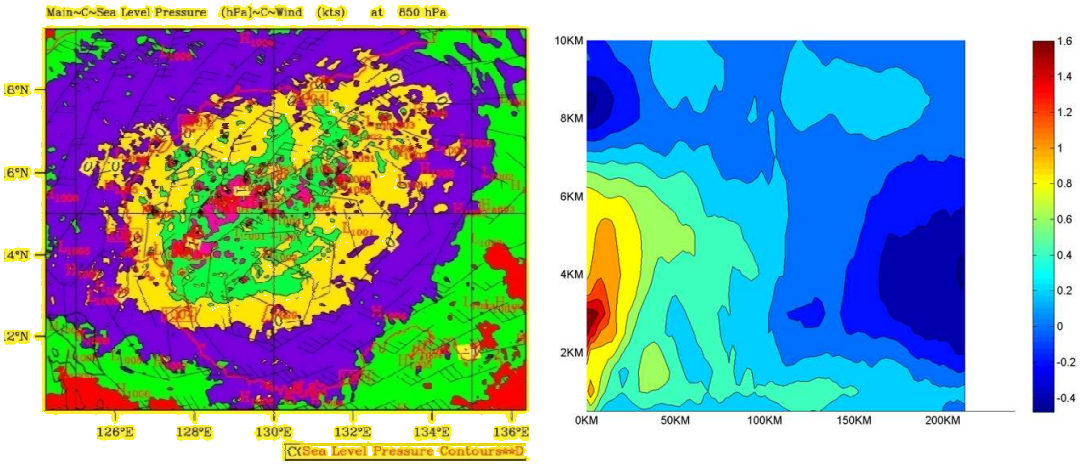

Fig. 5.12 (Left panels) Simulated mean sea level pressure (contour), 850-hPa winds (barbs) and temperature anomaly (shaded) at 1800 UTC 17 October and 0900 UTC 18 October 2003. (Right panels) Simulated azimuthally average of temperature anomaly centred at the surface minimum pressure of Typhoon Ketsana at 1800 UTC 17 October and 1200 UTC 18 October 2003.

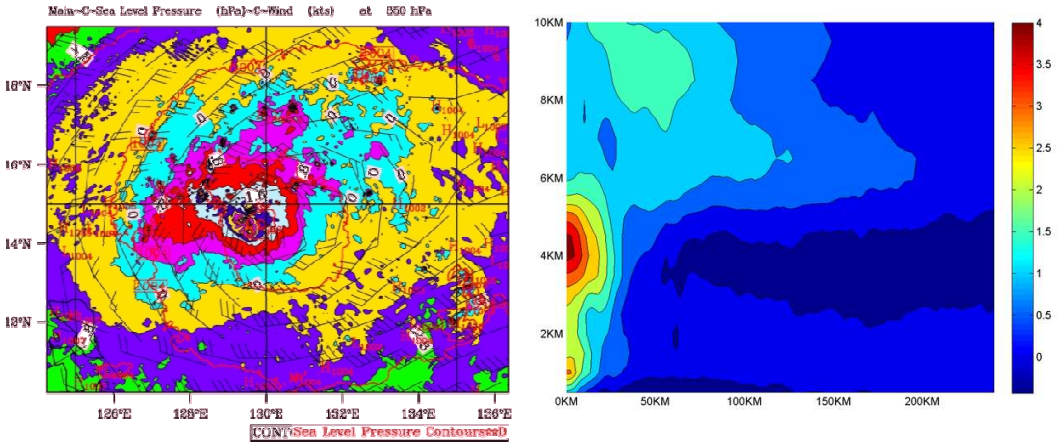

Fig. 5.12 (continued)

Azimuthally average temperature anomaly in the simulation shows that the heating concentrates in the mid to lower level because the strong core convective heating also contributes to these temperature anomalies. The heating diminishes for a while according to the reduced convective activity, and when MCS5 develops its associated heating almost collocates with the surface depression (Fig. 5.12 lower). Eventually this heating of MCS5 persists and develops to the mature warm-core structure of the simulated TC. Thus, it is believed that the inner-core heating associated with MCS5 effectively facilitates the TC formation and development.

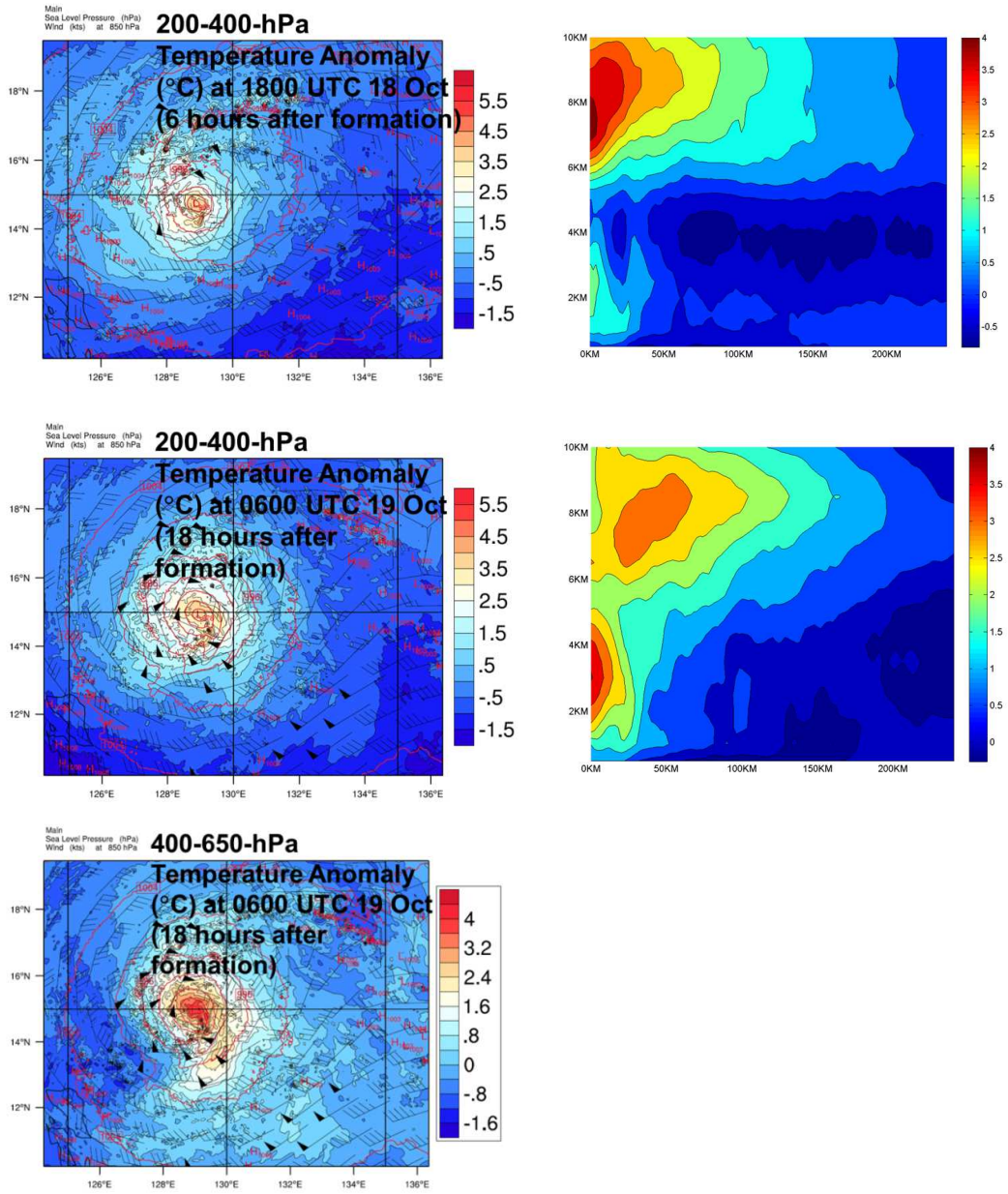

Fig. 5.13 (Left panels) Simulated mean sea level pressure (contour), 200-400-hPa, 400-650-hPa winds (barbs) and temperature anomaly (shaded) at 1800 UTC 18 October and 0600 UTC 19 October 2003. (Right panels) Simulated azimuthally average of temperature anomaly centred at the surface minimum pressure of Typhoon Ketsana at 1800 UTC 18 October and 0600 UTC 19 October 2003.

As in the observed warm core based on AMSU-A data, the simulated warm core a few hours after the formation time also concentrates at the upper level (Fig. 5.13). However, in the next 12 hours a warm centre develops at the low level too and is clearly shown in the 200-400-hPa and 400-650-hPa layer-average temperature anomalies, as well as that azimuthally average. This low-level warm core cannot be verified by the microwave data because the signal attenuation problem is quite serious at those levels (not shown). Thus, numerical simulations provide an effective way to analyse the generation mechanism of this warm core structure.

In general, the development of the warm-core structure is due to the diabatic heating at the eyewall. When the inner-core temperature anomaly increases at the mid to upper levels, the static stability increases and then the TC reaches a steady state. Consequently a dynamical balance is obtained between the TC circulation [especially the transverse circulation, see Vigh and Schubert (2009)] and the temperature field. However, depending on the synoptic environment there are possibly different mechanisms of developing the warm-core structure during the formation stage and early development stage. For example, Dolling and Barnes (2012) reported that during the development of Hurricane Humberto (2001) a pathway existed for a MCS to evolve into the warm-core structure. In other hurricanes that develop from initially cold-core, low-level wave disturbances such as pre-Hurricane Felix (2007) as simulated by Wang et al. (2010), other pathways may exist. Since the low-level warm core in Typhoon Ketsana developed almost right after the last episode of deep convection occurred before the TC formation, it is plausible to assume that adiabatic decent mechanism associated

with MCS proposed in Dolling and Barnes (2012) is a likely pathway to this warm core structure.

5.5.3 Potential temperature budget

To verify the aforementioned ideas, the budget of potential temperature change in the simulated Typhoon Ketsana is examined. In general, the rate of change in potential temperature θ can be decomposed according to the budget equation:

$$\frac{\Delta\theta}{\Delta t} = (adv) + (diab) + (pbl) + (diff) \ ,$$

where (adv) is total advection including that by horizontal and vertical wind, (diab) the diabatic heating, (pbl) the boundary layer parameterization and (diff) subgrid-scale diffusion. Ohno and Satoh (2015) also separated radiation as a budget item but usually that is a very small contribution compared with the others. On the other hand, the (pbl) usually has a small contribution near the surface.

Both Stern and Zhang (2013) and Ohno and Satoh (2015) found that total advection is the dominating term in the budget. Subgrid-scale horizontal diffusion was found by Stern and Zhang (2013) to be important to maintain the warm core structure in the mature phase of storm. In the case of Ohno and Satoh (2015) that analysed the very upper-level warm core, advection by the subsidence in the low stratosphere was identified as the major factor. Thus, we focus on the total advection and diabatic heating versus the total change of θ in this analysis.

After about 6 hours of Typhoon Ketsana's formation, an upper-level warm core forms in the model simulation. The warming is mostly northwest of the circulation

centre with a maximum rate of nearly 3 K per hour (i.e., less than 0.001 K s^{-1}, Fig. 5.14a). During early 19 October, warming at the low level also occurs. The warming is again mostly northwest of circulation centre and maximum rate reaches about 3 K per hour (Fig. 5.14b).

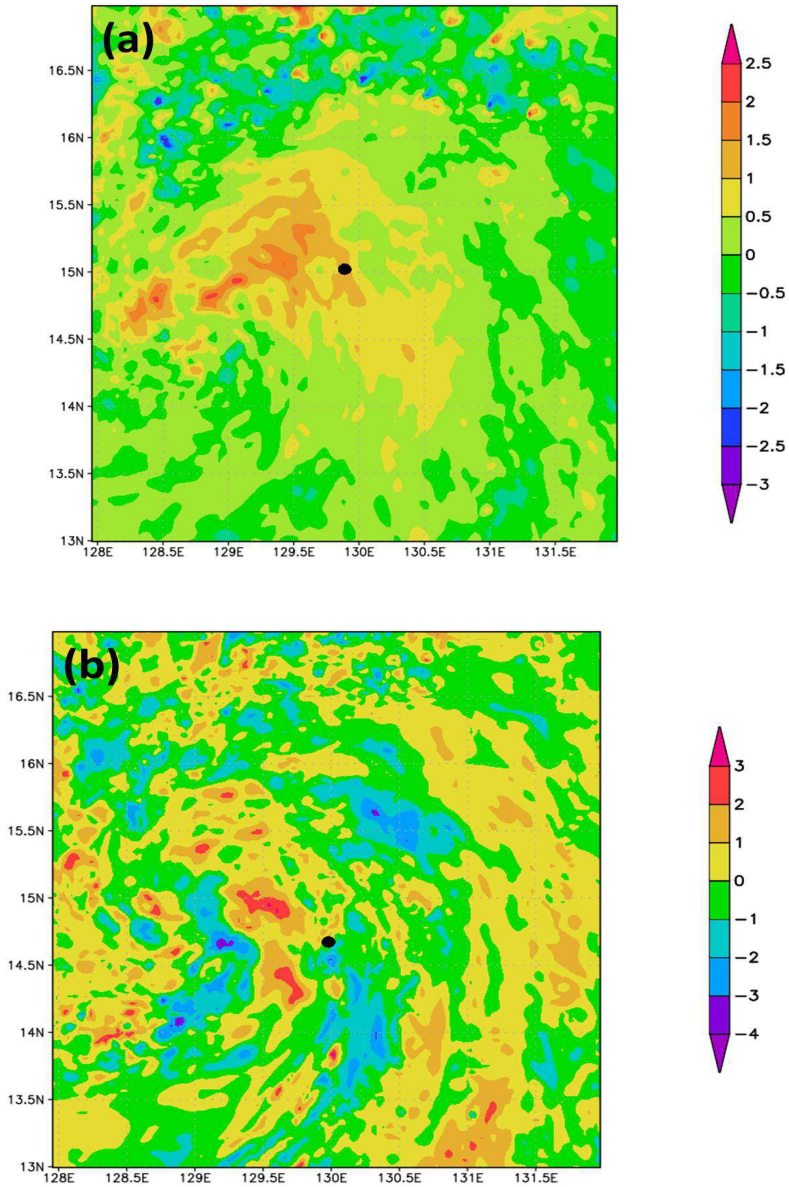

Fig. 5.14 Change in potential temperature (K per hour) in the simulated Typhoon Ketsana at (a) 1900 UTC 18 October, altitude 8 km and (b) 0500 UTC 19 October 2003, altitude 3 km.

Within the total advection contribution to the potential temperature change budget, the vertical advection is found to be much larger than the horizontal advection (by about an order of magnitude). As expected, vertical advection of potential temperature in the high resolution simulation is much affected by the convective-scale updraft and downdraft. Nevertheless, mesoscale regions of warm and cold advection have been identified. A few hours after the formation time of Typhoon Ketsana, the upper-level warm core emerged in the model (Fig. 5.13 upper panels). Vertical advection of potential temperature at 7-8 km altitude indicates a patch of warming near the low-level circulation centre and the last MCS before formation (Fig. 5.15a). Downdrafts, which are southeast of the major convective updrafts, exist in that area, are responsible for the warm advection (not shown). Diabatic heating in the model simulation concentrates at the convective-scale updraft (Fig. 5.15b) and in other locations having cooling. It is noted that the maximum vertical advection of the order of 0.1 K s^{-1} (and with similar contribution from diabatic heating in the updrafts) actually exceeds the change in potential temperature depicted in Fig. 5.14. Thus, advection is offset by diabatic cooling and subgrid-scale diffusion in the budget equation.

It has been discussed that during early development on 19 October, a low-level warm core also developed in the simulation (Fig. 5.13 lower panels). During the first few hours of 19 October, there is warm advection southwest and south of the low-level circulation centre at altitude of 3 km, which is again associated with a mesoscale area of downdraft at that altitude (Fig. 5.15c). Similar contribution from diabatic heating is

found as in the upper-level warm core, which concentrates at the convective-scale updrafts (Fig. 5.15d) initializing from near surface. Outside the updrafts, cooling is found in the other areas.

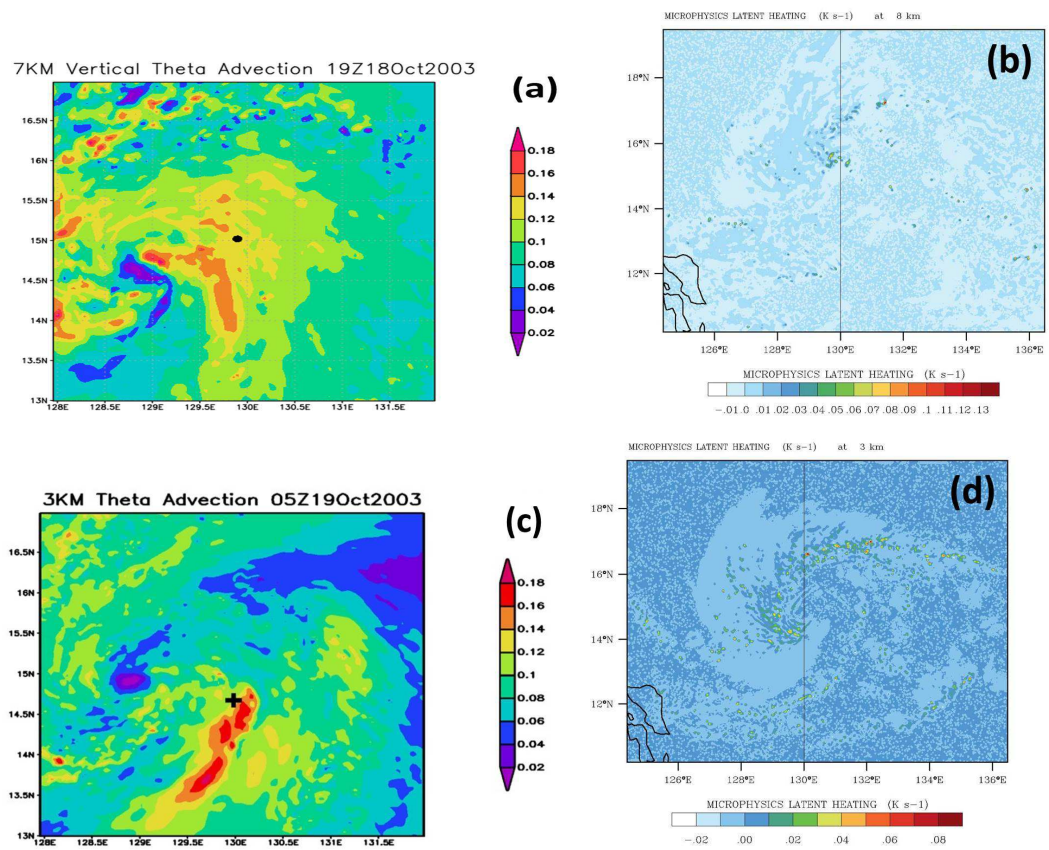

Fig. 5.15 (a) Advection of potential temperature by vertical wind at 7 km (K s^{-1}) and (b) diabatic heating (K s^{-1}) at 8 km at 1900 UTC 18 October. (c) and (d) are as in (a) and (b) except with altitude 3 km at 0500 UTC 19 October 2003.

With such consideration of potential temperature advection, it seems that the hypothesis in Dolling and Barnes (2012) of warming due to mesoscale decent of air (and

companied adiabatic warming) is valid in the simulation of Typhoon Ketsana, with respect to the generation of the initial upper-level warm core right after formation and the low-level one afterward. The association of MCS activity is supported by examination of the vertical profile of vertical velocity, such as that during early 19 October when the low-level warm core develops (Fig. 5.16). The vertical cross section has been selected ahead of the major convection at that time, and within the high resolution simulation domain manifested as small-scale convective cores. The profile is quite typical of stratiform rain region within MCS, with decent of air in the low-to-mid level and updraft aloft. Certainly, at about the same time there exists an upper-level warm core as well, which is likely to be maintained by the diabatic heating of convection at that level.

Although analyses show that the upper-level warm core of the simulated Typhoon Ketsana concentrates below 10 km, the vertical profile in Fig. 5.16 also reveals subsidence of air aloft about 16 km. Thus, the possibility of warming of such subsidence of air to the very high altitudes as has been discussed in Ohno and Satoh (2015) cannot be disregarded.

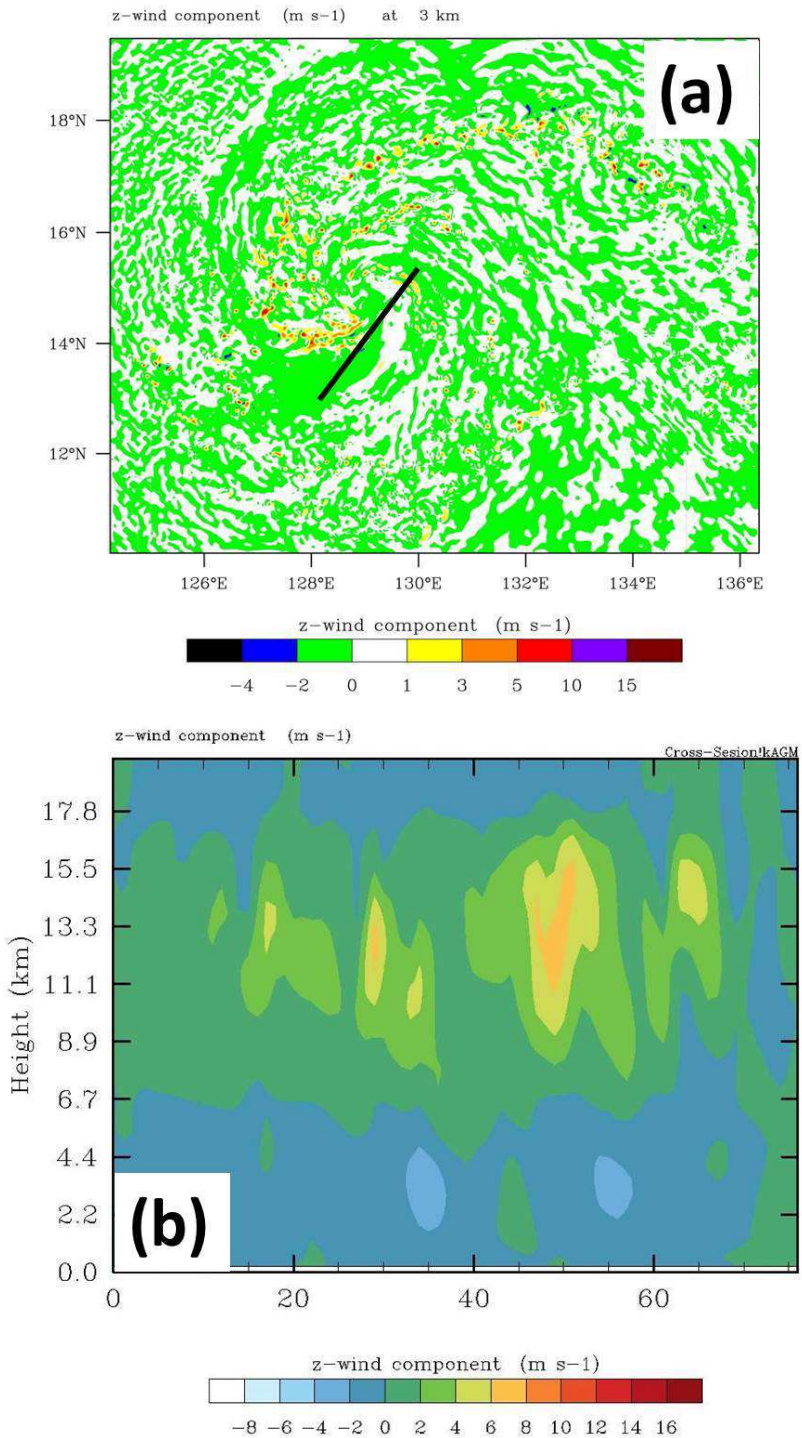

Fig. 5.16 (a) Vertical velocity with altitude 3 km at 0500 UTC 19 October 2003. The vertical cross section at the black line in (a) is shown in (b). Horizontal axis is grid point number.

6 Summary

The motivation of this study is to investigate the roles of MCSs and convective-scale systems during the formation process of TCs including the generation of warm core and its structure. Literature review of related studies and methodology applied are presented in Chapter 1 and 2 respectively, followed by analysis work in the later chapters. Both numerical and observational studies are carried out to investigate the mechanisms involved in the formation process and early development stage of TC. The conclusions that have been drawn from these results are summarised in this chapter.

The simulation of the formation of Typhoon Ketsana (2003) using the WRF model is analysed as follow up to the earlier study of Lu et al. (2012). While Lu et al. focused on the role of MCSs in the formation of the Typhoon, this study considers the physical and dynamical processes associated with the warm core generation, as well as contributions from the convective-scale systems. The results indicate that the last MCS during the TC formation is in close vicinity of the surface low pressure centre, and its associated heating almost directly transforms to the warm-core structure of the TC. It is argued with the theory of the response of a balanced vortex to diabatic heating (Hack and Schubert 1986; Vigh and Schubert 2009) that the heating location from this last MCS is relatively effective (compared with earlier MCS activities) in overcoming the inner-core high inertial stability to generate the necessary transverse circulation, and increase the static stability there for facilitating the pathway to a steady state of the vortex. Such contributions have also been revealed in the EP-flux analysis.

Comparison of Typhoon Ketsana (2003) with Typhoon Dan (1999), which was similar monsoon trough formation but with only one MCS involved, is carried out to examine their different paces of development. MCS activities and the rate of formation are analysed through the simulated CAPE. Results show that in these two cases, the rate of TC formation is synoptic pattern dependent; it is much faster to form a TC from unorganised disturbance for a single MCS than from multiple convection episodes associated with multiple MCSs. Compared with the single MCS pattern, spinning up of relative vorticity within different areas in the incipient vortex with multiple-MCS convection pattern does not expedite the TC development process, but rather hamper it. This mechanism may be explained from the point of view of competing for convective resources, or through the convective energy consumption and recovery circle. Development of deep convection consumes the environmental CAPE, which results in unfavourable environment for new convection development. Until the environmental CAPE increases again by heat and moisture fluxes from the ocean surface, it is not possible to develop a new convection system. This conclusion is also in agreement with previous study, (e.g. Fang and Zhang, 2011), which showed that in the simulated formation of Hurricane Dolly (2008), similar processes were found under the TC system scale.

Following the investigation of MCS activities and TC formation, the convective activities in Typhoon Ketsana are further analysed after spectral decomposition. Results show that both the area-averaged meso-α and meso-γ scale relative vorticity start to increase since the first MCS, but area-averaged meso-β scale vorticity is negative and

shows a decreasing trend with peaks consistent with the MCSs activities. This is mainly attributed to the mesoscale downdrafts associated with negative relative vorticity, and there is no apparent merging of vorticity centres within this scale.

The roles of VHTs or CVAs are then analysed. Results show that positive and negative vorticity indeed are dynamically linked with each other due to the same trend for both meso-β scale and meso-γ scale vorticity time series. For meso-γ scale both positive vorticity anomalies of the CVAs and negative vorticity anomalies associated with downdrafts are identified in the simulation, and they persist during the TC formation. A dynamical explanation of the surface vortex formation is investigated based on the self-aggregation of the CVAs and how the effect from the negative vorticity anomalies is reduced during the up-scale energy cascade process.

A quantitative measure of the merger index developed in Venkatesh (2003) is applied to examine the aggregation of vortices. Results also point out that the evolutions of the meso-γ scale vortices with positive and negative vorticity are highly correlated. The positive VHTs or CVAs do merge together to form the core vortex, on the other hand the negative ones either weaken or are expelled out of the core region. This is consistent with studies such as Fang and Zhang (2011), in which the positive CVAs get closer to the centre through advection by the secondary circulation, while the negative CVAs become weaker.

The OWZP is also applied to our high-resolution simulation of Typhoon Ketsana, which shows that it is a good indicator of TC formation when the grid distance is larger than 10 km, but the threshold of the parameter has to increase to about 1000 to detect TC

formation. Thus, besides the previous applications of the OWZP on detection of TC vortices in coarse-resolution climate model simulation, it is also feasible for applying to predictions of individual TC cases. Such applicability of OWZP as a diagnostic tool with the appropriate scale has also been illustrated by its correlation with the column-integrated moist entropy and midlevel relative vorticity in the simulation, which has been identified previously based on observations (Raymond and Carrillo 2011).

In addition, the unique feature of TC with the warm core structure is analysed with both observations and numerical modelling. Seventeen TCs that occurred in the monsoon trough of WNP are analysed with the AMSU-A microwave brightness temperature data obtained from the NOAA-15, NOAA-16, NOAA-18 and METOP-2 satellites. Results show that the heating associated with deep convection within a small area is clearly demonstrated for each TC case. Due to the low spatial resolution and signal attenuation, previous Research (e.g. Barnes and Nolan, 2012) found that remote-sensing data mostly overestimated the height of TC warm core. However, with consideration of the scattering issue, microwave information is a valuable resource to monitor the thermodynamic development in TC to indicate warm core structure in the mid to lower troposphere. However, the secondary warm core developed cannot be resolved via these data due to the contamination by strong scattering during the intensification of Typhoon Ketsana.

In the WRF simulation of Typhoon Ketsana, three stages of warm core development have been identified. First, mesoscale heating is located in the lower troposphere before formation, and then mature warm core development is found in the upper troposphere not

long after formation. Afterward, a secondary warm core formation is identified during early intensification. That is, the 'conventional' or 'typical' upper-level warm core may develop, however, there are mechanisms that lead to mid-to-low-level warm core as revealed in the simulation.

It is widely believed that the warm core of a TC is located in the upper level because during TC formation thermal wind requirement results in the upper-level warm core. However, recent studies showed different warm core heights of TCs. Similar to Stern and Zhang (2013) and Shno and Satoh (2015), the largest contribution to the potential temperature tendency from the total advection process is examined in our simulation of Typhoon Ketsana. Vertical advection is found to be the dominating component compared with horizontal advection. A typical stratiform profile of vertical velocity and heating is identified in the Typhoon's individual mesoscale convective episodes. As a consequence, the low-level mesoscale decent of air is responsible for the secondary warm core in the typhoon that develops after formation, similar to the effect of dry adiabatic descent discussed in Dolling and Barnes (2012). On the other hand, the upper-level heating associated with convection is likely to be responsible for maintaining the warm core at that level. How general a phenomenon for the development of secondary warm core at the mid-to-low level will be further explored in the future.

The study in this dissertation is certainly limited by the numbers of cases because there are only 2 TCs ever simulated and analysed. More cases should be studied, with both similar synoptic pattern of monsoon trough as in Typhoon Dan and Ketsana and TCs under other synoptic situations, to confirm the validity of results shown in this study.

These include the role of mesoscale heating to TC formation, CAPE cycles and the rates of TC development, convective systems organization dynamics, scale issue in applying the OWZP parameter and the warm core structure.

There are also a few directions that should be pursued in future research. The CAPE characteristics relative to MCS activities is only studied via model outputs, because there was no observation for the TC cases. The hypotheses put forward in the study should be further investigated via observations, which can confirm the model results.

The merger index of vortex applied here was originally designed to study mesoscale vortex mergering. Although it can be used to examine convective scale vortex interaction, it would be more rigorous to develop a convective-scale vortex merger index. This is particularly the case when the number of vortices under interaction is much larger under convective scale. The application of linear regression with varying number of vortices to obtain the merger index might need revision.

Moreover, currently there is still limitation in the application of passive microwave data to retrieve low-level temperature accurately and for deducing warm core structure in TC. When advances in data retrieval techniques have been made in the future, more of these satellite products should be used to validate the model simulated warm core structure as seen in the case of Typhoon Ketsana. It is only this way that the theories on the various potential warm core structures can be verified effectively.

References

Abbott, P. L. 2006: Natural disasters. *McGraw-Hill Higher Education.*

ATCR, 1999: Annual Tropical Cyclone Report, *Joint Typhoon Warning Centre, U. S. Naval Pacific Meteorology and Oceanography Centre,* 214 pp.

ATCR, 2003: Annual Tropical Cyclone Report, *Joint Typhoon Warning Centre, U. S. Naval Pacific Meteorology and Oceanography Centre,* 827 pp.

Adler, R.F., 2005: Estimating the benefit of TRMM tropical cyclone data in saving lives. *15th Conference on Applied Climatology, Amer. Meteor. Soc., Savannah, GA,* 20-24 June 2005.

Andrews, D. G., J. R. Holton, and C. B. Leovy, 1987: *Middle Atmospheric Dynamics*. Academic Press, 489 pp.

Augustine, J. A, and K.W. Howard, 1988: Mesoscale convective complexes over the United States during 1985. *Mon. Wea. Rev.*, **116**, 685–701.

Bartels, D. L., and R. A. Maddox, 1991: Midlevel cyclonic vortices generated by mesoscale convective systems. *Mon. Wea. Rev.*, **119**, 104–118.

Bessho, K., T. Nakasawa, S. Nishimura, and K. Kato, 2010: Warm core structures in organised cloud clusters developing or not developing into tropical storms observed by the Advanced Microwave Sounding Unit. *Mon. Wea. Rev.*, **138**, 2624–2643.

Bister, M., and K.A. Emanuel, 1997: The genesis of Hurricane Guillermo: TEXMEX analyses and a modelling study. *Mon. Wea. Rev*., **125**, 2662–2682.

Bosart, L. F., and F. Sanders, 1981: The Johnstown flood of July 1977: a long-lived convective storm. *J. Atmos. Sci.*, **38**, 1616–1642.

Bosart L. F., and J. A. Bartlo, 1991: Tropical storm formation in a baroclinic environment. *Mon. Wea. Rev.*, **119**, 1979–2013.

Brandes, E. A., 1990: Evolution and structure of the 6–7 May 1985 mesoscale convective system and associated vortex. *Mon. Wea.Rev.*, **118**, 109–127.

Braun, S. A. 2002: A cloud-resolving simulation of Hurricane Bob (1991): Storm structure and eyewall buoyancy. *Mon. Wea. Rev.,* **130**, 1573–1592

Camargo, S. J., K. A. Emanuel, and A.H. Sobel, 2007: Use of a genesis potential index to diagnose ENSO effects on tropical cyclone genesis. *J. Climate*, **20**, 4819-4834.

Charney J. G., and A. Eliassen, 1964: On the growth of the hurricane depression. *J. Atmos. Sci.*, **21**, 68–75.

Chang, C.-P., J. M. Chen, P. A. Harr, and L. E. Carr, 1996: Northwestern-propagating wave patterns over the tropical western North Pacific during summer. *Mon. Wea. Rev.*, **124**, 2245–2266.

Chen, S. A., and W. M. Frank, 1993: A numerical study of the genesis of extratropical convective mesovortices. Part I: Evolution and dynamics. *J. Atmos. Sci.*, **50**, 2401–2426.

Chen, T.-C., S.-Y.Wang, M.-C. Yen, and W. A. Gallus Jr., 2004: Role of the monsoon gyre in the interannual variation of tropical cyclone formation over the Western North Pacific. *Wea. Forecasting*, **19**, 776–785.

Chen, Y., and M. K. Yau, 2001: Spiral bands in a simulated hurricane. Part I: Vortex Rossby wave verification. *J. Atmos. Sci.*, **58**, 2128–2145.

Chen, Y., and M. K. Yau, 2003: Asymmetric structures in a simulated landfalling hurricane. *J. Atmos. Sci.,* **60**, 2294–2312.

Chen, W., M. Takahashi, and H.-F. Graf (2003): Interannual variations of stationary planetary wave activity in the northern winter troposphere and stratosphere and their relations to NAM and SST, *J. Geophys. Res.*, **108** (D24), 4797.

Cheung, K. K. W., 2004: Large-scale environmental parameters associated with tropical cyclone formations in the western North Pacific. *J. Climate*, **17**, 466–484.

——, and R. L. Elsberry, 2006: Model sensitivities in numerical simulations of the formation of Typhoon Robyn (1993).*Terr. Atmos. Oceanic Sci.*, **17**, 53−89.

Churchill, D. D., and R. A. Houze, Jr., 1984: Mesoscale updraft magnitude and cloud-ice content deduced from the ice budget of the stratiform region of a tropical cloud cluster. *J. Atmos. Sci.,* **41**, 1717−1725.

Collier, C. G., S. Lovejoy, and G. L. Austin, 1980: Analysis of bright bands from 3D radar data. Preprints, *19th Conf. on Radar Meteorology, Miami Beach, FL, Amer. Meteor. Soc.,* 44–47.

Cotton W. R., M.-S. Lin, R. L. McAnelly, and C. J. Tremback, 1989: A composite model of mesoscale convective complexes. *Mon. Wea. Rev.*, **117**, 765–783.

DeMaria, M., J. A. Knaff, and C. Sampson, 2007: Evaluation of long-term trends in tropical cyclone intensity forecasts. *Meteor. Atmos. Phys.*, **97**, 19–28.

Dolling, K., and G. M. Barnes, 2012: Warm core formation in Tropical Storm Humberto (2001). *Mon. Wea. Rev.*, **140**, 1177−1190.

Dritschel, D. G., and D. W. Waugh, 1992: Quantification of the inelastic interaction of

unequal vortices in two-dimensional vortex dynamics. *Phys. Fluids,* **A4**, 1737–1744.

Dudhia, J. 1989: Numerical Study of Convection Observed During the Winter Monsoon Experiment Using a Mesoscale Two-Dimensional Model. *J. Atmos. Sci.*, **46**, 3077–3107.

Dunkerton, T. J., M. T. Montgomery, and Z. Wang, 2009: Tropical cyclogenesis in a tropical wave critical layer: Easterly waves. *Atmos. Chem. Phys.*, **9**, 5587–5646

Ek, M. B., K.E. Mitchell, Y. Lin, E. Rogers, P. Grummann, V. Koren, G. Gayno, and J. D. Tarpley, 2003: Implementation of Noah land-surface model advances in the CEP operational mesoscale Eta mode. *J. Geophys. Res.*, **108** (D22): 8851.

Eliassen A., 1951: Slow thermally or frictionally controlled meridional circulation in a circular vortex. *Astro. phys. Norv.*, **5**, 19–60.

Eliassen, A., N., and E. Palm, 1960: On the transfer of energy in stationary mountain wave. *Geof. Pub.*, **22**, 1–23.

Emanuel, K. A., 1986: An Air-Sea Interaction Theory for Tropical Cyclones. Part I: Steady-State Maintenance. *J. Atmos. Sci.*, **43**, 585–605.

——, 1993: The effect of convective response time on WISHE modes. *J. Atmos. Sci*., **50**, 1763–1775.

——, and D. S. Nolan, 2004: Tropical cyclone activity and global climate preprints, *26th Conf. on Hurricanes and Tropical Meteorology, Miami, FL, Amer. Meteor. Soc.*, 240–241.

Emanuel, K, 2001: Contribution of tropical cyclones to meridional heat transport by the oceans. *J. Geophys. Res.*, **106** (D14), 14771–14781.

——, J. Callaghan, and P. Otto, 2008: A hypothesis for the redevelopment of warm-core

cyclones over northern Australian. *Mon. Wea. Rev.*, **136**, 3863−3872.

Fang, J., and F. Zhang, 2011: Initial development and genesis of Hurricane Dolly (2008), *J. Atmos. Sci.*, **67**, 655–672.

Frank, W.M., 1987: Tropical cyclone formation. A Global View of Tropical Cyclones, R.L. Elsberry, Ed., *U.S. Office of Naval Research, Marine Meteorology Program,* Washington, DC, 53–90.

Fu, B., T. Li, M. S. Peng, and F. Weng, 2007: Analysis of tropical cyclogenesis in the western North Pacific for 2000 and 2001. *Wea. Forecasting*, **22**, 763–780.

Ferreira, N. R., and W. H. Schubert, 1999: On the role of tropical cyclones in the formation of tropical upper tropospheric troughs. *J. Atmos. Sci.*, **56**, 2891–2907.

Ferrel, W., 1856: An essay on the winds and currents of the oceans. *Nashville Journal of Surgery and Medicine,* **11**, 287−301.

Gray, W. M., 1968: Global view of the origin of tropical disturbances and storms. *Mon. Wea. Rev.*, **96**, 669−700.

——, 1979: Tropical cyclone intensity determination through upper-troposphere aircraft reconnaissance. *Bull. Amer. Meteor. Soc.*, **60**, 1069−1074.

Hack, J. J., and W. H. Schubert, 1986: Nonlinear response of atmospheric vortices to heating by organised cumulus convection. *J. Atmos. Sci.*, **43**, 1559−1573.

Halverson, J. B., J. Simpson, G. Heymsfield, H. Pierce, T. Hock, and E. A. Ritchie, 2006: Warm core structure of Hurricane Erin diagnosed from high altitude dropsondes during CAMEX-4. *J. Atmos. Sci.,* **63**, 309–324.

Harr, P. A., and R. L. Elsberry, 1996: Structure of a mesoscale convective system embedded in Typhoon Robyn during TCM-93. *Mon. Wea. Rev.,* **124**, 634–652.

Haurwitz, B., 1935: The height of tropical cyclones and the "eye" of the storm. *Mon. Wea. Rev.*, **63**, 45-49.

Hawkins H. F., and D. T. Rubsam, 1968: Hurricane Hilda. *Mon. Wea. Rev.*, **96**, 701–707.

——, and S. M. Imbembo, 1976: The structure of a small, intense hurricane – Inez 1966. *Mon. Wea. Rev.*, **10**, 418–442.

Hendricks, E. A., M. T. Montgomery, and C. A. Davis, 2004: The role of "vortical" hot towers in the formation of tropical cyclone Diana (1984). *J. Atmos. Sci.*, **61**, 1209−1232.

Hobbs, P. V., 1973: Anomalously high ice particle concentrations in clouds. *8th International Conf. on Nucleation,* Leningrad, September 1973.

Hong, S-.Y., J. Dudhia, and S.-H. Chen, 2004: A revised approach to ice-microphysical processes for the bulk parameterization of cloud and precipitation, *Mon. Wea. Rev.*, **132**, 103−120.

Houze**,** R. A., Jr., 1973: A climatological study of vertical transports by cumulus-scale convection. *J. Atmos. Sci.,* **30**, 1112−1123.

——, 1982: Cloud clusters and large-scale vertical motions in the tropics. *J. Meteor. Soc. Japan*, **60**, 396−410.

——, 1989: Observed structure of mesoscale convective systems and implications for large-scale heating. *Quart. J. Roy. Meteor. Soc.,* **115**, 425−461.

——, W.-C. Lee, and M. M. Bell, 2009: Convective contribution to the genesis of Hurricane Ophelia (2005). *Mon. Wea. Rev.,* **137**, 2778–2800.

——, and D. D. Churchill, 1984: Microphysical structure of precipitating clouds in winter MONEX. Postprints, *15th Technical Conference on Hurricanes and Tropical Meteorology,* Miami, Amer. Meteor. Soc., 527–532.

——, and D. D. Churchill, 1987: Mesoscale organization and cloud microphysics in a Bay of Bengal depression. *J. Atmos. Sci.,* **44**, 1845–1867.

Ide, K., P. Courtier, M. Ghil, and A. Lorenc, 1997: Unified notation for data assimilation: Operational, sequential and variational. *J. Meteor. Soc. Japan*, **75**, 181–189.

Kain, J. S., 2004: The Kain–Fritsch Convective Parameterization: An update. *J. Appl. Meteor.*, **43**, 170–181.

Karyampudi, V. M., and H. F. Pierce, 2002: Synoptic-scale influence of the Saharan air layer on tropical cyclogenesis over the Eastern Atlantic. *Mon. Wea. Rev.*, **130**, 3100–3128.

Kieu, C. Q., and D.-L. Zhang, 2008: Genesis of Tropical Storm Eugene (2005) from merging vortices associated with ITCZ breakdowns, Part I: Observational and modelling analyses, *J. Atmos. Sci.,* **65**, 3419–3439.

Knight, C. A., W. A. Cooper, D. W. Breed, I. R. Paluch, P. L. Smith, and G. Vali, 1982: Microphysics. *Chapter 7 of Hailstorms of the Central High Plains, Vol. 1, The National Hail Research Experiment*. National Centre for Atmospheric Research and Colorado Associated University Press, Boulder, CO., 282 pp.

Kuo, H.-C., W. H. Schubert, C.-L.Tsai, and Y.-F. Kuo, 2008: Vortex interactions and barotropic aspects of concentric eyewall formation. *Mon. Wea. Rev.*, **136**, 5183–5198.

Laing, A., and J. Evans, 2011: Tropical Cyclones. *Chapter 8 of Introduction to Tropical Meteorology, 2nd Edition*. Online textbook developed through COMET, University Corporation of Atmospheric Research.

Lander, M. A. 1996: Specific tropical cyclone track types and unusual tropical cyclone motions associated with a reverse-oriented monsoon trough in the western North Pacific. *Wea. Forecasting*, **11**, 170–186.

La Seur, N. E., and H. F. Hawkins, 1963: An analysis of Hurricane Cleo (1958): Based on data from research reconnaissance aircraft. *Mon. Wea. Rev.*, **91**, 694–709.

Lee, C.-S., K. K. W. Cheung, J. S. N. Hui, and R. L. Elsberry, 2008: Mesoscale features associated with tropical cyclone formations in the western North Pacific. *Mon. Wea. Rev.*, **136**, 2006–2022.

Liu, Y., D.-L. Zhang, and M. K. Yau, 1997: A multiscale numerical study of Hurricane Andrew (1992). Part I: Explicit simulation and verification. *Mon. Wea. Rev.*, **125**, 3073–3093.

Lorenc, A. C., 1986: Analysis methods for numerical weather prediction. *Q. J. R. Meteorol. Soc.*, **112**, 1177–1194.

Lu, X., K. K. W. Cheung, and Y. Duan, 2012: Numerical study on the formation of Typhoon Ketsana (2003). Part I: Roles of the mesoscale convective systems. *Mon. Wea. Rev.*, **140**, 100–120.

Maddox, R. A., 1980: Mesoscale convective complexes: *Bull. Amer. Meteor. Soc.,* **61**, 1374–1387.

Marks, F. D., Jr., and R. A. Houze, Jr., 1984: Airborne Doppler-radar observations in Hurricane Debby. *Bull. Amer. Meteor. Soc.,* **65**, 569–582.

——, P. G. Black, M. T. Montgomery, and R. W. Burpee, 2008: Structure of eye and eyewall of Hurricane Hugo (1989). *Mon. Wea. Rev.*, **136**, 1237–1259.

Martinez, Y., G. Brunet, M. K. Yau, *and* X. Wang, 2011: On the dynamics of concentric eyewall genesis: Space-time empirical normal modes diagnosis, *J. Atmos. Sci.,* **68**, 457–476.

Matejka, T. J., Houze, R. A. Jr, and Hobbs, P. V., 1980: Microphysics and dynamics of clouds associated with mesoscale rainbands in extratropical cyclones. *Q. J. R. Meteorol. Soc.*, **106**, 29–56.

Maue, R. N., 2011: Recent historically low global tropical cyclone activity, *Geophys. Res. Lett.*, **38**, L14803.

McBride, J. L., 1995: Tropical cyclone formation. *Global Perspectives on Tropical Cyclones*, R. L. Elsberry, Ed., WMO/TD-No. 693, World Meteorological Organization, Geneva, 63–105.

McWilliams, J. C., 1984: The emergence of isolated, coherent vortices in turbulent flow. *J. Fluid Mech.*, **146**, 21-43.

Menkes, C. E., M. Lengaigne, P. Marchesiello, N.C. Jourdain, E.M. Vincent, J. Lefèvre, F. Chauvin, and J. F. Royer, 2011: Comparison of tropical cyclogenesis indices on seasonal to interannual timescales. *Climate Dyn.*, **38**, 301–321.

Mlawer, E. J., S. J. Taubman, P. D. Brown, and M. J. Iacono, 1997: Radiative transfer for inhomogeneous atmospheres: RRTM, a validated correlated-k Model for the longwave.

J. Geophys. Res., **102**, 16663–16682.

Molinari, J., S. Skubis, and D. Vollaro, 1995: External influences on hurricane intensity. Part III: Potential vorticity evolution. *J. Atmos. Sci.*, **52**, 3593–3606.

Molinari, J., D. Vollaro, F. Alsheimer, and H. E. Willoughby, 1998: Potential vorticity analysis of tropical cyclone intensification. *J. Atmos. Sci.*, **55**, 2632–2644.

——, ——, and K. L. Corbosiero, 2004: Tropical cyclone formation in a sheared environment: A case study. *J. Atmos. Sci.*, **61**, 2493–2509.

Monteverdi, J. P., and R. Edwards, 2010: The redevelopment of a warm core structure in Erin: A case of inland tropical storm formation. Electronic. *J. Severe Storms Meteor.*, **5**, 1–18.

Montgomery, M. T., and R. J. Kallenbach, 1997: A theory for vortex Rossby-waves and its application to spiral bands and intensity changes in hurricanes. *Q. J. R. Meteorol. Soc.*, **123**, 435–465.

——, M. E. Nicholls, T. A. Cram, and A. B. Saunders, 2006: A vortical hot tower route to tropical cyclogenesis. *J. Atmos. Sci.*, **63**, 355–386.

——, and J. Enagonio, 1998: Tropical cyclogenesis via convectively forced vortex Rossby waves in a three-dimensional quasigeostrophic model. *J. Atmos. Sci.*, **55**, 3176–3207.

——, Wang, Z., and T. J. Dunkerton, 2010: Coarse, intermediate and high resolution numerical simulations of the transition of a tropical wave critical layer to a tropical storm, *Atmos. Chem. Phys.*, **10**, 10803–10827.

Noh, Y., W. G. Cheon, S.-Y. Hong, and S. Raasch, 2003: Improvement of the K-profile model for the planetary boundary layer based on large eddy simulation data. *Bound.-Layer Meteor.*, **107**, 401–427.

Nguyen, S. V., R. K. Smith, and M. T. Montgomery, 2008: Tropical-cyclone intensification and predictability in three dimensions. *Q. J. R. Meteorol. Soc.*, **134**, 563–582.

Ohno, T., and M. Satoh, 2015: On the warm core of a tropical cyclone formed near the troposphere. *J. Atmos. Sci.*, **72**, 511–571.

Okubo, A., 1970: Horizontal dispersion of floatable particles in the vicinity of velocity singularities such as convergences, *Deep-Sea Res.*, **17**, 445–454.

Oyama, R., 2014: Estimation of tropical cyclone central pressure from warm core intensity observed by the Advanced Microwave Sounding Unit-A (AMSU-A). *Papers Meteorol. Geophys.*, **65**, 35–56.

Palmén, E., and C. Newton, 1969: *Atmospheric Circulation Systems (Their Structure and Physical Interpretation)*. Academic Press, 603 pp.

Parrish, D. F., and J. C. Derber, 1992: The National Meteorological Centre's spectral statistical interpolation analysis system. *Mon. Wea. Rev.*, **120**, 1747–1763.

Rappaport, E. N., and Coauthors, 2009: Advances and challenges at the national hurricane centre. *Wea. Forecasting*, **24**, 95–419.

Raymond, D. J., and López Carrillo, C., 2011: The vorticity budget of developing typhoon Nuri (2008). *Atmos. Chem. Phys.*, **11**, 147–163.

Reasor, P. D., M. T. Montgomery, and L. F. Bosart, 2005: Mesoscale observations of the genesis of Hurricane Dolly (1996), *J. Atmos. Sci.*, **62**, 3151–3171.

——, ——, F. D. Marks, and J. F. Gamache, 2000: Low-wavenumber structure and evolution of the hurricane inner core observed by airborne dual-Doppler radar. *Mon. Wea. Rev.*, **128**, 1653–1680.

Riehl, H., and J. S. Malkus, 1958: On the heat balance in the equatorial trough zone. *Oeophysica (Helsinki)*, **6**, 503−538.

Ritchie, E. A., and G. J. Holland, 1993, On the interaction of tropical-cyclone-scale vortices. II: Discrete vortex patches. *Q. J. R. Meteorol. Soc.*, **119**, 1363–1379.

——*, and* ——, 1997: Scale interactions during the formation of Typhoon Irving*, Mon. Wea. Rev.,* **125***,* 1377–1396.

——, and ——, 1999: Large-scale patterns associated with tropical cyclogenesis in the western Pacific. *Mon. Wea. Rev.*, **127**, 2027−2043.

Royer, J.-F., F. Chauvin, B. Timbal, P. Araspin, and D. Grimal, 1998: A GCM study of impact of greenhouse gas increase on the frequency of occurrence of tropical cyclones. *Climate Dyn.*, **38**, 307–343.

Schubert, W. H., 1985: Wave, mean-flow interactions and hurricane development. *16th Conf. on Hurricanes and Tropical Meteorology, Houston, Texas, Amer. Meteor. Soc.*, 140−141.

Shaw, N., 1922: The birth and death of cyclones. *Geophys. Mem.*, **2**, 213−227.

Simpson, J., E. A. Ritchie, G. J. Holland, J. Halverson and S. Stewart, 1997: Mesoscale interactions in tropical cyclone genesis. *Mon. Wea. Rev.*, **125**, 2643−2661.

Shapiro, L. J., and H. E. Willoughby, 1982: The response of balanced hurricanes to local sources of heat and momentum. *J. Atmos. Sci.*, **39**, 378–394.

Sippel, J. A., J. W. Nielsen-Gammon, and S. E. Allen, 2006: The multiple-vortex nature of tropical cyclogenesis. *Mon. Wea. Rev.*, **134**, 1796–1814.

Skamarock, W. C., J. B. Klemp, J. Dudhia, D. O. Gill, D. M. Barker, M. G. Duda, X.-Y. Huang, W. Wang, and J. G. Powers, 2008: *A description of the advanced research WRF version 3*. NCAR Technical Note 475.

Stern, D. P., and D. S. Nolan, 2012: On the height of the warm core in tropical cyclones. *J. Atmos. Sci.*, **69**, 1657–1680.

——, and F. Zhang, 2013: How does the eye warm? Part I: A potential temperature budget analysis of an idealised tropical cyclone. *J. Atmos. Sci.*, **70**, 73–90.

Steiner, M., and R. A. Houze, Jr., 1993: Three-dimensional validation at TRMM ground truth sites: Some early results from Darwin, Australia. Preprints, *26th Conference on Radar Meteorology, Norman*, Amer. Meteor. Soc., 417-420.

——, ——, and S. E. Yuter, 1995: Climatological characterization of three-dimensional storm structure from operational radar and rain gauge data. *J. Appl. Meteor.*, **34**, 1978–2007.

Stone, P. H., and G. Salustri, 1984: Generalization of the Quasi-Geostrophic Eliassen-Palm flux to include eddy forcing of condensation heating. *J. Atmos. Sci.*, **41**, 3527–3535.

Tippett, M. K., S. J. Camargo, and A. H. Sobel, 2011: A Poisson regression index for tropical cyclone genesis and the role of large-scale vorticity in genesis, *J. Climate.,* **24**, 2335–2357.

Tory, K. J., and W. M. Frank, 2010: Tropical Cyclone Formation. Global Perspectives on Tropical Cyclones: From Science to Mitigation. *World Scientific*, 55–91.

——, M. T. Montgomery, and N. E. Davidson, 2006a: Prediction and diagnosis of tropical cyclone formation in an NWP system. Part I: The critical role of vortex enhancement in deep convection. *J. Atmos. Sci.*, **63**, 3077–3089.

——, ——, ——, and J. D. Kepert, 2006b: Prediction and diagnosis of tropical cyclone formation in an NWP system. Part II: A diagnosis of Tropical Cyclone Chris formation. *J. Atmos. Sci.*, **63**, 3091–3113.

——, R. A. Dare, N. E. Davidson, J. L. McBride, and S. S. Chand, 2013: The importance of low-deformation vorticity in tropical cyclone formation. *Atmos. Chem. Phys.*, **13**, 2115–2132.

Venkatesh, T. N., 2003: A Vortex Merger Theory for Tropical Cyclone Genesis, Ph.D. Thesis, *Indian Institute of Science*, 167 pp.

Velasco, I., and J. M. Fritsch, 1987: Mesoscale convective complexes in the Americas. *J. Geophys. Res.*, **92**, 9561–9613.

Vigh, J. L., and W. H. Schubert, 2009: Rapid development of the tropical cyclone warm core. *J. Atmos. Sci.*, **66**, 3335–3350.

Wang, Y., 2001: An explicit simulation of tropical cyclones with a triply nested movable mesh primitive equation model: TCM3. Part I: Model description and control experiment. *Mon. Wea. Rev.*, **129**, 1370–1394.

——, 2002a: Vortex Rossby waves in a numerically simulated tropical cyclone. Part I: Overall structure, potential vorticity, and kinetic energy budgets. *J. Atmos. Sci.*, **59**, 1213–1238.

——, 2002b: Vortex Rossby waves in a numerically simulated tropical cyclone. Part II: The role in tropical cyclone structure and intensity changes. *J. Atmos. Sci.*, **59**, 1239–1262.

Wang, Z., M. T. Montgomery, and Fritz, C., 2012: A first look at the structure of the wave pouch during the 2009 PREDICT-GRIP dry runs over the Atlantic, *Mon. Wea. Rev.*, **140**, 1144–1163.

——, ——, and T. J. Dunkerton, 2010: Genesis of pre-Hurricane Felix (2007). Part II: Warm core formation, precipitation evolution, and predictability. *J. Atmos. Sci.*, **67**, 1730−1743.

Wang, C., and G. Magnusdottir, 2006: The ITCZ in the central and eastern Pacific on synoptic time scales. *Mon. Wea. Rev.*, **134**, 1405–1421.

Wang, Z, 2014: Characteristics of Convective Processes and Vertical Vorticity from the Tropical Wave to the Tropical Cyclone Stage in the High-resolution Numerical Model Simulations of Tropical Cyclone Fay (2008). J. Atmos. Sci., 71, 896-915.

Weiss, J., 1991: The dynamics of entropy transfer in two-dimensional hydrodynamics, *Phys. D*, **48**, 273–294.

Xiao, Q., Y.-H. Kuo, Z. Ma, W. Huang, X.-Y. Huang, X. Zhang, D. M. Barker, J. Michalakes, and J. Dudhia, 2008: Application of an adiabatic WRF adjoint to the investigation of the May 2004 McMurdo, Antarctica severe wind event. *Mon. Wea. Rev.*, **136**, 3696–3713.

Zehr, R. M., 1992: *Tropical cyclogenesis in the western North Pacific*. NOAA Technical Report NESDIS 61, U. S. Department of Commerce, Washington, DC 20233, 181 pp.

Zhu, T., and F. Weng, 2013: Hurricane Sandy warm-core structure observed from advanced Technology Microwave Sounder. *Geophys. Res. Lett.*, **40**, 3325–3330.

Zipser, E. J., 1982: Use of a conceptual model of the life cycle of mesoscale convective systems to improve very-short-range forecasts. *Nowcasting*, *K. Browning, Ed., Academic Press,* 191–221.